

Complete Analytical Model of GaN MESFETs for High Power and Microwave Frequency Applications

A Thesis Submitted

to

the Department of Electrical and Electronic Engineering in Partial Fulfillment of the Requirements for the Degree of Bachelor of Science in Electrical and Electronic Engineering

By

<u>Name</u>	<u>Student Id.</u>
Aysha Siddique Shanta	09221146
Tasneem Rumman Huq	09221147
Daraksha Binte Hossain	09221149
Riaz Mahmood	09221074

Thesis Supervisor:

Professor Md. Shafiqul Islam, PhD



**Department of Electrical and Electronic Engineering
BRAC University, Dhaka
December 2011**

DECLARATION

We hereby declare that this thesis is based on the results found by ourselves. Materials of work found by other researcher are mentioned by reference. This thesis, neither in whole nor in part, has been previously submitted for any degree.

Aysha Siddique Shanta

Tasneem Rumman Huq

Daraksha Binte Hossain

Riaz Mahmood

Signature of Supervisor

ACKNOWLEDGMENT

We would like to express our sincere gratitude and appreciation to everyone who made this thesis possible. Most of all, we would like to thank our supervisor, Professor Dr. Md. Shafiqul Islam for his guidance in achieving our thesis objective. It was an honour getting the privilege to work under his supervision.

Second, we would like to thank our teacher Mehdi Zahid Sadi for his heartiest assistance and invaluable feedbacks for our thesis.

Last, but most importantly, we would specially like to thank our classmates for their support and encouragements.

TABLE OF CONTENTS

DECLARATION.....	i
ACKNOWLEDGMENT	ii
TABLE OF CONTENTS	iii
LIST OF TABLES	vi
LIST OF FIGURES	vi
ABSTRACT	x
CHAPTER 1 INTRODUCTION	1
1.1 MESFET Operation	1
1.2 Types of MESFET	2
1.3 I-V Characteristics of MESFET	4
1.4 C-V Characteristics of MESFET	7
1.5 Structure of MESFET	8
1.6 Equivalent Circuit of a MESFET	9
1.7 Applications of MESFET	11
CHAPTER 2 MOTIVATION	13
2.1 Factors of Motivation	13
2.2 Comparison Between GaAs, SiC and GaN.....	14
2.3 More on GaN and SiC FETs.....	14
CHAPTER 3 LITERATURE REVIEW	18
3.1 Comparison Between R_{ON} and Breakdown Voltage of Different Materials	18
3.2 Potential Performance of SiC and GaN Based MESFETS	18

3.3 Pulsed Measurements of GaN MESFETS	20
3.4 Investigation of Cross Sectional Potential Distribution in GaN-Based FETs by Kelvin Probe Force Microscopy.....	22
3.5 Double-Ion-Implanted GaN MESFETS with Extremely Low Source/Drain Resistance.....	27
CHAPTER 4 PARAMETERS OF GaN MESFET	34
4.1 Study of One-Dimensional Channel Potential Variation	34
4.2 Two Dimensional Channel Potential Distribution of GaN MESFET.....	38
4.3 Variation of Drain-Source Current with Drain-Source Voltage keeping Gate-Source Voltage constant.....	46
4.4 Transconductance	48
4.5 Noise figure.....	54
4.6 Gate-drain capacitance	59
4.7 Gate-source capacitance.....	66
4.8 Total internal device capacitance	68
CHAPTER 5 CONCLUSIONS.....	70
CHAPTER 6 SUGGESTIONS FOR FURTHER RESEARCH	71
REFERENCES.....	73
APPENDIX A MATLAB CODES FOR SIMULATION.....	A.1
One Dimensional Channel Potential Variations for Different Values of Applied Voltage.....	A.1
Two Dimensional Channel Potential.....	A.3
Variation of Drain-Source Current with Drain-Source Voltage	A.7
Variation of Transconductance with Gate-Source Voltage	A.13
Variation of Optimum Noise Figure with Frequency	A.17
Variation of Gate-Drain Capacitance with Drain-Source Voltage	A.28

Variation of Gate-Source Capacitance with Respect to Gate-Source Voltage	A.29
Variation of Total Internal Device Capacitance with Gate Length.....	A.30

LIST OF TABLES

Table 2.1: Comparison Between SiC, GaAs and GaN.....	14
Table 2.2: Material Parameters of SiC and GaN Compared to GaAs and Si	15

LIST OF FIGURES

Figure 1.1: MESFET under negative voltage at gate electrode	2
Figure 1.2: Depletion type MESFET	3
Figure 1.3: Enhancement type MESFET	4
Figure 1.4: I-V characteristics curve	4
Figure 1.5: Linear and saturation regions	7
Figure 1.6: Self aligned MESFET	8
Figure 1.7: Non self aligned MESFET	9
Figure 1.8: Equivalent circuit component superimposed on the cross sectional view of a MESFET	10
Figure 1.9: Equivalent circuit of MESFET	11
Figure 2.1: Schematic of MESFET structure	17
Figure 3.1: R_{ON} vs. Breakdown voltage	18
Figure 3.2: Relationship between electron drift velocity and electric field for GaN (circles) and SiC (triangles)	18
Figure 3.3: Static I-V characteristics for GaN and SiC MESFETs for effective gate voltages of -1V to -5 V	19

Figure 3.4: Transconductance as a function of gate bias	20
Figure 3.5: Current gain cut-off frequency as a function of gate bias.....	20
Figure 3.6: DC I-V characteristics of a $2 \times 50 \times 0.3 \mu\text{m}^2$ GaN MESFET with and without light	21
Figure 3.7: Pulsed I-V characteristics of a $2 \times 50 \times 0.3 \mu\text{m}^2$ GaN MESFET with and without light	22
Figure 3.8: Schematic cross section of (a) fabricated FET structure and (b) diagram of the KFM measurement system	23
Figure 3.9: Electric field distribution between the drain and source edges near the surface of AlGaIn/GaN HFET (a) without and (b) with SiN_x passivation layer. Electric field is concentrated at the midpoint of the drain and gate electrodes	24
Figure 3.10: Electric field distribution between the drain and source edges at the mid-depth of GaN buffer of AlGaIn/GaN HFET (a) without and (b) with SiN_x passivation layer	25
Figure 3.11: Electric field distribution under the gate electrode of AlGaIn/GaN HFET (a) without (b) with SiN_x passivation layer. Electric field is concentrated near the GaN/SiC interface except for the case of which GaN layer is $0.5 \mu\text{m}$ without SiN_x passivation	26
Figure 3.12: GaN MESFET structure with ion implanted channel and source/drain regions (Double Ion Implanted GaN MESFET)	28
Figure 3.13: $I_{ds}-V_{ds}$ characteristics of DII MESFET and CII MESFET	29
Figure 3.14: Transconductance of DII MESFET and IIC MESFET	30
Figure 3.15: On-state resistance of ion implanted GaN MESFET	31
Figure 3.16: On-state resistance components of ion implanted GaN MESFET	32
Figure 3.17: I_{dss} as a function of gate length of DII and IIC MESFETs	33
Figure 3.18: Transconductance as a function of gate length of DII and IIC MESFETs ..	33
Figure 4.1: Parameters used for studying the variation of channel potential	34
Figure 4.2: Variation of 1D channel potential for different V_a	37
Figure 4.3: Typical MESFET Structure under Gate and Drain Bias.....	38
Figure 4.4: Separated Channel Region	39

Figure 4.5: 3D view of 2D channel potential.....	45
Figure 4.6: 2D view of 2D channel potential.....	46
Figure 4.7: I_{ds} - V_{ds} characteristics of GaN MESFET [14].....	48
Figure 4.8: Variation of Transconductance with Gate-Source Voltage for different Drain-Source Voltage	49
Figure 4.9: Variation of Transconductance with Gate-Source Voltage for $R_s = 75\Omega$	50
Figure 4.10: Variation of Transconductance with Gate-Source Voltage for $R_s = 55\Omega$	51
Figure 4.11: Variation of Transconductance with Gate-Source Voltage for $R_s = 35\Omega$	51
Figure 4.12: Variation of Transconductance with Gate-Source Voltage for $R_s = 15\Omega$	52
Figure 4.13: Variation of Transconductance with Gate-Source Voltage for $R_s = 5\Omega$	53
Figure 4.14: Variation of Transconductance with Gate-Source Voltage for $V_{ds} = 10V$	53
Figure 4.15: Variation of Optimum Noise Figure with Frequency for different Gate Length	55
Figure 4.16: Variation of Optimum Noise Figure with Frequency for $R_s = 75\Omega$	55
Figure 4.17: Variation of Optimum Noise Figure with Frequency for $R_s = 55\Omega$	56
Figure 4.18: Variation of Optimum Noise Figure with Frequency for $R_s = 35\Omega$	57
Figure 4.19: Variation of Optimum Noise Figure with Frequency for $R_s = 15\Omega$	57
Figure 4.20: Variation of Optimum Noise Figure with Frequency for $R_s = 5\Omega$	58
Figure 4.21: Variation of Optimum Noise Figure with Frequency for $L = 1\mu m$	59
Figure 4.22: Variation of Gate-Drain Capacitance with Drain-Source Voltage for different Gate-Source Voltage.....	60
Figure 4.23: Variation of Gate-Drain Capacitance with Drain-Source Voltage for $L = 4\mu m$, $Z = 100\mu m$	60
Figure 4.24: Variation of Gate-Drain Capacitance with Drain-Source Voltage for $L = 3\mu m$, $Z = 75\mu m$	61
Figure 4.25: Variation of Gate-Drain Capacitance with Drain-Source Voltage for $L = 2\mu m$, $Z = 50\mu m$	62

Figure 4.26: Variation of Gate-Drain Capacitance with Drain-Source Voltage for $L = 1\mu\text{m}$, $Z = 25\mu\text{m}$	63
Figure 4.27: Variation of Gate-Drain Capacitance with Drain-Source Voltage for $L = 0.5\mu\text{m}$, $Z = 12.5\mu\text{m}$	64
Figure 4.28: Variation of Gate-Drain Capacitance with Drain-Source Voltage for $L = 0.25\mu\text{m}$, $Z = 6.25\mu\text{m}$	65
Figure 4.29: Variation of Gate-Drain Capacitance with Drain-Source Voltage for $V_{GS} = 0\text{V}$	65
Figure 4.30: Variation of Gate-Source Capacitance with Gate-Source Voltage	66
Figure 4.31: Variation of Gate-Source Capacitance with Gate-Source Voltage for different gate lengths	67
Figure 4.32: Variation of Total Internal Device Capacitance with Gate Length for different Gate-Source Voltage.....	68
Figure 4.33: Variation of Total Internal Device Capacitance with Gate Length for different Gate SourceVoltage.....	69

ABSTRACT

In the past few years, growing interest has been paid to the wide band gap materials such as GaN because of its low thermal generation rate and high breakdown field for its potential use in high power, high temperature and microwave frequency applications. The use of GaN based devices for efficient, linear high power RF amplifiers has already been grown for military applications. GaN Metal Semiconductor Field Effect Transistors (MESFETs) have received much attention as its structure is simpler to analyze than that of High Electron Mobility Transistors (HEMTs) and its epi-layers and the physical effects are easier to realize and interpret. Flourishing interest in exploiting the properties and performance of GaN based devices requires the development of simple physics-based analytical models to simplify the device parameter acquisition and to be able to use it for computer-aided design of GaN integrated circuits (ICs). Few analytical models on GaN MESFETs are reported, though significant experimental work is available. Therefore more analytical models should be developed to understand the device operation accurately.

In this thesis, analytical one- and two-dimensional channel potential models are developed for long-channel GaN MESFETs based on the solution of Poisson's equation. The developed analytical channel potential model can be used for short-channel MESFETs with some modifications and assumptions. Analytical models for I-V and C-V characteristics of GaN MESFET are also presented considering the effect of parasitic resistances and gate length modulation. The models evaluate the transconductance and optimum noise figure. The models developed in this thesis will be very helpful to understand the device behaviour in nanometer regime for future applications.

CHAPTER 1

INTRODUCTION

MESFET is an abbreviation for **Metal Semiconductor Field Effect Transistor**. It is a unipolar device where the current conduction occurs by flow of majority carriers only. An n-type MESFET involves current produced by flow of electrons, while in a p-type MESFET, holes cause the current conduction. MESFET consists of a conducting channel through which the device conducts electricity. This channel is positioned between source and drain contacts, as illustrated in Figure 1.1. The flow of free carrier, and hence the current through the channel is regulated by adjusting the gate voltage which causes the thickness of the depletion layer to be varied underneath the metal contact. The Schottky barrier is a potential formed at the metal-semiconductor junction, which exhibits rectifying characteristics that makes it suitable to be used as a diode as well [1].

1.1 MESFET Operation

As demonstrated in Figure 1.1, the MESFET involves 3 terminals, namely Gate, Source and Drain. A semi-insulating GaN substrate is used below the conduction channel. The n-doped region, which acts as the channel can be formed in two ways: by ion implantation or by growing an epitaxial layer. Ion implantation involves ion diffusion in the lightly n-doped layer. Epitaxial growth is a process where crystals are grown in a particular orientation over another crystal and can be of two kinds. If both crystals are of the same material, the process is known as homoepitaxy, and if the materials are different, it is known as heteroepitaxy. An n^+ doped region is implanted on both sides of the n-doped channel which acts as Source and Drain. Metal contacts are then placed on top of the Gate, Source and Drain forming the three distinct terminals of a MESFET. The gate metal and n-doped material junction created forms a Schottky barrier as mentioned earlier.

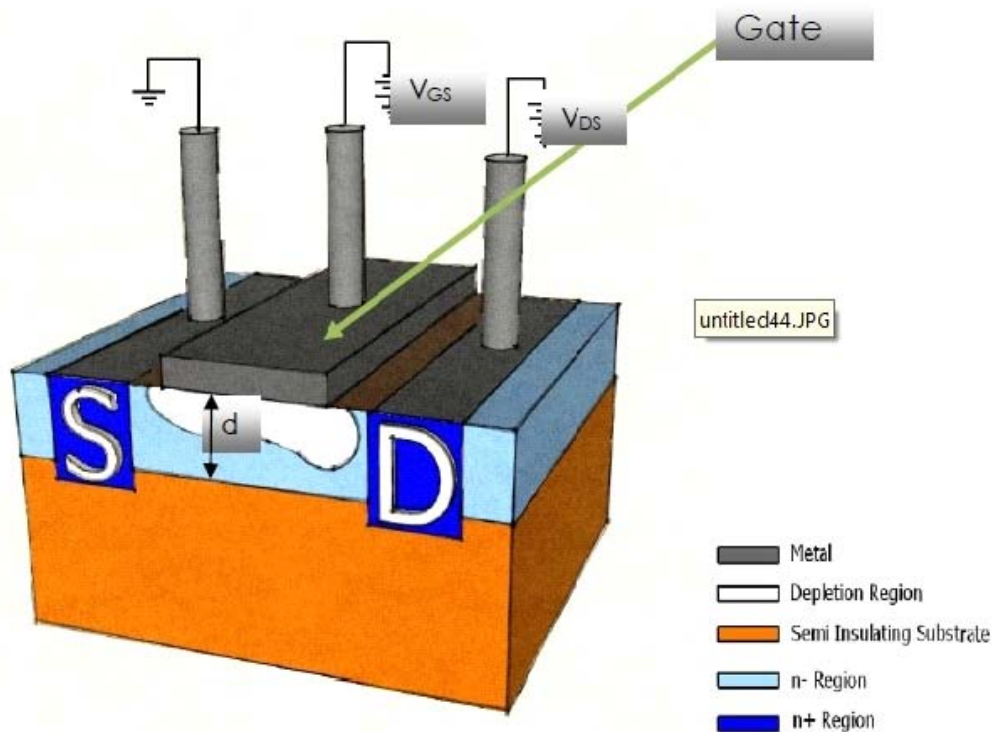


Figure 1.1: MESFET under negative voltage at gate electrode [1]

1.2 Types of MESFET

There are two categories of MESFET operation: depletion MESFET and enhancement MESFET.

1.2.1 Depletion MESFET

In n-channel **depletion MESFET** (Fig. 1.2), the depletion width is varied by altering voltage at the gate terminal. Applying a negative voltage at the gate-to-source causes the depletion width to expand and make the channel width narrow, obstructing the flow of carriers. The junction between gate and channel thus becomes reverse biased. If the depletion region is expanded such that it completely blocks the channel, or pinches-off the channel, the resistance of the channel from source to drain becomes large, causing the MESFET to be turned off like a switch.

Applying a positive gate-to-source voltage will cause the depletion width to minimize allowing the channel size to increase again turning the MESFET on again [1].

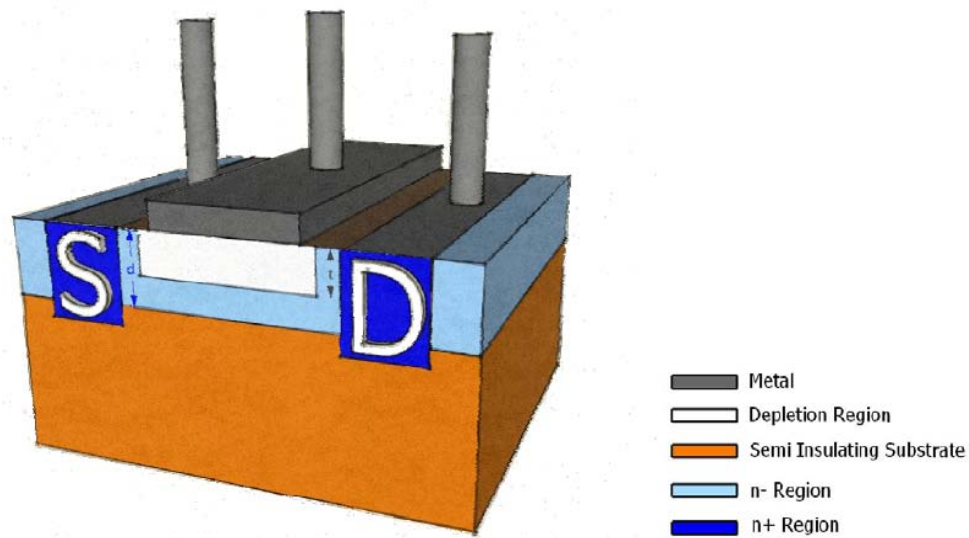


Figure 1.2: Depletion type MESFET [1]

1.2.2 Enhancement MESFET

In an n-channel **enhancement MESFET** (Fig. 1.3), the depletion region completely covers the channel region naturally, and the device remains switched off. In order to allow carriers to flow, the channel needs to be expanded, which is done by narrowing the depletion region. A positive voltage is thus applied at the gate terminal, making the junction between the gate and channel forward biased. As the channel width increases, the device starts to conduct again and current flows [1].

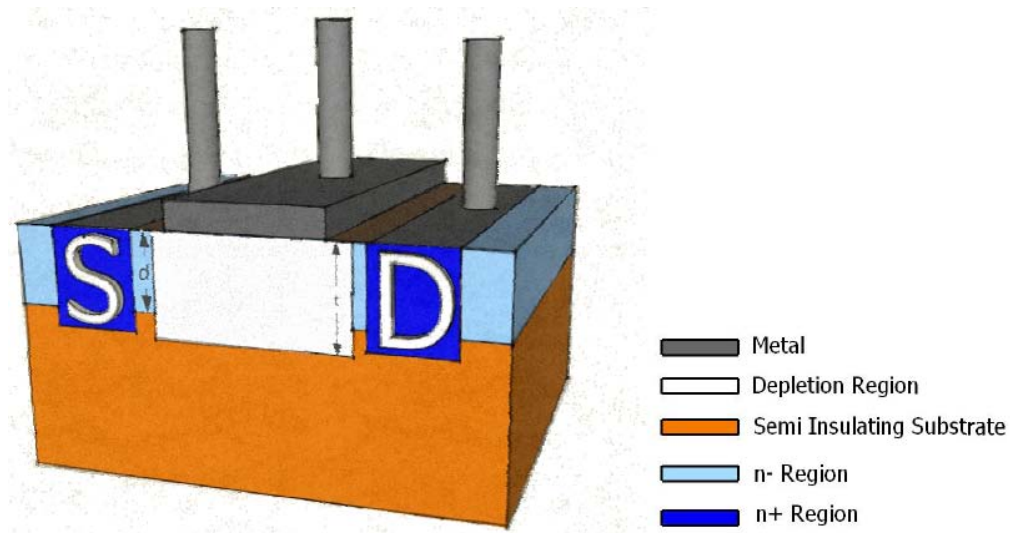


Figure 1.3: Enhancement type MESFET [1]

1.3 I-V Characteristics of MESFET

There are great similarities in the I-V characteristics of a MOSFET and JFET with a typical MESFET. The I-V characteristics of a typical MESFET are shown in the Figure 1.4.

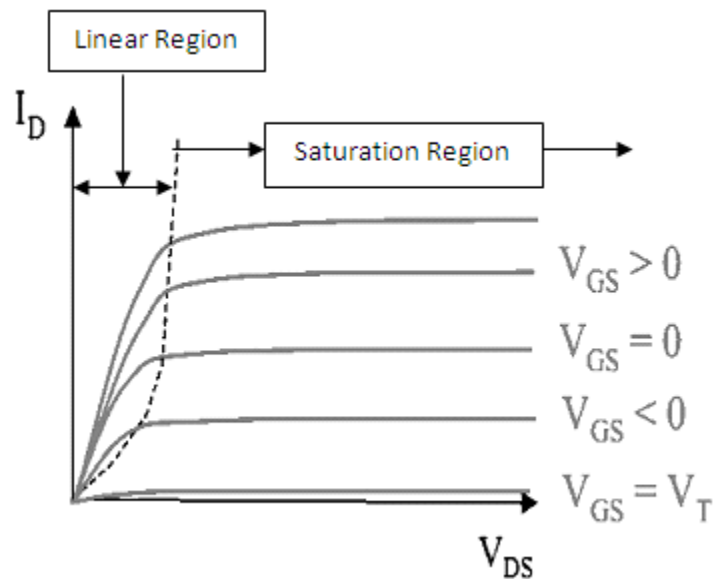


Figure 1.4: I-V characteristics curve [1]

In Figure 1.4, drain current (I_{DS}) is plotted against drain-source voltage (V_{DS}). As we know that the drain current is also a function of gate-source voltage (V_{GS}) so an individual curve in the figure represents the dependency of drain current (I_{DS}) in drain-source voltage (V_{DS}) for a particular value of gate-source voltage (V_{GS}). Figure 1.4 represents the I-V characteristics of a depletion type and an enhancement type MESFET. There is another mode of operation of MESFET which is known as the breakdown mode. In this mode excessive drain-source voltage is applied.

To operate the MESFET in depletion mode, necessary voltage should be given at the gate electrode. The application of more negative voltage at the gate electrode makes the junction more reversed biased results in increase of the depletion region. The channel gets entirely depleted, if we keep increasing the negative voltage at gate electrodes. Therefore, no current flows. Here a new term is introduced named *threshold voltage*. Threshold voltage of a MESFET is the voltage required to fully deplete the doped channel layer. From Figure 1.4, we can see that the value of I_D is very low for lower V_{GS} . Further increase in the negative voltage on the gate will stop the channel. Therefore, we can say that the threshold voltage of the figure above is near the lowest V_{GS} curve. Denoting V_T as the threshold voltage, it can be said that current conducting region are valid for $V_{GS} > V_T$ [1].

There are different types of regions of operation of a MESFET. A short description of each region is given below.

1.3.1 Linear Region ($0 < V_{DS} < V_{DSsat}$)

This region is only valid for low value of V_{DS} . Figure 1.5 shows that, for low value of V_{DS} drain current I_D depends almost linearly on V_{DS} for a particular value of V_{GS} . Here the dependency is linear, so the region is called linear region, which is also known as the triode region. This region is applicable for the value of $V_{DS} < V_{DSsat}$. Where

$$V_{DSsat} = V_{GS} - V_{to} \dots \dots \dots (1)$$

The dotted locus shows the change of V_{DSsat} with respect to the values of V_{GS} [1].

1.3.2 Saturation Region ($V_{DS} > V_{DSsat}$)

In linear region, I_D increases with the increase of V_{DS} . But after a certain value of V_{DS} , with the increase in V_{DS} , the value of I_D does not change significantly. When $V_{DS} = V_{DS sat}$, only then the saturation of I_D current is attainable. One can see that in Figure 1.5, the drain current still tends to increase though the saturation is achieved. The pinch off point shifts toward the source from drain results this phenomenon, which eventually decreases the channel length effectively. The decrease in channel length results in increase of current I_D . Depending upon the material used, saturation may occur in two different ways for a MESFET. They are discussed below:

1.3.2.1 Saturation by pinch-off

Figure 1.5 illustrates the saturation by pinch off. In the MESFET device fabricated by the material like Si (which has reasonable high saturation E-field value), I_D saturates by pinching off the channel between the drain and source.

High saturation electric field value means the drift velocity of carrier saturates at a higher value of E-field along the channel. The case is such that, the mobility may be considered as constant during the process and depletion on drain side increases with the increase in V_{DS} voltage. After reaching a certain value, the drain side depletion pinches off the channel.

So at this stage drain side channel possesses high impedance and does not let carriers to pass through. But with the high electric field some of the carriers are swept off to the drain side and thus saturates the current. Figure 1.5 shows the case of pinch off while applied $V_{DS} > V_{DS sat}$.

1.3.2.2 Saturation by velocity saturation

The drift velocity of the carrier saturates comparably at a lower electric field for the material like GaAs. The electric field is high as a greater value of V_{DS} is applied beyond the saturation. This high electric field saturates the velocity of the carriers through the channel. The device has short channel as it ensures greater strength of the electric field which is expected to happen. Due to the

velocity saturation of the carrier the saturation in drain current I_{DS} occurs in this type of device [1].

An overview of different regions of operation of a MESFET is shown in a table below:

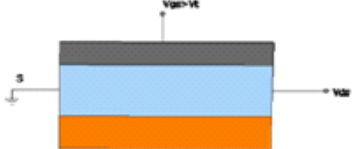
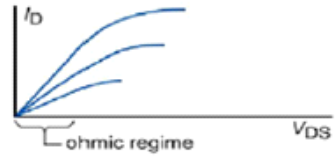
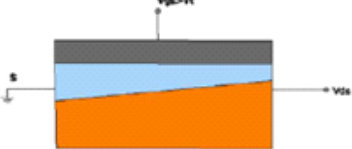
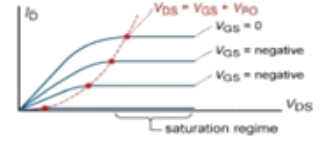
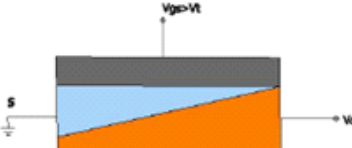
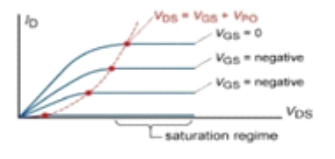
Region	Device Cross section	I-V Curve
Linear		
Saturation (due to velocity saturation)		
Saturation (due to pinch off)		

Figure 1.5: Linear and saturation regions [1]

1.4 C-V Characteristics of MESFET

An accurate capacitance model is highly desirable for reliable simulation of high-speed digital and analogue circuits. The internal gate-source capacitance (C_{GS}) is very important for microwave applications as it has a significant impact on both device input impedance and ultimate frequency performance. For a GaN MESFET, the lateral structure makes it a very low charge device. It can switch hundreds of volts in nanoseconds, giving it multiple megahertz capability. Gate-drain capacitance (C_{GD}) is most important in switching. As it has a lateral structure, C_{GD} comes only from a small corner of the gate. An extremely low C_{GD} leads to the very rapid voltage switching capability of GaN transistors. The junction from the gate to the channel and the capacitance of the dielectric between the gate and the field plate are included in

C_{GS} . Comparing with C_{GD} , C_{GS} is large. C_{DS} is also small, being limited to the capacitance across the dielectric from the field plate to the drain. If capacitance is small, RC time constant will be small as well. As a result of smaller RC time constant, the switching frequency will be very high [2].

1.5 Structure of MESFET

The structure of MESFETS can be of two kinds, self aligned source and drain MESFET and non self aligned source and drain MESFET.

1.5.1 Self-aligned source and drain

This structure (Fig. 1.6) requires the gate to be formed first so that the annealing process is required after the formation of the source and drain areas by ion implantation. The gate contact must be able to withstand the high temperatures. The length of the channel is minimized and gate contact covers the whole length. Such a structure has very limited number of materials where it can be suitable [1].

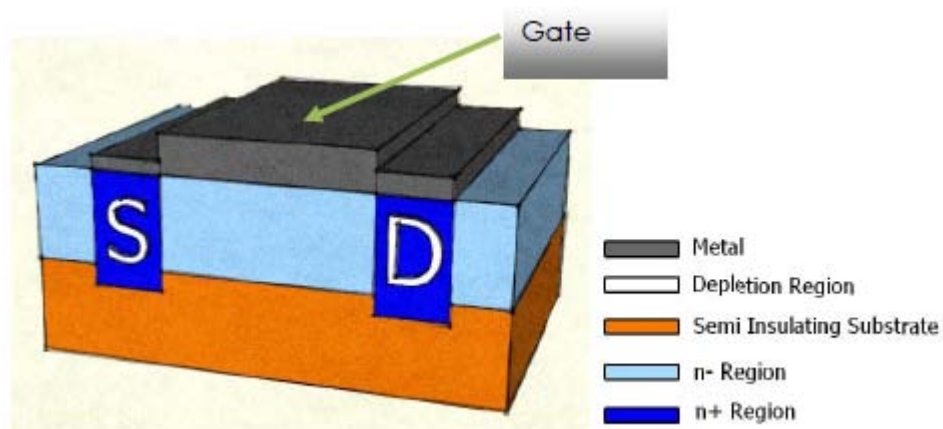


Figure 1.6: Self aligned MESFET [1]

1.5.2 Non self-aligned source and drain

Non-self aligned source and drain structure requires the source and drain contacts to be formed before the gate (Fig. 1.7). The gate is placed on a section of the channel. It does not cover the whole of the length of the channel [1].

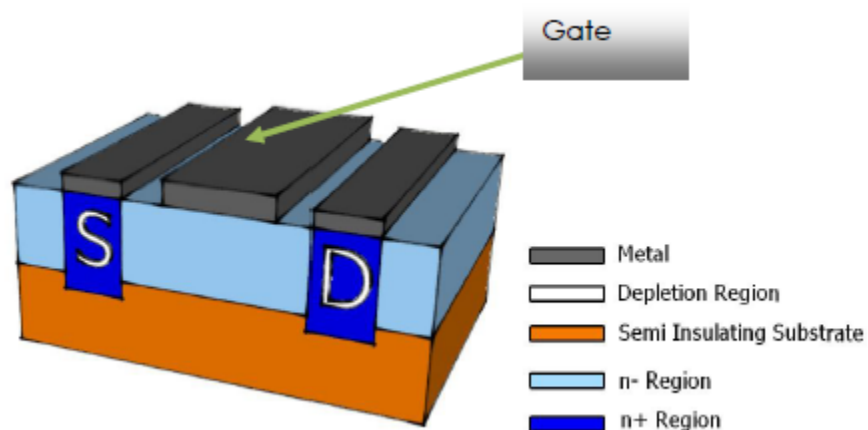


Figure 1.7: Non self aligned MESFET [1]

1.6 Equivalent Circuit of a MESFET

It is possible to predict an equivalent circuit of a MESFET if we know the modes of operation of a MESFET. Figure 1.8 shows us the equivalent circuit superimposed on the cross sectional view of a MESFET [1].

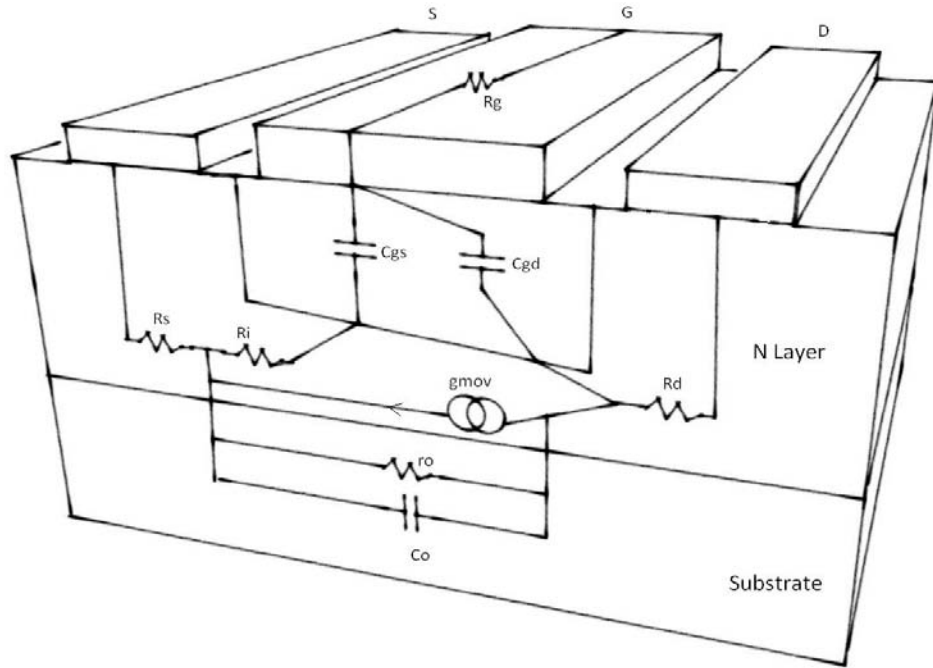


Figure 1.8: Equivalent circuit component superimposed on the cross sectional view of a MESFET [1]

In Fig. 1.8, it is assumed that the MESFET is an n-MESFET.

- C_{gs} : Capacitance represents the charge storage in the depletion region at source gate region
- C_{gd} : Capacitance represents the charge storage in the depletion region at gate drain region
- R_s : Resistance represents the bulk resistance of N-layer in the source gate region together with any contact resistance at the source ohmic metallization
- R_d : Resistance represents the bulk resistance of N-layer in the gate drain region together with any contact resistance at the drain ohmic metallization
- R_g : parasitic resistance at the gate
- R_i : internal source-gate resistance
- g_{mov} : represents the drain current flow along the channel from drain to source

- r_o : substrate resistance
- C_o : substrate capacitance
- v : voltage from gate to source direction

The equivalent circuit for the behaviour analysis of MESFET modeling is shown in Fig. 1.9.

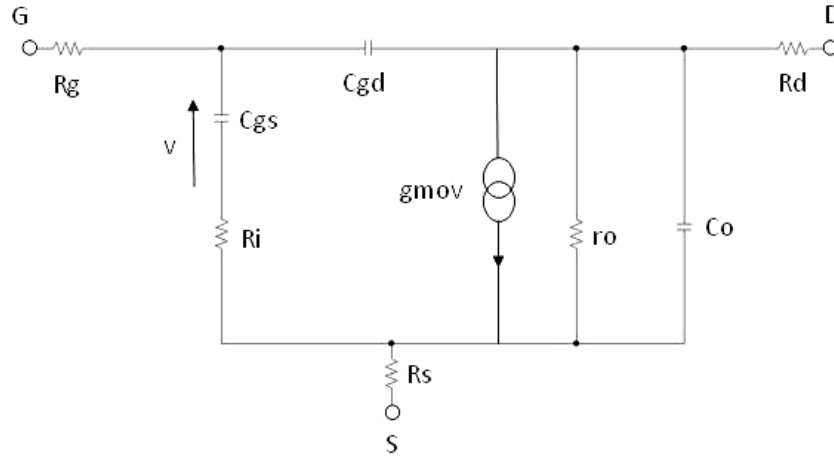


Figure 1.9: Equivalent circuit of MESFET [1]

1.7 Applications of MESFET

- MESFET involves high electron mobility and lower levels of stray capacitance, which makes it useful in RF amplifier applications. MESFET thus makes itself useful in microwave power amplifiers, broadband amplifiers, high frequency low noise RF amplifiers and oscillators.
- Technology utilizing shorter gate lengths make use of MESFETs in high frequency telecommunication and aerospace applications too, such as in wireless communications involving base station cellular application, satellite and radar systems and personal communication systems.
- Nowadays, with Blue-ray disc technology, GaN-based violet laser diodes are used in this application too. GaN has another potential in the application of fabrication of blue laser diodes (LDs) in high density optical storage systems. Further research may originate

application of GaN in energy efficient lighting, communication, printing, projection TV and even in surgeries. In addition, researchers are trying to make use of GaN-based LEDs and develop LED light bulbs. Large scale use of GaN LEDs and LED lighting technology will cause a vast reduction of greenhouse gases, improving environmental conditions along with saving energy.

- MESFET's Schottky diode property allows them to be used in switching applications and mixers.
- High power electronics also makes use of MESFETs, for example in automotive and electric car applications. Nanotubes of GaN are being tried out in nanoscale electronics, optoelectronics and biochemical-sensing applications as well [3].

CHAPTER 2

MOTIVATION

2.1 Factors of Motivation

Some important properties of GaN made it very useful for high power and microwave frequency applications. Some advantages of GaN over other materials are as follows:

- GaN has higher mobility compared to other materials such as SiC and Si which makes it the best material for very high frequencies.
- Almost the entire visible range of wavelengths is spanned in the Group III nitride alloy system. The band gap of nitride based materials ranges from 1.9eV to 6.2eV.
- GaN possesses low dielectric constants and high thermal conductivity pathways.
- GaN has high bond strengths and very high melting temperatures. These high bond strengths improve its reliability compared to other materials.
- The nitrides are resistant to chemical etching and allow GaN based devices to be operated in harsh environments.
- GaN light sources will be compact and highly reliable and could result in enormous cost savings compared to conventional light sources.
- The use of GaN based LEDs may result in reduction of greenhouse gases and minimize the risk of global warming.
- Large application of GaN is in fabricating blue laser diodes for extremely high density optical storage systems [3].

2.2 Comparison Between GaAs, SiC and GaN

Table 2.1 shows the comparison between SiC, GaAs and GaN.

Table 2.1: Comparison between SiC, GaAs and GaN.

Material Property	SiC	GaAs	GaN
Band gap (eV) [4]	3.2	1.43	3.4
Electron Mobility (cm ² /V-sec)[5]	900	8500	2000
Electron Saturation Velocity (10 ⁶ cm/sec)[6]	22	12	25
Thermal Conductivity (Watts/cm ² ·K) [7]	5	0.5	1.3
High/Low Power Device [8]	High	Low	High

2.3 More on GaN and SiC FETs

SiC MESFETs and GaN HEMTs have an enormous potential in high-power amplifiers at microwave frequencies due to their wide bandgap features of high electric breakdown field strength, high electron saturation velocity and high operating temperature. The high power density combined with the comparably high impedance attainable by these devices also offers new possibilities for wideband power microwave systems.

2.3.1 Wide Bandgap SiC and GaN Transistors

The fundamental physical limitations of Si operation at higher temperature and powers are the strongest motivations for switching to wide bandgap semiconductors such as SiC and GaN for

these applications. For phase array radars, wireless communication market and other traditional military applications require demanding performance of microwave transistors. In several applications, as well as in radar and military systems, the development of circuits and sub-systems with broadband capabilities is required. From transmitter point of view the bottleneck, and the critical key factor, is the development of high performance PA.

Next generation cell phones require wider bandwidth and improved efficiency. The development of satellite communications and TV broadcasting requires amplifiers operating both at higher frequencies and higher power to reduce the antenna size of terminal users. The same requirement holds for broadband wireless internet connections as well. This high power and high frequency applications require transistors with high breakdown voltage, high electron velocity and high thermal conductivity.

The wide band gap materials, like GaN and SiC are preferable as we can see from Table 2.2.

Table 2.2: Material parameters of SiC and GaN compared to GaAs and Si [9].

Material	Bandgap [eV]	Critical electric field [MV/cm]	Thermal conductivity [W/cm-K]	Electron mobility [cm ² /Vs]	Saturated electron drift velocity [cm/s]	Relative dielectric constant
4H-SiC	3.26	2	4.5	700	2×10^7	10
GaN	3.49	3.3	1.7	900	1.5×10^7	9
GaAs	1.42	0.4	0.5	8500	1×10^7	12.8
Si	1.1	0.3	1.5	1500	1×10^7	11.8

The high output power density of WBG transistors allows the fabrication of smaller size devices with the same output power. The operation at high voltage due to its high breakdown electric field not only reduces the need for voltage conversion, but also provides the potential to obtain high efficiency. The wide bandgap enables it to operate at elevated temperatures. These

attractive features in power amplifier enabled by the superior properties make these devices promising candidates for microwave power applications.

The critical electric field is the maximum field that the material can sustain before the onset of breakdown and is closely related to bandgap. When the electric field is so high that the carriers can acquire a kinetic energy larger than the band gap, new electron-hole pairs can be created through impact ionization. These newly created carriers are in turn accelerated and, if the electric field is sufficiently high the process is repeated again and again. This causes an increase in the current that will degrade the efficiency and output power and ultimately destroy the device due to the heat generated. Therefore the critical field limits the supply voltage that can be used for the transistor and hence output power.

The maximum current in the device under high electric field is controlled by the saturated electron velocity (by limiting the flux of electrons). A higher V_{sat} will allow higher current and hence higher power. SiC and GaN has higher V_{sat} compared to Si and GaAs according to Table 2.2.

The electron mobility of SiC and GaN is inferior to that of Si and GaAs. This reduces the efficiency of the device by increasing the knee voltage especially in the case of SiC MESFET but this effect is reduced by the high breakdown voltage of SiC, which enables a sufficiently high supply voltage that the knee voltage becomes small in comparison. The relatively low mobility of SiC also reduces the high frequency capability of devices. But the impact of the low mobility of SiC on the high frequency performance is partially offset by the high V_{sat} . Due to higher mobility and the ability to use high electron mobility transistor (HEMT) structures, GaAs and GaN transistors can be used at substantially higher frequencies than Si or SiC transistors.

Heat removal is a critical issue in microwave power transistors especially for class-A power amplifier operation and continuous wave (CW) applications. The thermal conductivity of SiC is substantially higher than that of GaAs and Si. The large bandgap and high temperature stability of SiC and GaN also makes them possible to operate devices at very high temperatures. At temperatures above 300 °C, SiC and GaN have much lower intrinsic carrier concentrations than Si and GaAs. This implies that devices designed for high temperatures and powers should be fabricated from wide bandgap semiconductors, to avoid effects of thermally generated carriers.

The higher impedance (higher supply voltage) and lower relative dielectric constant (reduces parasitic capacitances) for both SiC and GaN compared to Si and GaAs simplifies broadband

impedance matching. Another important property of amplifiers is their linearity. Excellent linearity has been reported for SiC MESFETs both in power amplifiers and low noise amplifiers [9].

2.3.2 SiC MESFET

The hole mobility of SiC is low, so majority carrier devices, such as MESFETs are preferred, which do not rely on holes for their operation. The 4H-SiC has been the material of choice for high frequency SiC MESFETs (Fig. 2.1) because of the higher electron mobility in 4H-SiC. The first SiC MESFETs were fabricated on conducting substrates, which limits the frequency performance by creating large parasitic capacitances in the device. The solution is to process devices on highly resistive or semi-insulating (SI) substrates [9].

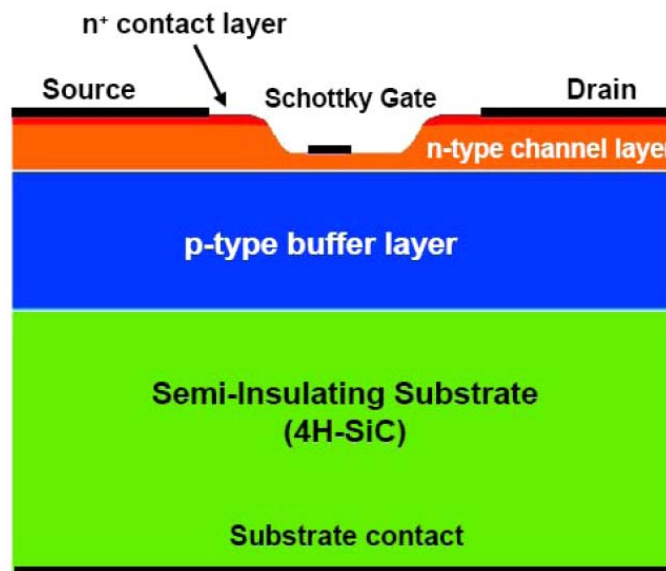


Figure 2.1: Schematic of SiC MESFET structure [9]

CHAPTER 3

LITERATURE REVIEW

3.1 Comparison Between R_{ON} and Breakdown Voltage of Different Materials

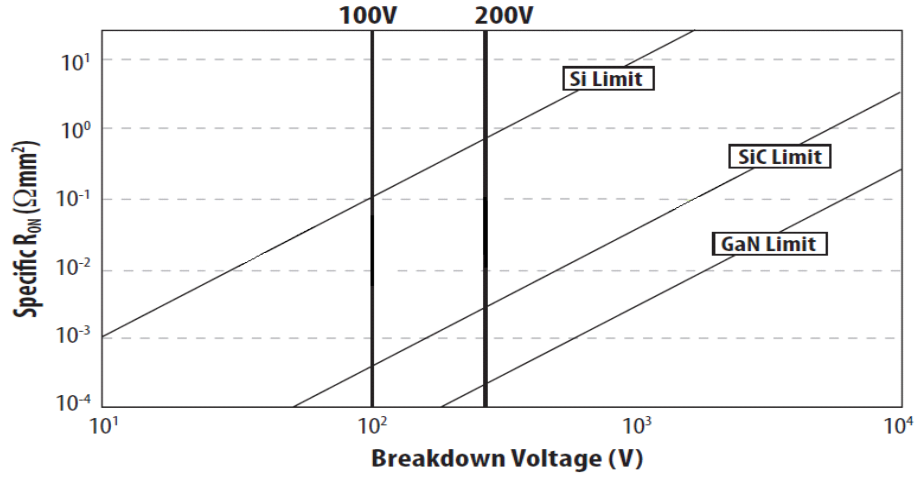


Figure 3.1: R_{ON} vs. Breakdown voltage [2]

R_{ON} is the total resistance that the current experiences while flowing from source to drain. Lower R_{ON} is required for a MESFET to perform efficiently. From Figure 3.1, we can see that GaN has the least R_{ON} for higher breakdown voltage which is desirable for the operation [2].

3.2 Potential performance of SiC and GaN based MESFETs

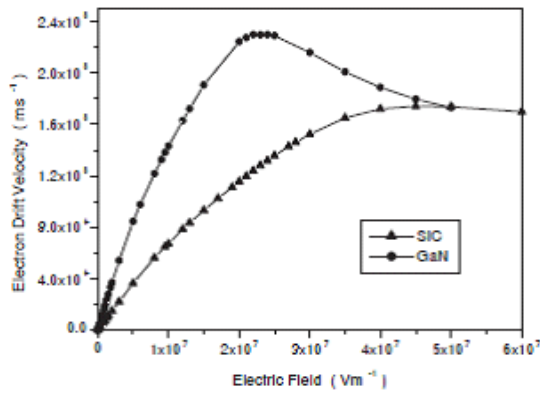


Figure 3.2: Relationship between electron drift velocity and electric field for GaN (circles) and SiC (triangles) [10]

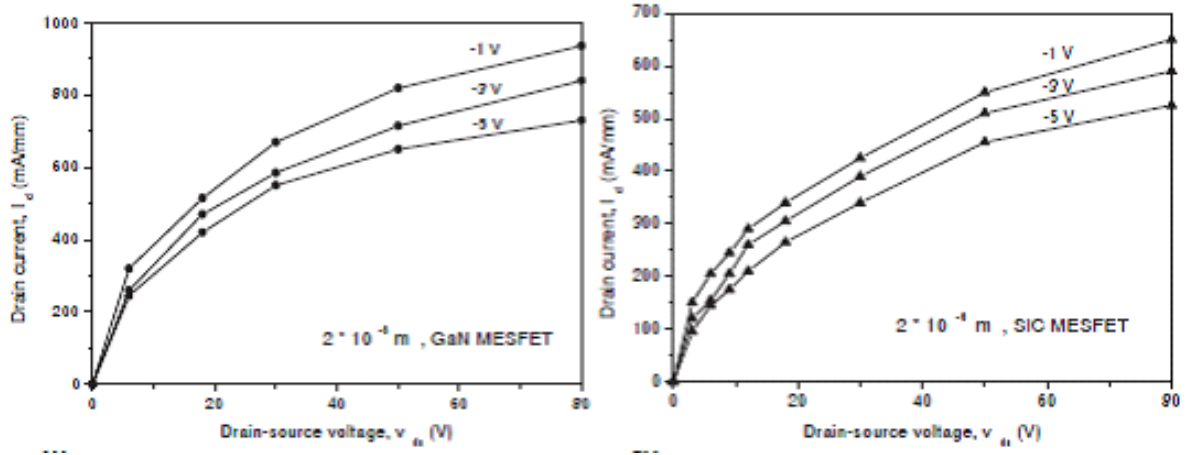


Figure 3.3: Static I-V characteristics for GaN and SiC MESFETs for effective gate voltages of -1 V to -5 V [10]

In the Figure 3.3 the computed $I_{ds}(V_{ds}, V_{gs})$ characteristics are presented for both GaN and SiC MESFET. The acquired characteristics are almost identical in shape. For both structures we can see that the output conductance is relatively high and even at a large negative gate bias the device is not entirely pinched-off. These two effects occur due to the short channel effects and strong electron injection in the buffer layer. We can obtain high drain current for both the structures which confirms us that GaN or SiC MESFETs are good for high power application. Furthermore, GaN has the better electronic transport properties than SiC. Consequently the GaN based MESFET shows 70% higher drain current density as compared with the SiC MESFET.

From Figure 3.3 we can also study the effect of device length on output drain current. Clearly it is seen from the figure that, as the device length is reduced, higher drain current are reached as a result of the increase in longitudinal electric field and velocity overshoot effects [10].

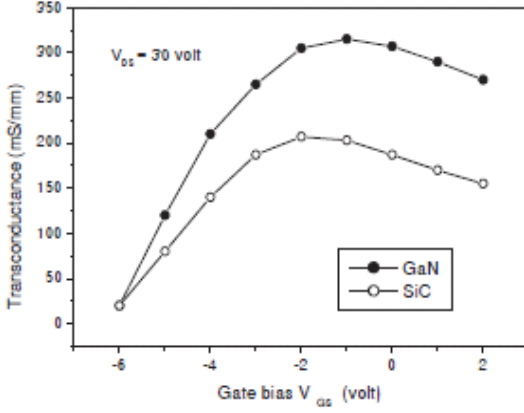


Figure 3.4: Transconductance as a function of gate bias [10]

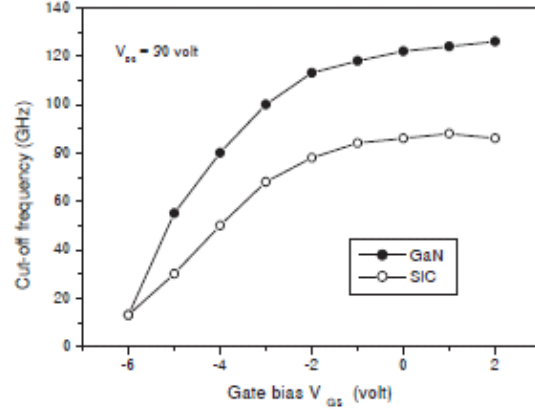


Figure 3.5: Current gain cut-off frequency as a function of gate bias [10]

Figures 3.4 and 3.5 show us transconductance (g_m) and cut-off frequency (f_c) versus gate voltage V_{gs} at a constant V_{ds} for both structures. GaN has better electronic properties and higher drain current densities. Therefore, GaN MESFETs exhibits 70% higher transconductance and cut-off frequency. These results show that GaN MESFETs may perform quite well for high frequency and high power applications [10].

3.3 Pulsed Measurements of GaN MESFETs

The GaN material has outstanding electronic properties. This material was widely investigated for use in high power RF transistors. The wide band gap of this material allows high supply voltages and high temperature applications. But till now all the devices electrical properties were not entirely understood [11].

3.3.1 DC Measurements

Static I-V measurements are shown in Fig. 3.6 for two different lighting conditions. For a V_{gs} of 1V and a V_{ds} of 18V, the transistor exhibits a drain current of about 305 mA/mm with light and 270 mA/mm without light. This difference can be explained by the existence of electrical traps

located in the material or/and at the surface. Further measurements were underway in order to determine their location [11].

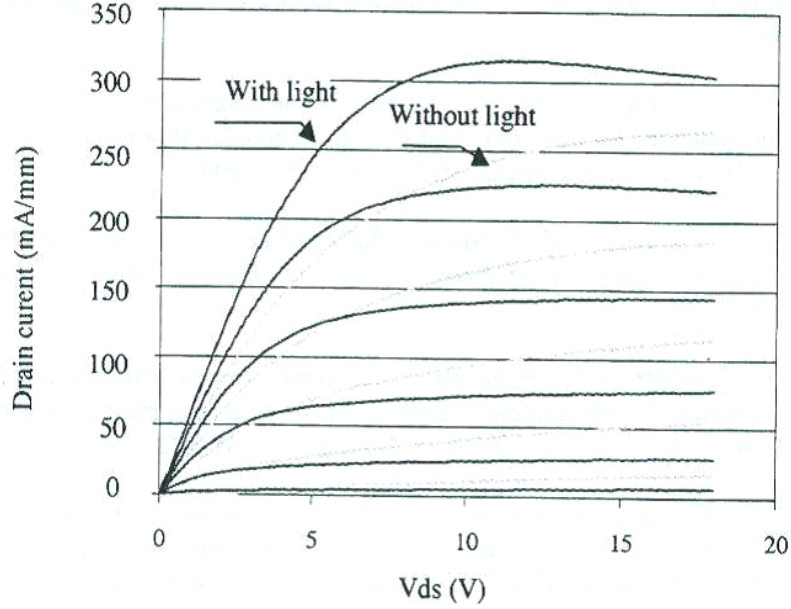


Figure 3.6: DC I-V characteristics of a $2 \times 50 \times 0.3 \mu\text{m}^2$ GaN MESFET with and without light [11]

3.3.2 Static Pulsed Measurements

Pulsed measurements were also performed on the same device. Figure 3.7 shows the pulsed I-V characteristics with and without lighting for a dormant bias voltage of $V_{ds} = 18 \text{ V}$ and $V_{gs} = -9 \text{ V}$. From the figure we can see that the maximum amount of drain current obtained without the presence of light is less than half of the current obtained under static conditions. As a result, this loss confirms us about the presence of electrical traps.

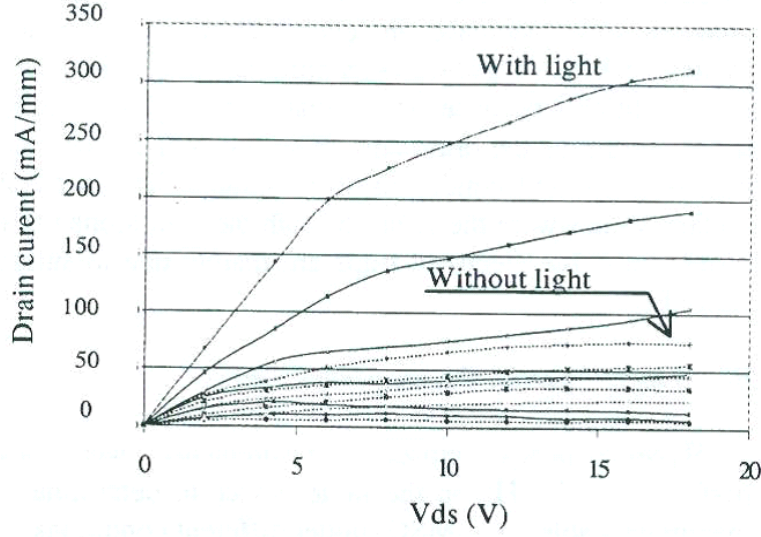


Figure 3.7: Pulsed I-V characteristics of a $2 \times 50 \times 0.3 \mu\text{m}^2$ GaN MESFET with and without light [11]

3.4 Investigation of Cross Sectional Potential Distribution in GaN-Based FETs by Kelvin Probe Force Microscopy

Kelvin probe force microscopy is a powerful measurement technique that can be used to determine the two dimensional electrical potential distribution. It has been used to investigate the potential of GaN-based FET at an operating state. The investigation has been carried out on a cleaved surface of an AlGaIn/GaN HFET without and with SiN_x passivation layer by using KFM under several device operation conditions and influences of the passivation effect on the electric field distribution has been discussed [12].

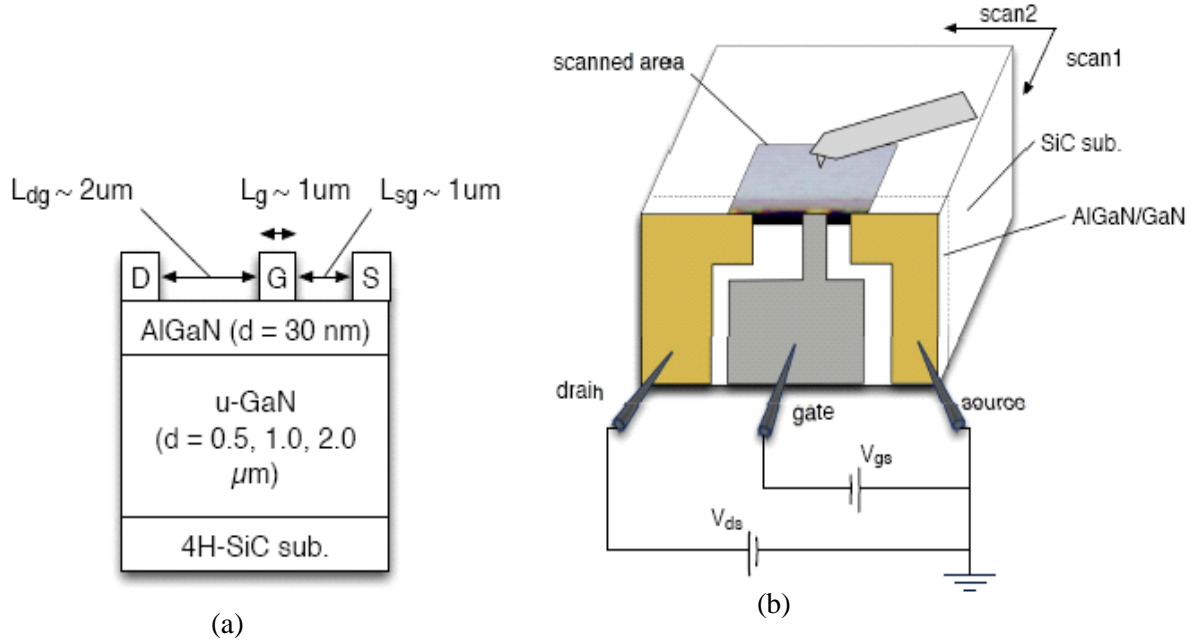


Figure 3.8: Schematic cross section of (a) fabricated FET structure and (b) diagram of the KFM measurement system [12]

Figure 3.8 (a) and (b) show a fabricated FET device structure and schematic diagram of the KFM measurement system used for the investigation. It is seen that source and drain ohmic contacts consisting of Ti/Al/Ti/Au layered structure and a gate Schottky contact consisting of a Ni/Au were formed on the sample surface. The gate length L_g , was about $1 \mu\text{m}$. The source-gate distance, L_{sg} , and the gate-drain distance, L_{dg} , were about $1 \mu\text{m}$ and $2 \mu\text{m}$, respectively. FET structures with and without passivation by Si_xN_y was prepared in order to investigate any advantage of surface passivation [12].

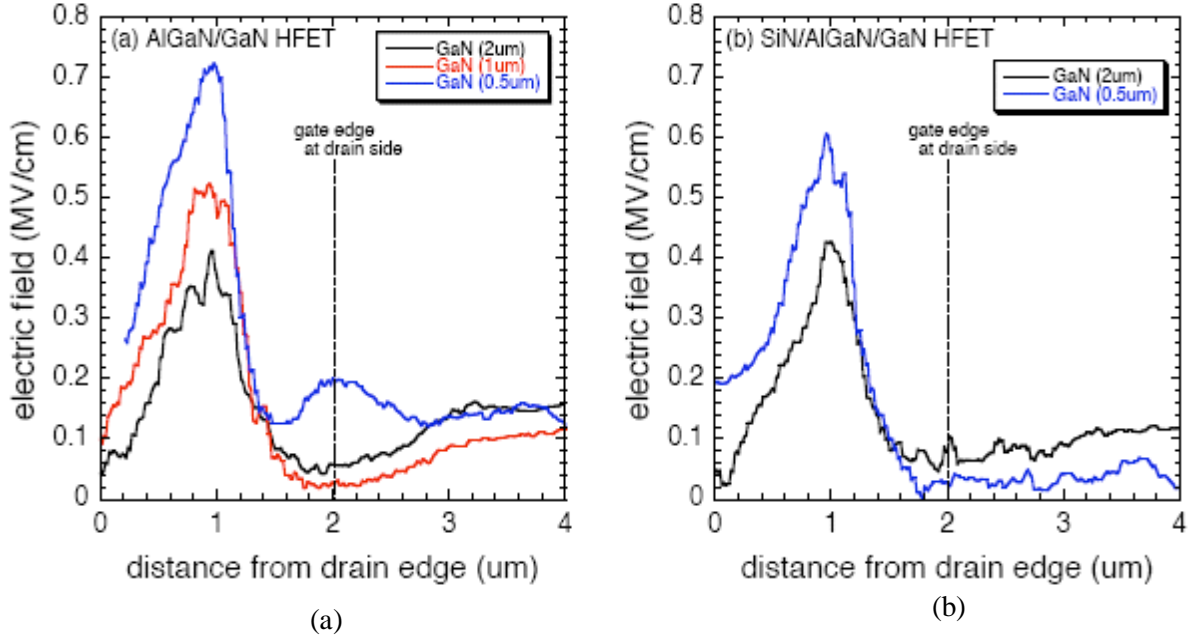


Figure 3.9: Electric field distribution between the drain and source edges near the surface of AlGaIn/GaN HFET (a) without and (b) with SiN_x passivation layer. Electric field is concentrated at the midpoint of the drain and gate electrodes [12]

Figure 3.9 shows a comparison of a profile plot of the electric field distribution between the drain and source electrodes near the surface of AlGaIn/GaN HFETs (a) without and (b) with the SiN_x passivation layer. In both cases, the maximum intensity of the electric field at the surface is seen to be increasing with decreasing GaN buffer thickness. Also, the maximum electric fields in passivated AlGaIn/GaN HFETs are the same or slightly lower than in the non-passivated AlGaIn/GaN HFETs. However, the electric field distribution near the surface of the passivated AlGaIn/GaN HFETs is weak compared to the non-passivated AlGaIn/GaN HFETs [12].

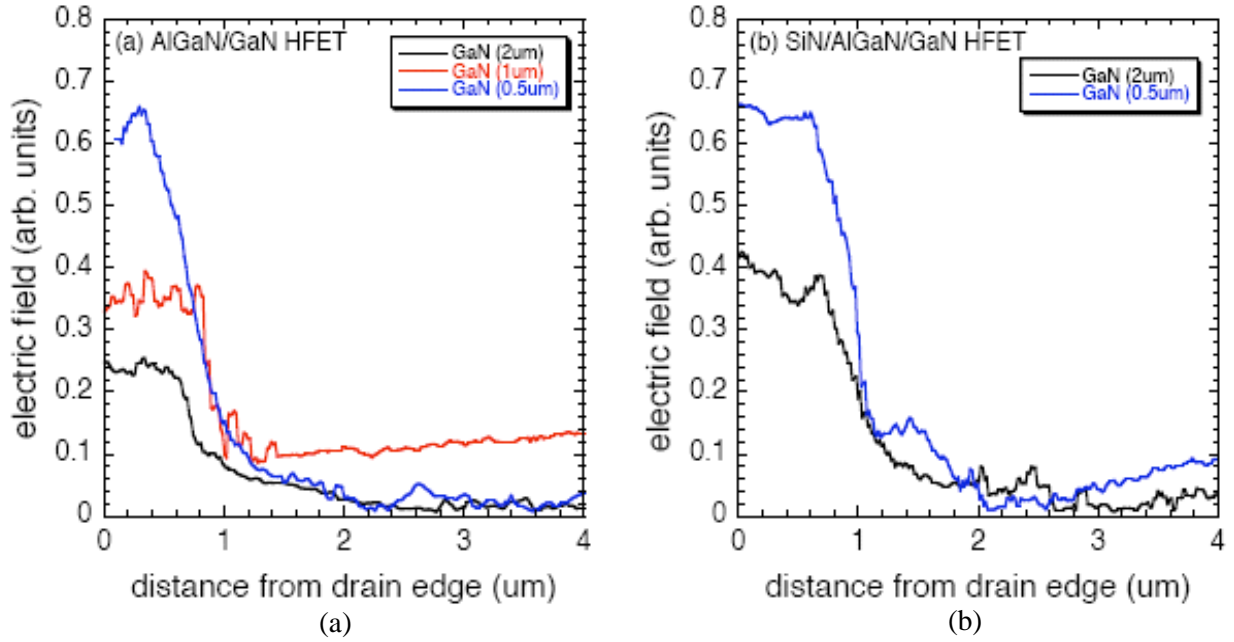


Figure 3.10: Electric field distribution between the drain and source edges at the mid-depth of GaN buffer of AlGaIn/GaN HFET (a) without and (b) with SiN_x passivation layer [12]

Figure 3.10 shows a comparison of the electric field distribution at the mid-depth of the GaN buffer layer from the drain edge to the source edge of AlGaIn/GaN HFETs (a) without and (b) with the SiN_x passivation layer. As seen in the case of the electric field near the AlGaIn/GaN surface, the electric field distribution shows a tendency to increase with decreasing GaN buffer layer. In the case of a thick GaN buffer layer ($\text{GaN} = 2\mu\text{m}$), the SiN_x -passivated AlGaIn/GaN HFET showed a slightly stronger electric field concentration.

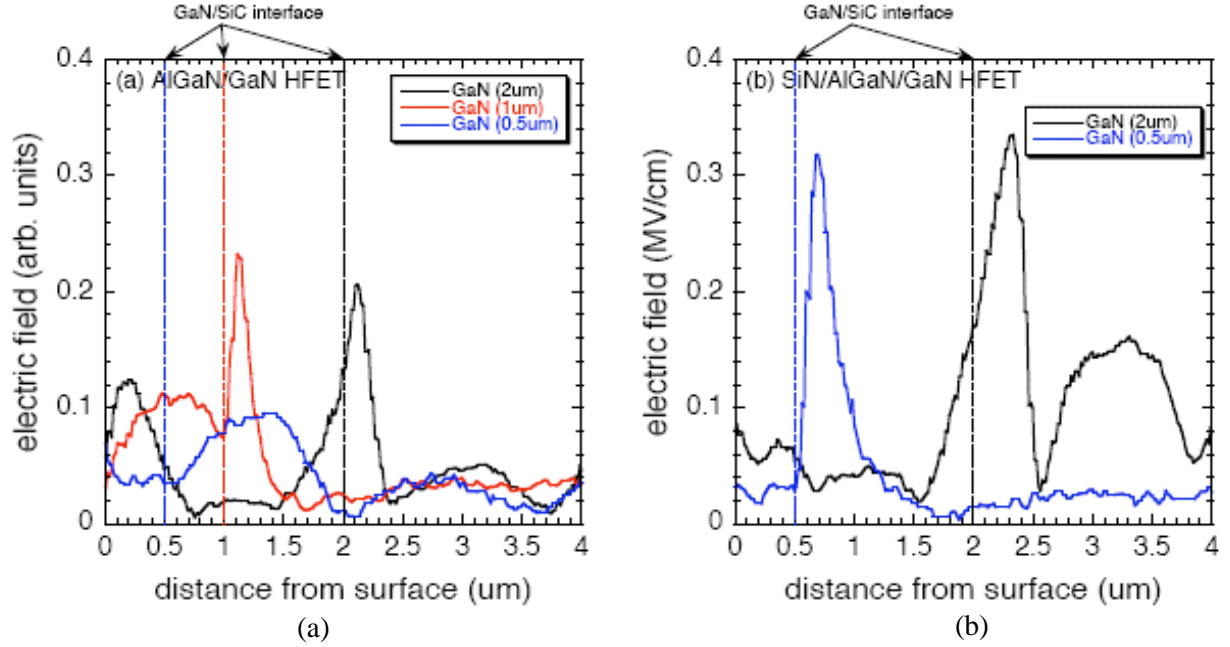


Figure 3.11: Electric field distribution under the gate electrode of AlGaIn/GaN HFET (a) without (b) with SiN_x passivation layer. Electric field is concentrated near the GaN/SiC interface except for the case of which GaN layer is 0.5 μm without SiN_x passivation. [12]

Figure 3.11 compares the profile plot of electric field distribution under the gate electrode of AlGaIn/GaN HFETs (a) without and (b) with the SiN_x passivation layer. In each sample, it is observed that the electric field is concentrated on the SiC side near the interface between the GaN buffer and the SiC substrate. It is also seen that the maximum intensity of the electric field is almost the same without being dependent on the GaN buffer thickness and slightly higher than that in the AlGaIn/GaN HFETs without the SiN_x passivation [12].

3.5 Double-Ion-Implanted GaN MESFETs with Extremely Low Source/Drain Resistance

Devices without ion implanted source/drain structure are conventionally used. Research with the aim to reduce the on-state resistance of MESFET so that the saturation drain current I_{DS} and transconductance (g_m) can be enhanced, led to the finding of double-ion-implantation of GaN MESFETs.

GaN FETs are known to be a wide bandgap semiconductor material with a high breakdown electric field, high saturation drift velocity and better thermal conductivity in comparison with the more commonly used GaAs and SiC MESFETs. To increase the efficiency of such devices, some properties may be adjusted in order to obtain, much better results, one of such properties being the on-state resistance of the device. A reduction in the on-state resistance will result in increased saturation drain current and increased maximum transconductance. This can be achieved by producing high concentration layers below the source and drain contacts.

One of the processes for fabricating high concentration regions is known as ion implantation for impurity doping. The resulting structure of GaN MESFET is shown in Fig. 3.12, due to ion implantation of both the channel and drain/source [13].

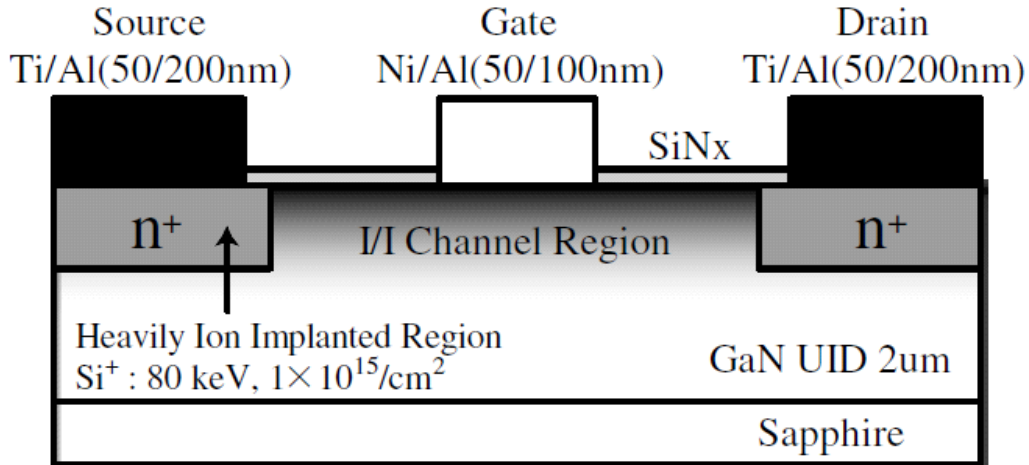


Figure 3.12: GaN MESFET structure with ion implanted channel and source/drain regions (Double Ion Implanted GaN MESFET) [13]

With disadvantages involved in this process, to minimize the damage caused by ion implantation, the process is carried out in very high temperatures. For instance, the activation and crystal damage recovery of an implanted GaN will require annealing at temperatures above 1500 °C.

Experiments were carried out to study the changes of the on-state resistance by utilizing the circular transmission line (C-TLM) to analyze the outcome of ion implanted source/drain regions, or double-ion-implantation.

The following are the graphical results obtained from research and experiment. The results for double-ion-implanted (DII) MESFETs have been compared with that of ion-implanted-channel (IIC) MESFETs, where the drain/source regions are not as heavily doped [13].

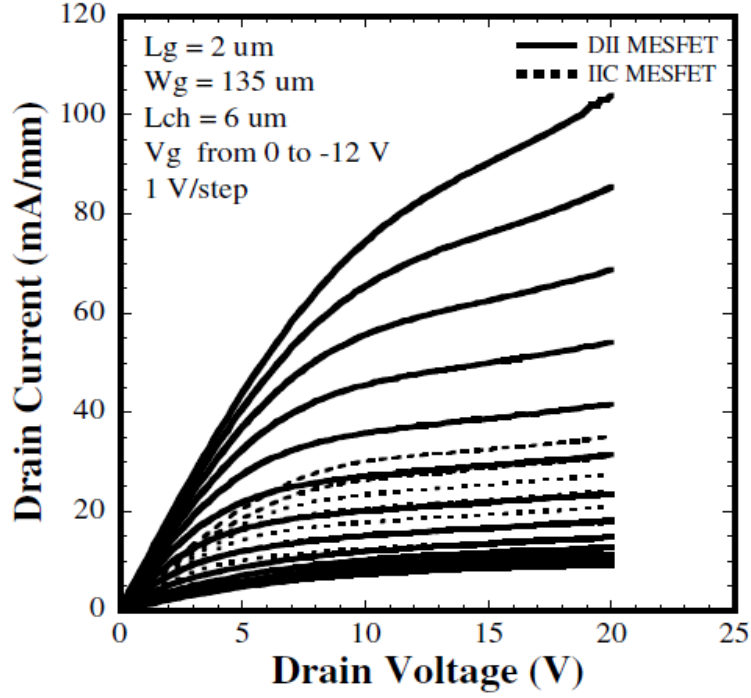


Figure 3.13: I_{ds} - V_{ds} characteristics of DII MESFET and CII MESFET [13]

Figure 3.13 illustrates how drain current, I_d for DII MESFET is much greater than that obtained with IIC MESFET for a specific value of drain voltage, V_{ds} . An increase in drain voltage increases the drain current. The inverse of the slope of the I_d - V_{ds} characteristic curve in its linear region is defined as the source/drain resistance of the device. As seen from the figure, for a particular range of drain voltage and its corresponding drain current, the slope of the curve is greater for DII MESFET as compared to IIC MESFET, implying the drain/source resistance is much smaller for DII MESFETs.

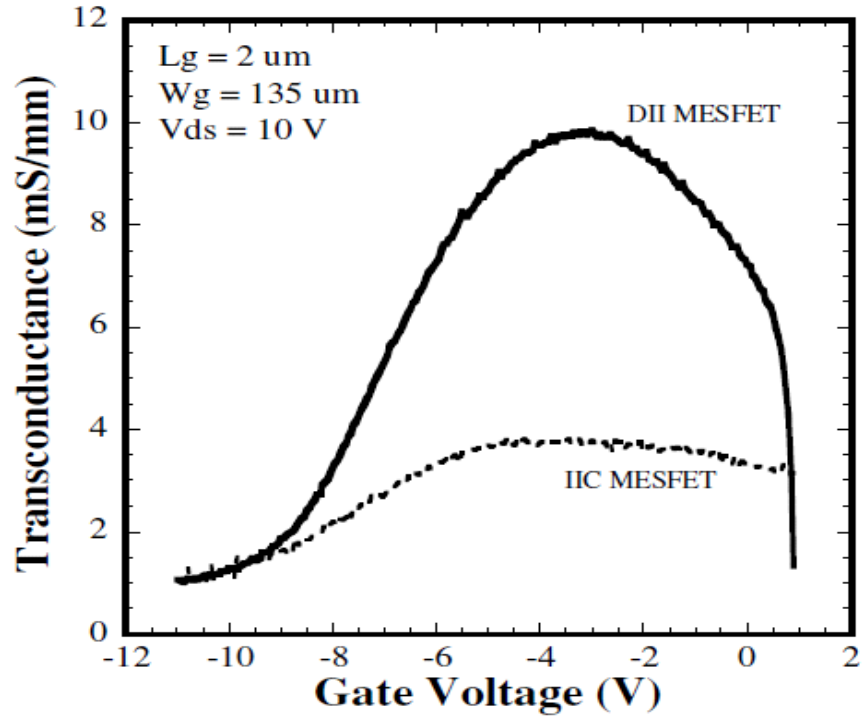


Figure 3.14: Transconductance of DII MESFET and IIC MESFET [13]

Figure 3.14 show that transconductance (g_m) is much greater for a DII MESFET than that for an IIC MESFET, with a variation in the gate voltage of the MESFETs.

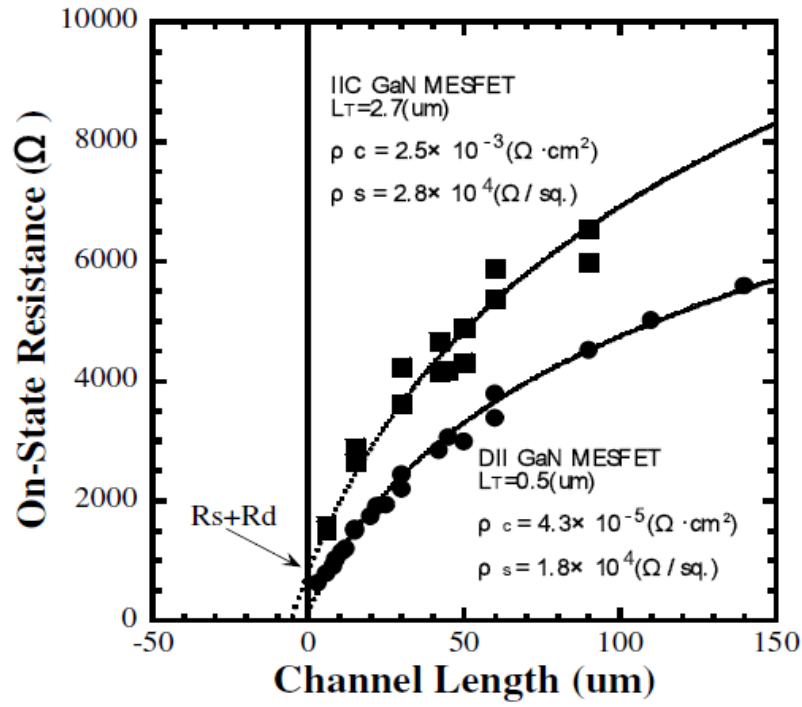


Figure 3.15: On-state resistance of ion implanted GaN MESFET [13]

The illustration above (Fig. 3.15) involves the variation of the on-state resistance as a function of channel length. The on-state resistances in a MESFET involved are illustrated in Fig. 3.16.

Where,

R_{ch} = channel sheet resistance

R_s = parasitic source resistance

R_d = parasitic drain resistance

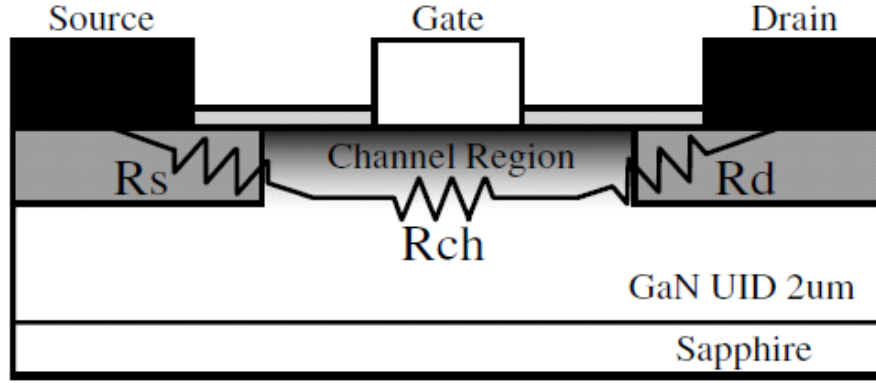


Figure 3.16: On-state resistance components of ion implanted GaN MESFET [13]

R_{ch} was found to be of same value for both DII and IIC MESFETs, but with lower values of R_s and R_d . This shows that highly doped ion-implanted source/drain regions minimizes the resistance between the metal and source/drain regions, sheet resistance of highly-doped-regions, and the sheet resistance of implanted-channel-regions between the gate and heavily doped regions.

Figures 3.17 and 3.18 represent curves showing the variation of I_{dss} and g_{mMAX} with changes in the gate length of the device. One way of increasing the values for I_{dss} and g_{mMAX} is reducing gate lengths to submicron order. For further improvements in these two parameters, a reduction in the on-state resistance is essential, especially when such devices are used for scaling purposes [13].

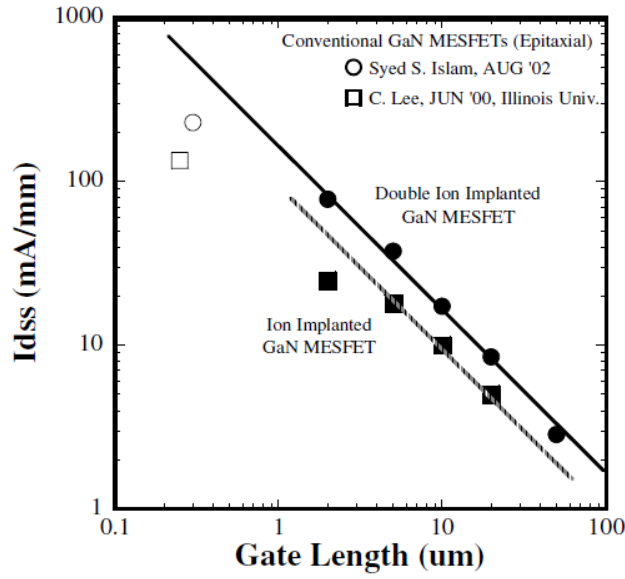


Figure 3.17: I_{dss} as a function of gate length of DII and IIC MESFETs. [13]

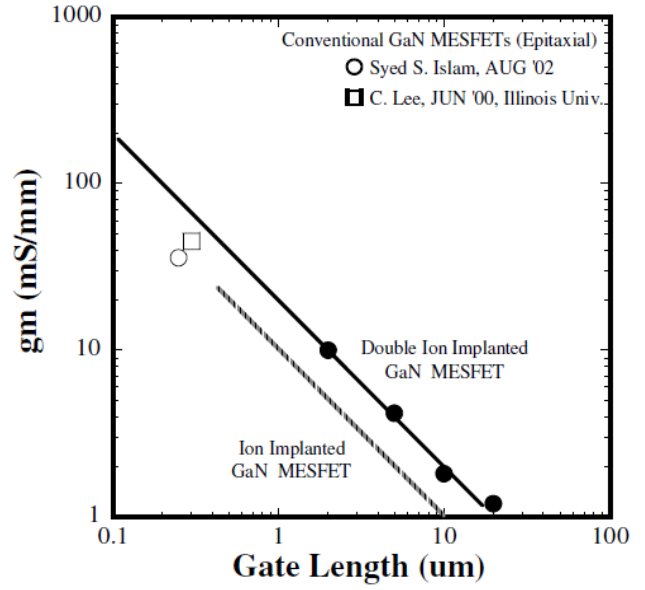


Figure 3.18: Transconductance as a function of gate length of DII and IIC MESFETs.

As a result of the mentioned adjustments made on a MESFET, the following conclusions have been drawn:

Increase in $I_{dss} = 200\%$

Increase in $g_m = 200\%$

Decrease in source/drain resistance = 94%

These were the figures obtained:

Saturation drain current increases from 36 mA/mm to 78 mA/mm

Maximum transconductance increases from 3.8 mS/mm to 10 mS/mm

On-state resistance reduces from 210 ohm-mm to 105 ohm-mm [13]

CHAPTER 4

PARAMETERS OF GaN MESFET

4.1 Study of One-Dimensional Channel Potential Variation

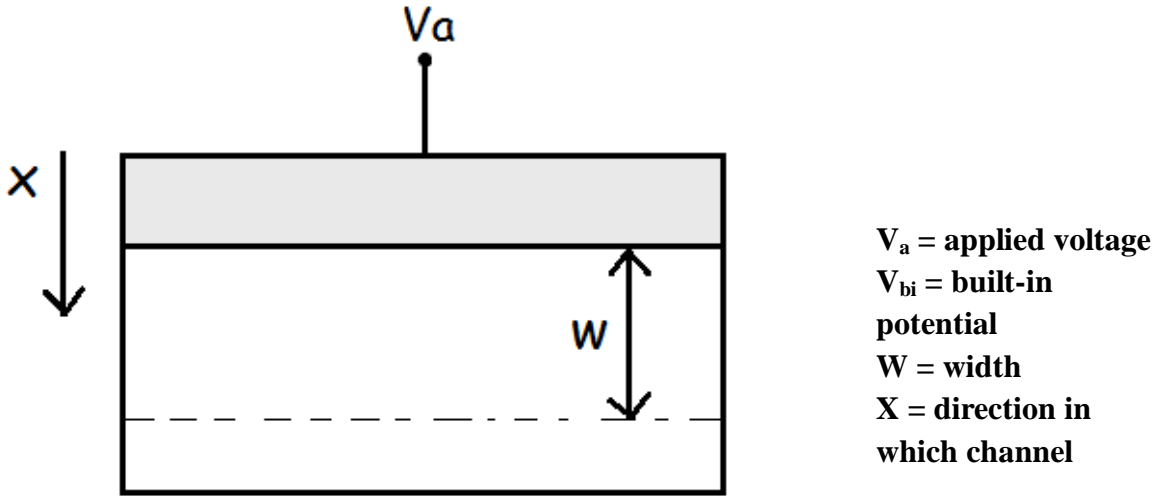


Figure 4.1: Parameters used for studying the variation of channel potential

Let's consider the Poisson's Equation in the x-direction:

$$\frac{d^2 \phi(x)}{dx^2} = -\frac{\rho_s}{\epsilon} \quad (4.1)$$

Integrating equation 4.1, we get

$$\int \frac{d^2 \phi(x)}{dx^2} dx = -\int \frac{\rho_s}{\epsilon} dx$$

$$\frac{d\phi(x)}{dx} = -\frac{\rho_s}{\epsilon} x + c_1$$

$$\frac{d\phi(x)}{dx} = -\frac{qN_D}{\epsilon} x + c_1 \quad (4.2)$$

At $x = w$, equation 4.2 equals zero. Thus,

$$\frac{d\phi(x)}{dx} = 0$$

Hence, we can write,

$$\left. \frac{d\phi(x)}{dx} \right|_{x=w} = 0$$

$$-\frac{qN_D}{\varepsilon} w + c_1 = 0$$

$$c_1 = \frac{qN_D}{\varepsilon} w$$

(4.3)

Substituting equation 4.3 in equation 4.2, we obtain,

$$\frac{d\phi(x)}{dx} = -\frac{qN_D}{\varepsilon} x + \frac{qN_D}{\varepsilon} w$$

$$\phi(x) = -\frac{qN_D}{2\varepsilon} x^2 + \frac{qN_D w}{\varepsilon} x + c_2$$

Now at $x=0$, $c_2 = V_a - V_{bi}$

$$\phi(x) \Big|_{x=0} = c_2 = V_a - V_{bi}$$

$$\phi(x) = -\frac{qN_D}{2\varepsilon} x^2 + \frac{qN_D w}{\varepsilon} x + (V_a - V_{bi})$$

(4.4)

Since the first derivative is zero when $x = w$, a maximum value exists. After double differentiation, the second derivative obtained is negative. Hence the extreme point is a maxima.

Now, letting $x = w$ in equation 4.4,

$$\phi(w) = -\frac{qN_D}{2\varepsilon} w^2 + \frac{qN_D w^2}{\varepsilon} + (V_a - V_{bi})$$

$$\phi(w) = -\frac{qN_D}{2\varepsilon} w^2 - (V_{bi} - V_a)$$

(4.5)

Next, using $\phi(w) = 0$ in equation 4.5, we can find an expression for w as following,

$$w = \sqrt{\frac{2\varepsilon(V_{bi} - V_a)}{qN_D}}$$

$$w^2 = \frac{2\varepsilon(V_{bi} - V_a)}{qN_D}$$

$$\begin{aligned}\varphi(w) &= \frac{qN_D}{2\varepsilon} \cdot \frac{2\varepsilon}{qN_D} (V_{bi} - V_a) - (V_{bi} - V_a) \\ &= (V_{bi} - V_a) - (V_{bi} - V_a) \\ &= 0\end{aligned}$$

where,

ϕ_m = metal work function

x = electron affinity of semiconductor

N_d = doping concentration

V_{bi} = built-in potential

$\epsilon = 8.9 \epsilon_o$ (for GaN)

The MATLAB code used for this variation is added on page A.1.

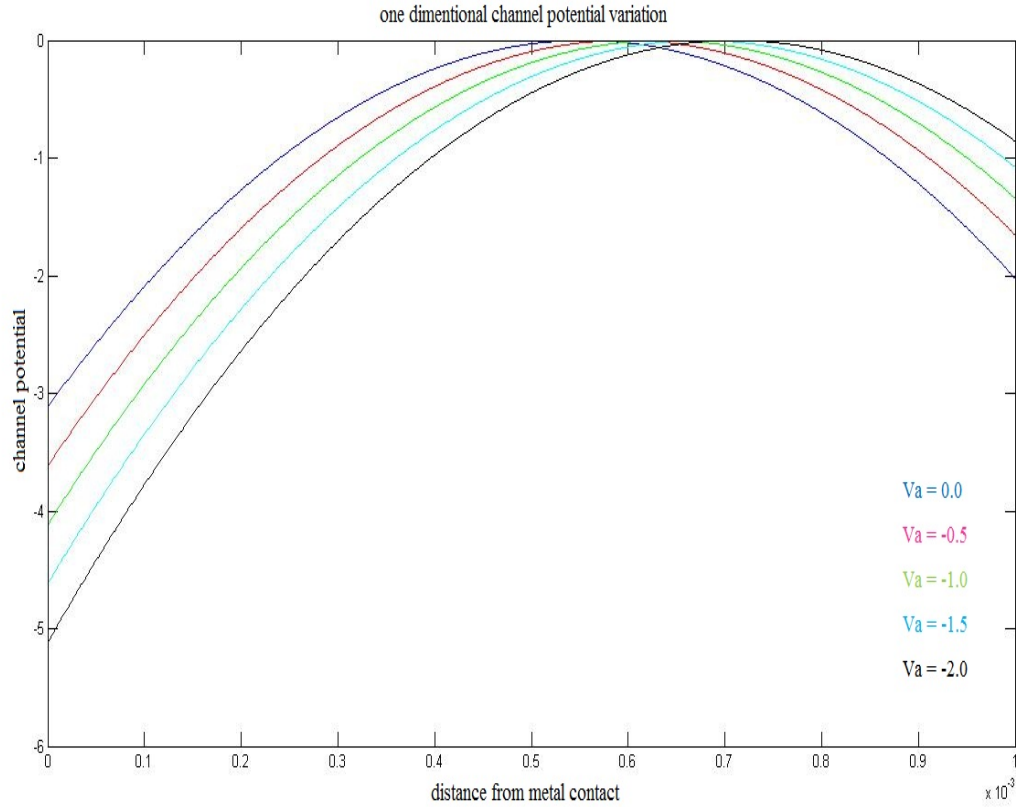


Figure 4.2: Variation of 1D channel potential for different V_a (volts) [15]

Figure 4.2 shows the resulting graph. The graph shows that as the distance is increased in the x-direction, away from the metal contacts, for different values of applied potential, V_a , the channel potential shows a certain kind of variation. At a fixed distance, increasing the applied potential causes the channel potential to increase. Keeping the value of V_a constant, if we move away from the metal contacts, the channel potential appears to increase with the increasing distance up to a certain point where we get a maximum value for the potential. Increasing the distance further after that point causes the potential to decrease. The graph also shows that for fixed values of applied potential, the maximum values of channel potential differ.

Hence, we can tell from the graphical interpretation that there must be a certain location within the channel for carriers between the metal contacts and the substrate, where a maximum value for the potential exists, such that the location appears to be at the midpoint of the channel [15].

4.2 Two Dimensional Channel Potential Distribution of GaN MESFET

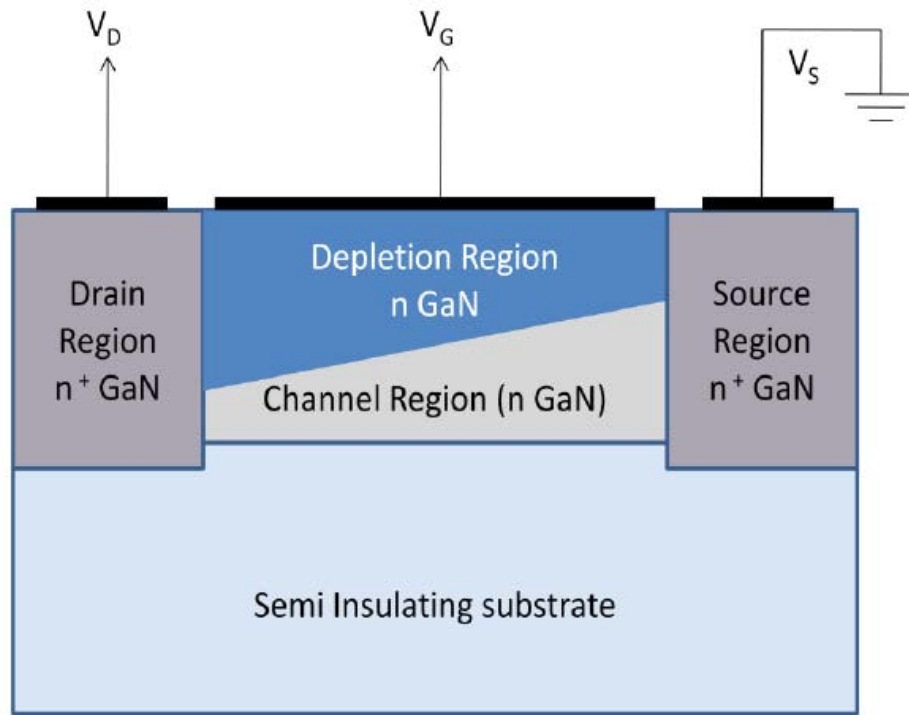


Figure 4.3: Typical MESFET Structure under Gate and Drain Bias [15]

In our study of the 2 dimensional potential distribution of a GaN MESFET, we will use the typical structure of the MESFET, as shown in Fig. 4.3, operating under the gate voltage V_g and the drain voltage V_d , where the source voltage, V_s along with the substrate is grounded. The substrate is semi-insulating GaN. The source and drain regions are highly doped with n^+ GaN, while the channel is moderately doped n GaN. Tungsten is used at the gate terminal to form the Schottky contact, and the drain and source terminals form the ohmic contacts.

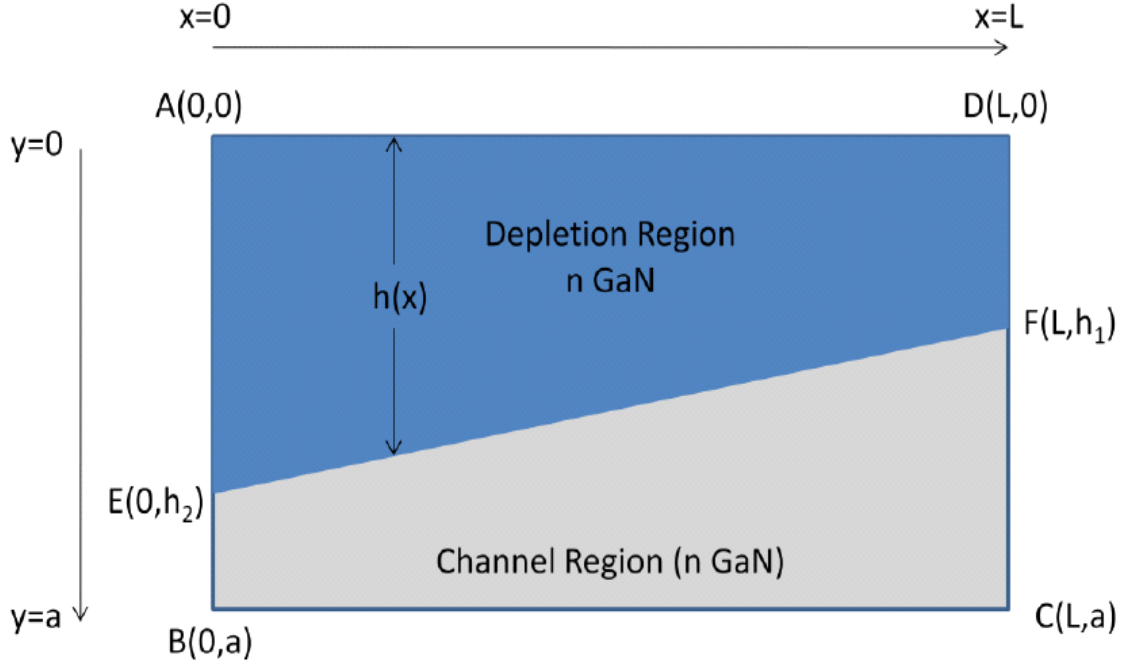


Figure 4.4: Separated Channel Region [15]

Figure 4.4 illustrates only the channel region labelled with different coordinates for which the potential distribution is observed. Point A is considered as the origin (0, 0) of Cartesian coordinate system. Values of x increase from left to right, while values of y increase from top to bottom. ' L ' signifies the length of the channel and ' a ' denotes the depth of the channel. Since we are studying the 2D potential distribution, the channel width that is perpendicular to the x - y plane is assumed to be constant.

A built-in potential exists at the Schottky contact due to the applied voltage V_G at the gate terminal. This causes the potential under the metal contact to be $V_G - V_{bi}$, where V_{bi} is the built-in potential of the Schottky contact. As a result of V_G being negative, a depletion region under the gate terminal is formed. The depth of this depletion region created can be altered by varying value of x due to the drain to source voltage, V_{DS} applied [15].

Let's assume the depletion width, h as a function of x , $h(x)$. For simplicity, assume the change of values of $h(x)$ with respect to x is linear. Thus, using the equation of the straight line, we can write,

$$\begin{aligned}
h(x) - h_2 &= \frac{h_1 - h_2}{L - 0}(x - 0); \\
\Rightarrow h(x) &= -\frac{\Delta h}{L}x + h_2; \\
\text{where,} \\
h_1 &= \sqrt{\frac{2\epsilon(V_{bi} - V_{GS})}{eN_D}};
\end{aligned}$$

where, at $x = L$, $h(x)$ has the lowest value.

$$h_2 = \sqrt{\frac{2\epsilon(V_{bi} - V_{GS} + V_{DS})}{eN_D}};$$

which is the depth of the depletion region at the drain terminal, at $x=0$, considered as the highest value of $h(x)$.

Now,

$$\begin{aligned}
\Delta h &= h_1 - h_2; \\
\epsilon &= \text{Permittivity of GaN} \\
e &= \text{charge of electron,} \\
V_{GS} &= \text{Gate to Source voltage,} \\
V_{DS} &= \text{Drain to Source voltage and} \\
N_D &= \text{Channel doping concentration.}
\end{aligned}$$

As the drain region is highly doped, conductivity is very high as there is negligible potential drop around this region, we can say that this region is of equal potential. Considering how small the built-in potential of the ohmic contact the drain terminal is, it can be assumed that the potential at the drain is V_D . For the same reason, the potential at the source terminal is V_S . Hence, the vertical electric field along the EF line can be said to be zero, and the rate of change of potential with respect to y is zero.

Assuming the two dimensional potential function is $\Phi(x, y)$. The potential distribution in the MESFET is given by the Poisson's equation as:

$$\begin{aligned}
\nabla^2 \varphi(x, y) &= -\frac{\rho}{\epsilon}; \\
\Rightarrow \frac{\partial^2 \varphi(x, y)}{\partial x^2} + \frac{\partial^2 \varphi(x, y)}{\partial y^2} &= -\frac{eN_D}{\epsilon} \tag{4.6} \\
\text{where, } \rho &= eN_D = \text{surface charge density.}
\end{aligned}$$

The boundary conditions of the space charge region are set as follows:

1. At AD line ($y=0$ line), Potential $\varphi(x, 0) = V_1 = V_{GS} - V_{bi}$;
2. At DC line ($x=L$ line), Potential $\varphi(L, y) = V_2 = V_S$;
3. At AB line ($x=0$ line), Potential $\varphi(0, y) = V_3 = V_D = V_2 + V_{DS}$;
4. At EF line, $\left[\frac{\partial \varphi(x, y)}{\partial y} \right]_{y=h(x)} = 0$;

Let the solution of the differential solution be,

$$\varphi(x, y) = A(x)y^2 + b(x)y + C(x) \quad (4.7)$$

Now, applying boundary condition, at $y=0$, $\varphi(x, y) = V_1$, we get

$$\varphi(x, 0) = C(x) = V_1 \quad (4.8)$$

Differentiating equation (4.7) with respect to y , we get

$$\frac{\partial \varphi(x, y)}{\partial y} = 2yA(x) + B(x) \quad (4.9)$$

Now, at $y = h(x)$, $\frac{\partial \varphi(x, y)}{\partial y} = 0$.

Now, at $y = h(x)$, $\frac{\partial \varphi(x, y)}{\partial y} = 0$

So, from equation (4.7)

$$2A(x)h(x) + B(x) = 0$$

$$\Rightarrow B(x) = -2A(x)h(x) \quad (4.10)$$

The potential equation becomes,

$$\varphi(x, y) = A(x)y^2 - 2A(x)h(x)y + V_1 \quad (4.11)$$

Differentiating the equation two times with respect to y , we get

$$\Rightarrow \frac{\partial \varphi(x, y)}{\partial y} = 2yA(x) - 2A(x)h(x)$$

$$\Rightarrow \frac{\partial^2 \varphi(x, y)}{\partial y^2} = 2A(x) \quad (4.12)$$

Once again, differentiating equation (4.11) twice with respect to x will give

$$\begin{aligned}
\varphi(x, y) &= A(x)y^2 - 2A(x)h(x)y + V_1 \\
\Rightarrow \frac{\partial \varphi(x, y)}{\partial x} &= y^2 \frac{\partial A(x)}{\partial x} - 2y \left\{ A(x) \frac{\partial h(x)}{\partial x} + h(x) \frac{\partial A(x)}{\partial x} \right\} \\
\Rightarrow \frac{\partial^2 \varphi(x, y)}{\partial x^2} &= y^2 \frac{\partial^2 A(x)}{\partial x^2} - 2y \left\{ A(x) \frac{\partial^2 h(x)}{\partial x^2} + \frac{\partial h(x)}{\partial x} \frac{\partial A(x)}{\partial x} + h(x) \frac{\partial^2 A(x)}{\partial x^2} + \frac{\partial A(x)}{\partial x} \frac{\partial h(x)}{\partial x} \right\} \\
\Rightarrow \frac{\partial^2 \varphi(x, y)}{\partial x^2} &= y^2 \frac{\partial^2 A(x)}{\partial x^2} - 2y \left\{ A(x) \frac{\partial^2 h(x)}{\partial x^2} + 2 \frac{\partial h(x)}{\partial x} \frac{\partial A(x)}{\partial x} + h(x) \frac{\partial^2 A(x)}{\partial x^2} \right\}
\end{aligned} \tag{4.13}$$

Now,

$$\begin{aligned}
h(x) &= -\frac{\Delta h}{L}x + h_2 \\
\frac{\partial h(x)}{\partial x} &= -\frac{\Delta h}{L} \\
\frac{\partial^2 h(x)}{\partial x^2} &= 0
\end{aligned}$$

Putting the values of $h(x)$, $\frac{\partial h(x)}{\partial x}$ and $\frac{\partial^2 h(x)}{\partial x^2}$ in equation 4.13, we get

$$\begin{aligned}
\frac{\partial^2 \varphi(x, y)}{\partial x^2} &= \{y^2 - 2yh(x)\} \frac{\partial^2 A(x)}{\partial x^2} - 4y \frac{\partial h(x)}{\partial x} \frac{\partial A(x)}{\partial x} \\
\Rightarrow \frac{\partial^2 \varphi(x, y)}{\partial x^2} &= \{y^2 - 2y(-\frac{\Delta h}{L}x + h_2)\} \frac{\partial^2 A(x)}{\partial x^2} - 4y(-\frac{\Delta h}{L}) \frac{\partial A(x)}{\partial x} \\
\Rightarrow \frac{\partial^2 \varphi(x, y)}{\partial x^2} &= (y^2 - 2yh_2) \frac{\partial^2 A(x)}{\partial x^2} + 2y \frac{\Delta h}{L} \frac{\partial^2 A(x)}{\partial x^2} + 4y \frac{\Delta h}{L} \frac{\partial A(x)}{\partial x}
\end{aligned} \tag{4.14}$$

Now, putting the values of $\frac{\partial^2 \varphi(x, y)}{\partial x^2}$ and $\frac{\partial^2 \varphi(x, y)}{\partial y^2}$ from equations (4.12) and (4.14)

respectively in equation 4.6 we get,

$$\begin{aligned}
\Rightarrow (y^2 - 2yh_2) \frac{\partial^2 A(x)}{\partial x^2} + 2y \frac{\Delta h}{L} \frac{\partial^2 A(x)}{\partial x^2} + 4y \frac{\Delta h}{L} \frac{\partial A(x)}{\partial x} + 2A(x) &= -\frac{eN_d}{\epsilon} \\
\Rightarrow \frac{\partial^2 A(x)}{\partial x^2} + \frac{2y \frac{\Delta h}{L}}{y^2 - 2yh_2} \frac{\partial^2 A(x)}{\partial x^2} + \frac{4y \frac{\Delta h}{L}}{y^2 - 2yh_2} \frac{\partial A(x)}{\partial x} + 2A(x) &= -\frac{eN_d}{\epsilon(y^2 - 2yh_2)}
\end{aligned} \tag{4.15}$$

Let,

$$a = \frac{2y \frac{\Delta h}{L}}{y^2 - 2yh_2}, \quad b = \frac{2}{y^2 - 2yh_2} \quad \text{and} \quad c = -\frac{eN_d}{\epsilon(y^2 - 2yh_2)}$$

Substituting values of a, b and c as shown above in equation (4.15) gives,

$$(1 + ax) \frac{d^2 A(x)}{dx^2} + 2a \frac{dA(x)}{dx} + b = c \tag{4.16}$$

The equation obtained now is an ordinary differential equation with respect to x

So, $\frac{\partial}{\partial x}$ can be written as $\frac{d}{dx}$

If we solve equation (4.16) using Wolfram Mathematica, we get the following solution:

$$A(x) = \frac{d_1 \sqrt{-\frac{b(\frac{1}{a} + x)}{a}} I_1 \left(\sqrt{-\frac{b(\frac{1}{a} + x)}{a}} \right)}{ax + 1} - \frac{d_2 \sqrt{-\frac{b(\frac{1}{a} + x)}{a}} K_1 \left(\sqrt{-\frac{b(\frac{1}{a} + x)}{a}} \right)}{ax + 1} + \frac{c}{b} \quad (4.17)$$

where $I_1(z)$ is the ‘first order modified Bessel function of first kind’ and $K_1(z)$ is the ‘first order modified Bessel function of second kind’.

d_1 and d_2 are arbitrary constants.

Let,

$$P_1(x) = \frac{\sqrt{-\frac{b(\frac{1}{a} + x)}{a}} I_1 \left(\sqrt{-\frac{b(\frac{1}{a} + x)}{a}} \right)}{ax + 1};$$

$$P_2(x) = \frac{\sqrt{-\frac{b(\frac{1}{a} + x)}{a}} K_1 \left(\sqrt{-\frac{b(\frac{1}{a} + x)}{a}} \right)}{ax + 1};$$

$$P_3 = \frac{c}{b};$$

So,

$$A(x) = d_1 P_1(x) - d_2 P_2(x) + P_3 \quad (4.18)$$

Now, putting $A(x) = d_1 P_1(x) - d_2 P_2(x) + P_3$ in equation (4.11), we get

$$\begin{aligned} \varphi(x, y) &= y^2 \{d_1 P_1(x) - d_2 P_2(x) + P_3\} - 2yh(x) \{d_1 P_1(x) - d_2 P_2(x) + P_3\} + V_1 \\ \Rightarrow \varphi(x, y) &= \{y^2 - 2yh(x)\} P_1(x) d_1 - \{y^2 - 2yh(x)\} P_2(x) d_2 + V_1 + \{y^2 - 2yh(x)\} P_3 \end{aligned} \quad (4.19)$$

Let,

$$M(x, y) = y^2 - 2yh(x);$$

So,

$$\varphi(x, y) = M(x, y)P_1(x)d_1 - M(x, y)P_2(x)d_2 + V_1 + M(x, y)P_3 \quad (4.20)$$

Now, let the boundary conditions be:

$$\text{at } x = L, \varphi(L, y) = V_2;$$

$$\text{at, } x = 0 \varphi(0, y) = V_3 = V_2 + V_{ds};$$

Putting these conditions in equation (4.20), we get,

$$M(0, y)P_1(0)d_1 - M(0, y)P_2(0)d_2 = V_3 - V_1 - M(0, y)P_3 \quad (4.21)$$

$$M(L, y)P_1(L)d_1 - M(L, y)P_2(L)d_2 = V_2 - V_1 - M(L, y)P_3 \quad (4.22)$$

Let,

$$Q_1 = M(0, y)P_1(0)$$

$$Q_2 = M(0, y)P_2(0)$$

$$Q_3 = V_3 - V_1 - M(0, y)P_3$$

$$Q_4 = M(L, y)P_1(L)$$

$$Q_5 = M(L, y)P_2(L)$$

$$Q_6 = V_2 - V_1 - M(L, y)P_3$$

After substitutions, equations (4.21) and (4.22) become:

$$Q_1d_1 - Q_2d_2 = Q_3 \quad (4.23)$$

$$Q_4d_1 - Q_5d_2 = Q_6 \quad (4.24)$$

Solving the equations (4.21) and (4.22) for d_1 and d_2 , we get,

$$d_1 = \frac{\begin{vmatrix} Q_3 & -Q_2 \\ Q_6 & -Q_5 \end{vmatrix}}{\begin{vmatrix} Q_1 & -Q_2 \\ Q_4 & -Q_5 \end{vmatrix}} = \frac{Q_2Q_6 - Q_3Q_5}{Q_2Q_4 - Q_1Q_5};$$

$$d_2 = \frac{\begin{vmatrix} Q_1 & Q_3 \\ Q_4 & Q_6 \end{vmatrix}}{\begin{vmatrix} Q_1 & -Q_2 \\ Q_4 & -Q_5 \end{vmatrix}} = \frac{Q_1Q_6 - Q_3Q_4}{Q_2Q_4 - Q_1Q_5};$$

Putting the values of d_1 and d_2 in equation (4.17), we get $A(x)$. Substituting this value of $A(x)$ in equation (4.11), we finally get the potential function $\Phi(x, y)$ [15].

Detailed code for the simulation of this variation is on A.3.

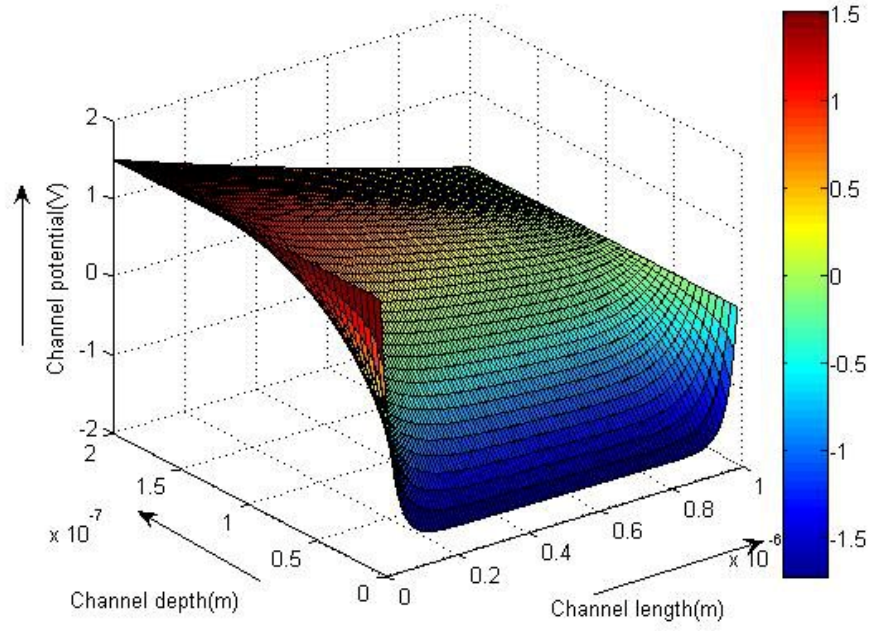


Figure 4.5: 3D view of 2D channel potential [15]

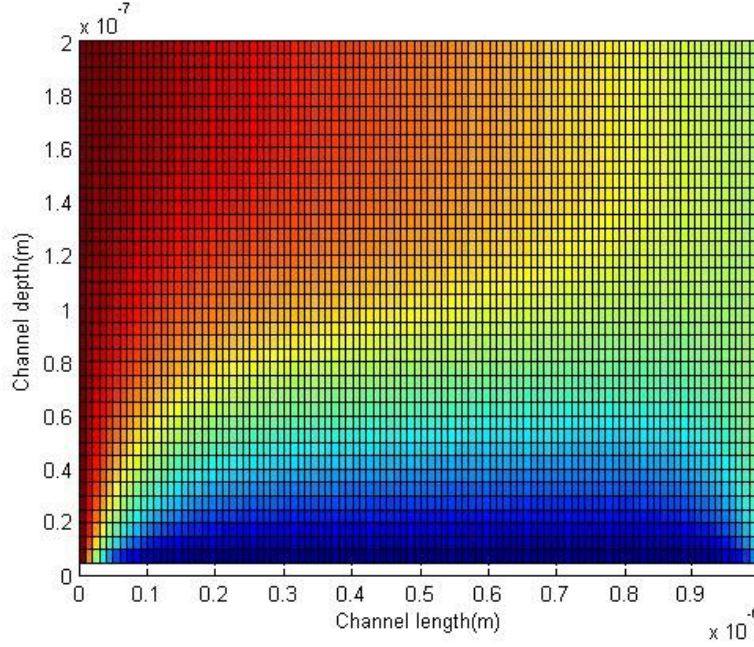


Figure 4.6: 2D view of 2D channel potential [15]

4.3 Variation of Drain-Source Current with Drain-Source Voltage Keeping Gate-Source Voltage Constant

The equation below represents the drain-source current as in the linear region, including the parasitic source and the drain resistances.

$$I_{ds} = \frac{qZ\mu N_d a}{L} \left(V_{ds} - I_{ds}(R_s + R_d) - \frac{2}{3V_p^{1/2}} \left[(V_{bi} - V_{gs} + V_{ds} - I_{ds}R_d)^{3/2} - (V_{bi} - V_{gs} + V_{ds} + I_{ds}R_s)^{3/2} \right] \right) \quad (4.25)$$

In this equation,

I_{ds} = drain-source current

μ = electron mobility

A = active channel thickness

L = gate length

Z = gate width

V_{ds} = applied drain-source voltage

R_s = parasitic source

R_d = drain resistances

V_p = pinch-off voltage

This equation is solved using iteration in order to get the value of current. Velocity saturation is attained as the electric field in the conducting channel increases.

Length of the channel, L_s is given as:

$$L_s = L - \frac{2a}{\pi} \sin^{-1} \left(\frac{\pi K_d (V_{ds} - V_{1s})}{2aE_s} \right)$$

The length, L_s in the gate-length spacing is given as

$$L'_s = \frac{(1 - K_d) V_{2s}}{E_s \cosh \left(\frac{\pi L_s}{2a} \right)}$$

where,

K_d = ratio of the voltage drop in the high field region to that in the conducting channel.

$V_{(2)s}$ = voltage drop in the channel.

Drain current in the saturation region is given as

$$I_{dsat} = \frac{1 + 2\beta R_s (V_{gs} - V_t) - (1 + 4\beta R_s (V_{gs} - V_t))^{1/2}}{2\beta R_s^2}$$

where,

$$\beta = \frac{2\epsilon_s v_{sat} Z}{a(V_p + 3E_s L_s)}$$

V_t is the threshold voltage, where

$$V_t = V_{bi} - V_p$$

In the region where $V_{ds} > V_{sat}$, the saturation value of V_{ds} , the drain-source current I'_{dsat} becomes

$$I'_{dsat} = I_{dsat} \left(1 + \frac{L_s + L'_s}{L} \right)$$

MATLAB code used for this simulation in order to obtain the graph on Figure 4.7 is added in on page A.7.

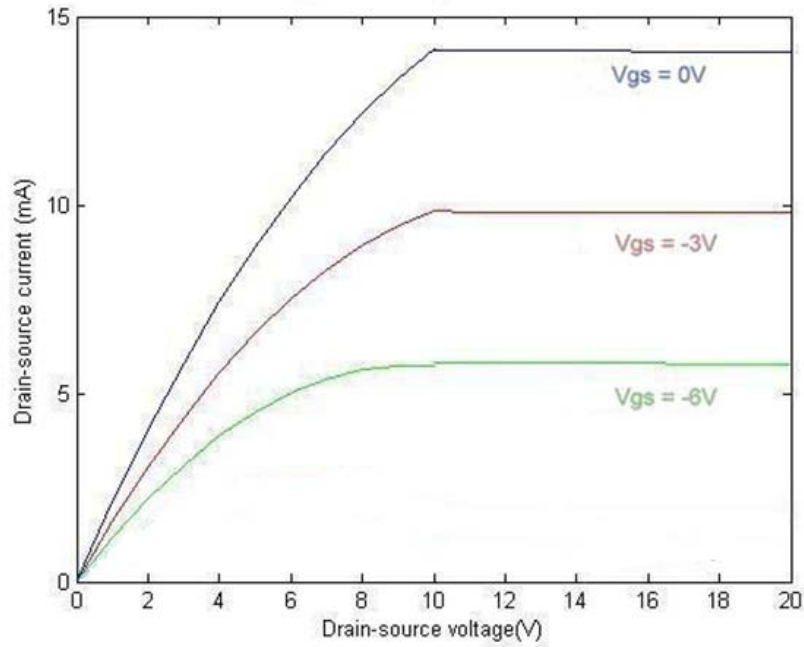


Figure 4.7: I_{ds} - V_{ds} characteristics of GaN MESFET [14]

4.4 Transconductance

The transconductance is one of the most important indicators of device quality for microwave application. It is affected by channel material properties and device dimensions. It is the slope of the I_{DS} - V_{GS} characteristics with V_{DS} constant.

$$g'_m = \frac{g_m}{1 + g_m R_s} \quad (4.26)$$

where,

$$g_m = \left. \frac{\partial I_{ds}}{\partial V_{gs}} \right|_{V_{ds}=const.}$$

and, g'_m = effective transconductance.

MATLab code as on page A.13 has been used in order to obtain the graphs shown in Fig. 4.8.

Figure 4.8 shows the variation of transconductance with gate-source voltage for different drain-source voltage. With the increase in negative gate bias, the transconductance decreases as the depletion layer width increases and channel layer width decreases. As a result drain current decreases.

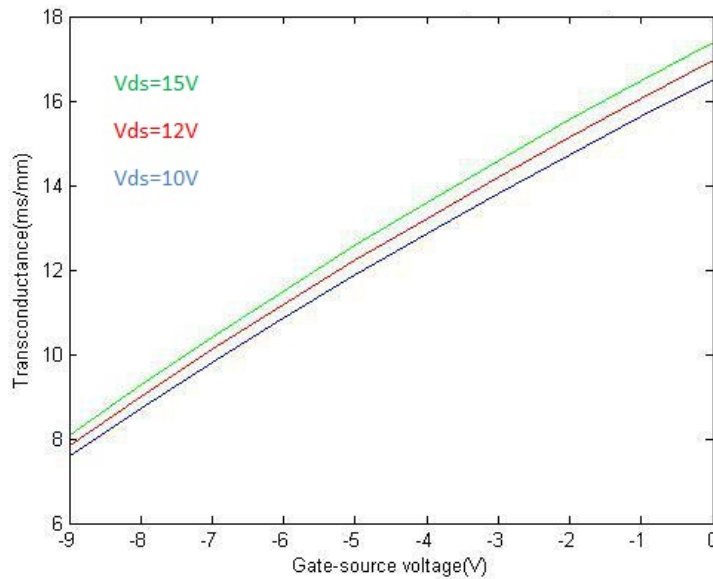


Figure 4.8: Variation of Transconductance with Gate-Source Voltage for different Drain-Source Voltage

It can be seen from equation (4.26) that effective transconductance (g'_m) is inversely proportional to the source resistance (R_s). If we decrease R_s , transconductance will increase. In the following figures the value of R_s has been decreased from 75Ω to 5Ω . As a result we can see that the value of g'_m increases.

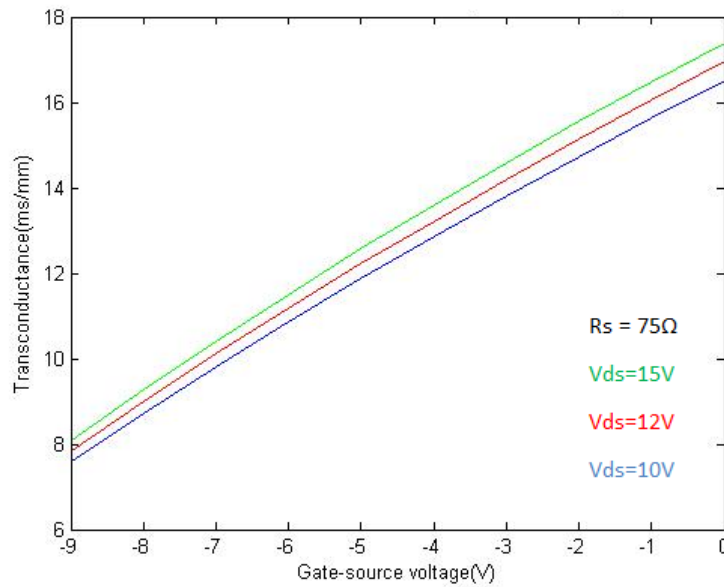


Figure 4.9: Variation of Transconductance with Gate-Source Voltage for $R_s = 75\Omega$

In Figure 4.9 we can see that for $R_s = 75\Omega$ the value of transconductance for $V_{ds} = 15V$ is approximately 17ms/mm.

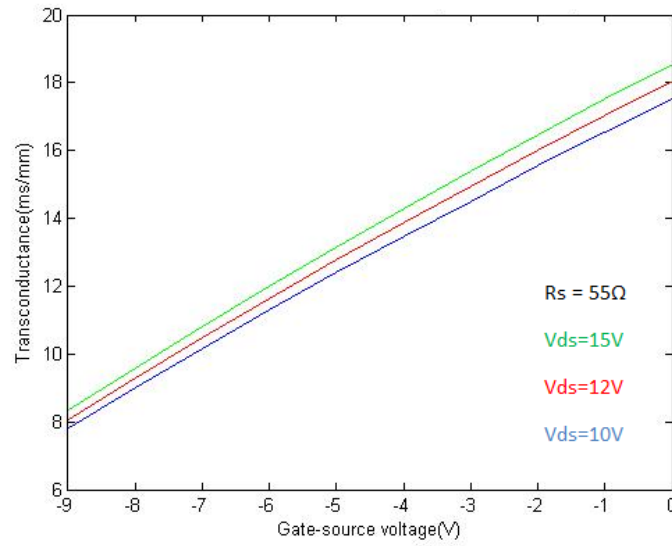


Figure 4.10: Variation of Transconductance with Gate-Source Voltage for $R_s = 55\Omega$

The value of transconductance is supposed to increase as R_s decreases from 75Ω to 55Ω . From figure 4.10 we can see that transconductance has increased from approximately 17ms/mm to 18.5ms/mm for $V_{ds} = 15V$.

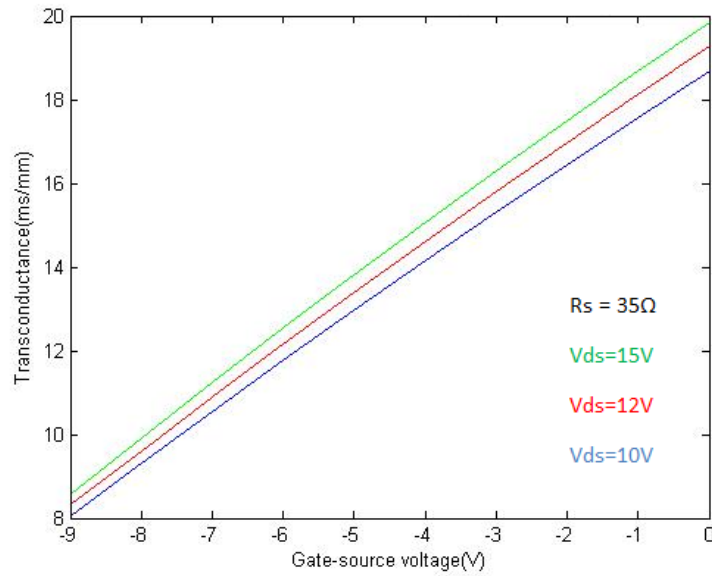


Figure 4.11: Variation of Transconductance with Gate-Source Voltage for $R_s = 35\Omega$

The value of transconductance is supposed to increase as R_s decreases from 55Ω to 35Ω . From Figure 4.11 we can see that transconductance has increased from approximately 18.5ms/mm to 20ms/mm for $V_{ds} = 15V$.

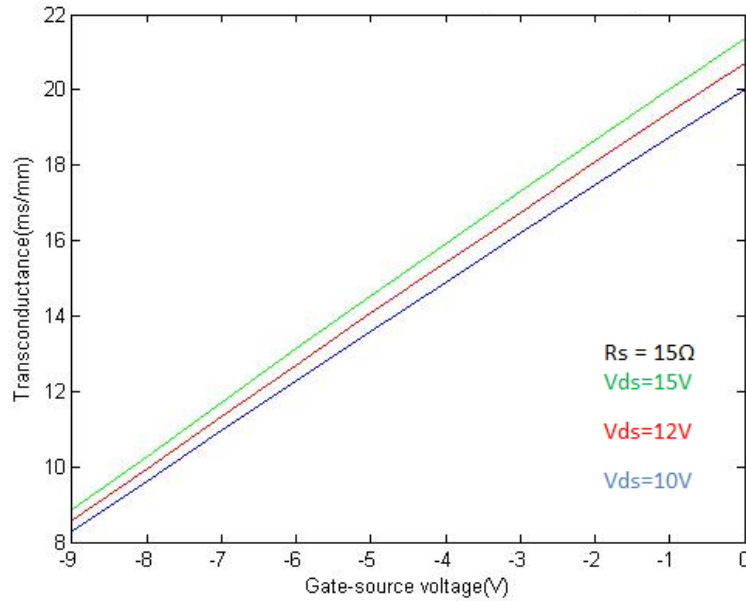


Figure 4.12: Variation of Transconductance with Gate-Source Voltage for $R_s = 15\Omega$

The value of transconductance is supposed to increase as R_s decreases from 35Ω to 15Ω . From Figure 4.12 we can see that transconductance has increased from approximately 20ms/mm to 21ms/mm for $V_{ds} = 15V$.

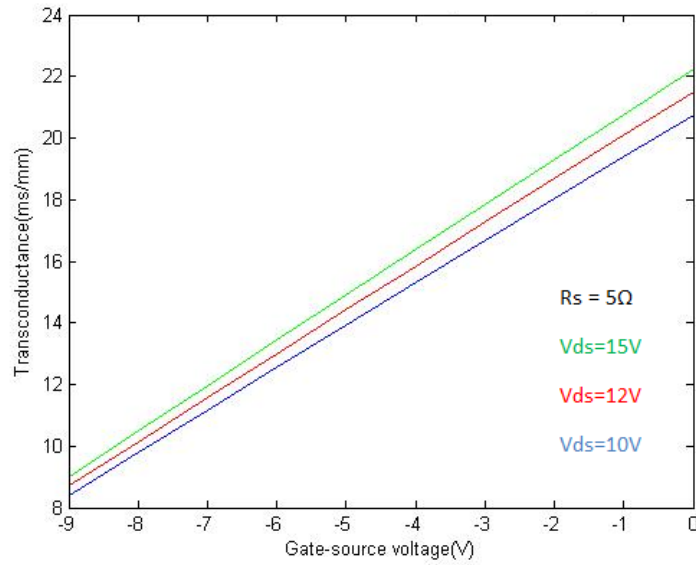


Figure 4.13: Variation of Transconductance with Gate-Source Voltage for $R_s = 5\Omega$

The value of transconductance is supposed to increase as R_s decreases from 15Ω to 5Ω . From Figure 4.13 we can see that transconductance has increased from approximately 21ms/mm to 22ms/mm for $V_{ds} = 15V$.

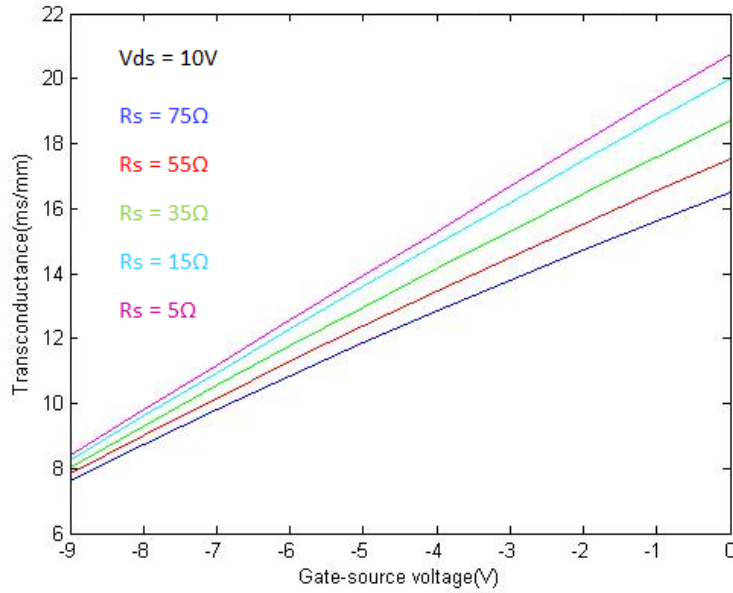


Figure 4.14: Variation of Transconductance with Gate-Source Voltage for $V_{ds} = 10V$

The value of transconductance is supposed to increase as R_s decreases from 75Ω to 5Ω . From Figure 4.14 we can see that transconductance has increased from approximately 16ms/mm to 21ms/mm for $V_{ds} = 10V$.

4.5 Noise figure

Noise figure plays a vital role when used as small signal amplifier components.

The equation for noise figure is as follows:

$$f_o = 10 \log_{10} \left(1 + 2.5 \frac{f}{f_t} \sqrt{g_m (R_s + R_g)} \right) \quad (4.27)$$

where,

R_g = metallization resistance

f = frequency in gigahertz

MATLAB code as shown in page A.17 was utilized in order to obtain the graphs as shown in Fig. 4.15.

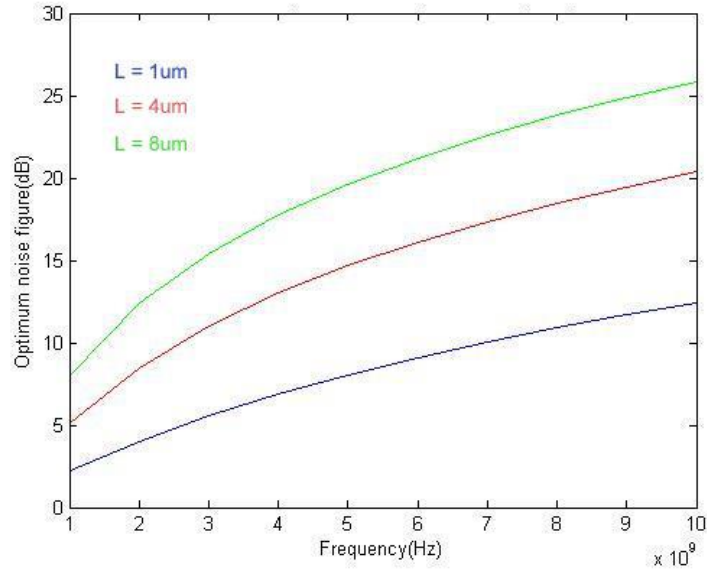


Figure 4.15: Variation of Optimum Noise Figure with Frequency for different Gate Length

It can be seen from equation (4.27) that noise figure (f_o) is proportional to the source resistance (R_s). If we decrease R_s , noise figure will decrease. In the following figures the value of R_s has been decreased from 75Ω to 5Ω . As a result we can see that the value of f_o decreases as well.

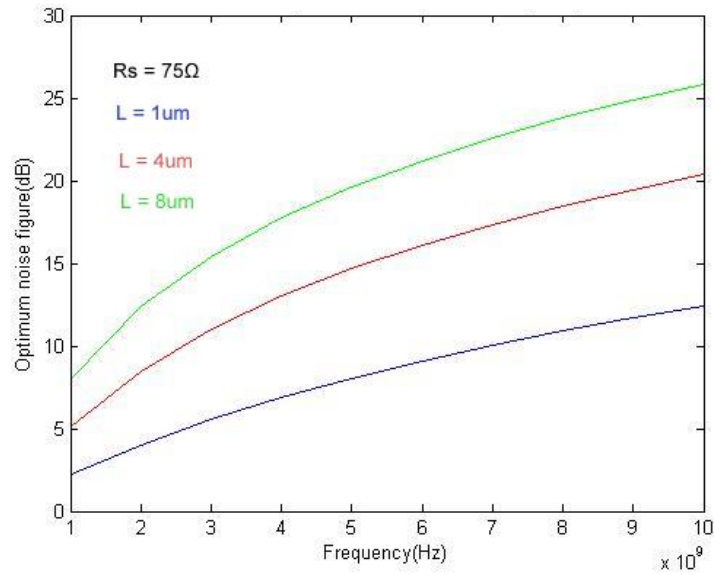


Figure 4.16: Variation of Optimum Noise Figure with Frequency for $R_s = 75\Omega$

In Figure 4.16 we can see that for $R_s = 75\Omega$, the value of noise figure for $L = 8\mu\text{m}$ is approximately 26 dB.

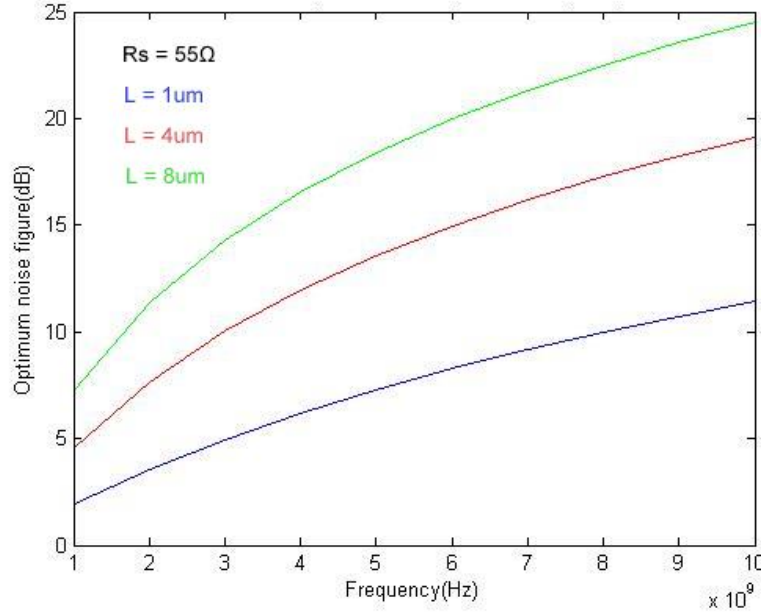


Figure 4.17: Variation of Optimum Noise Figure with Frequency for $R_s = 55\Omega$

The value of noise figure is supposed to decrease as R_s decreases from 75Ω to 55Ω . From Figure 4.17 we can see that noise figure has decreased from approximately 26 dB to 25 dB for $L = 8\mu\text{m}$.

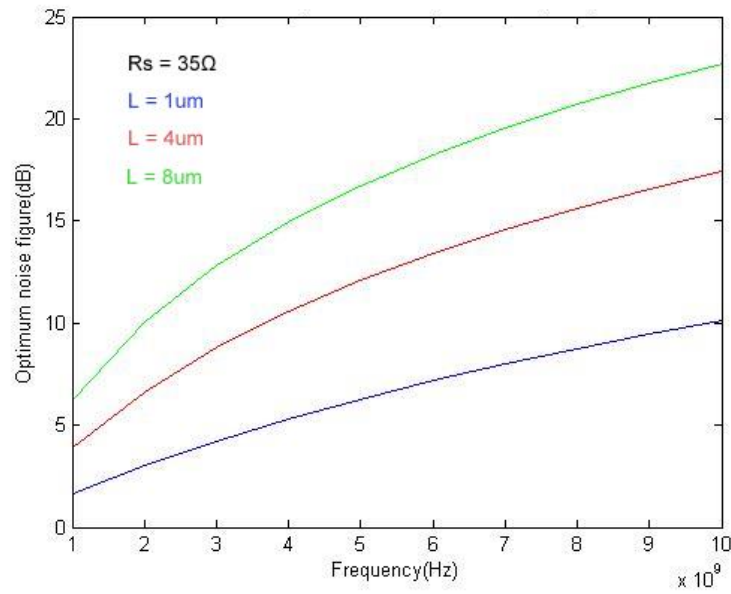


Figure 4.18: Variation of Optimum Noise Figure with Frequency for $R_s = 35\Omega$

The value of noise figure is supposed to decrease as R_s decreases from 55Ω to 35Ω . From Figure 4.18 we can see that noise figure has decreased from approximately 25dB to 23dB for $L = 8\mu\text{m}$.

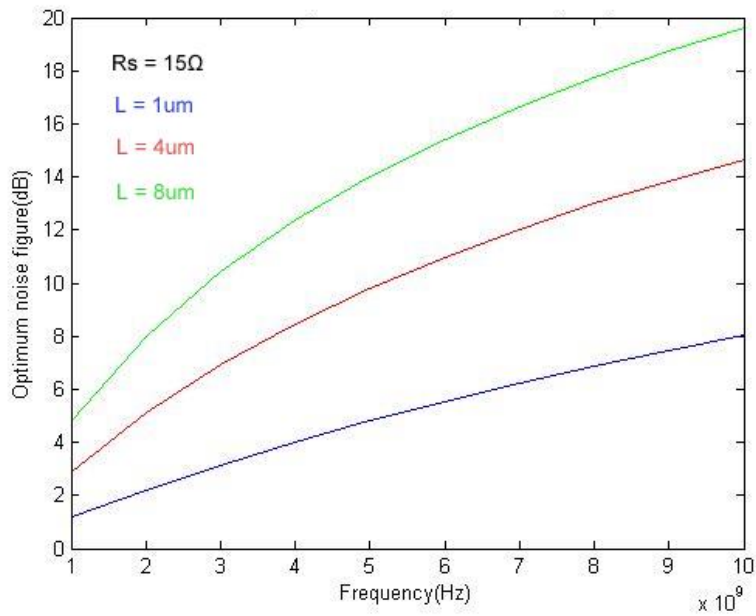


Figure 4.19: Variation of Optimum Noise Figure with Frequency for $R_s = 15\Omega$

The value of noise figure is supposed to decrease as R_s decreases from 35Ω to 15Ω . From Figure 4.19 we can see that noise figure has decreased from approximately 23 dB to 20 dB for $L = 8\mu\text{m}$.

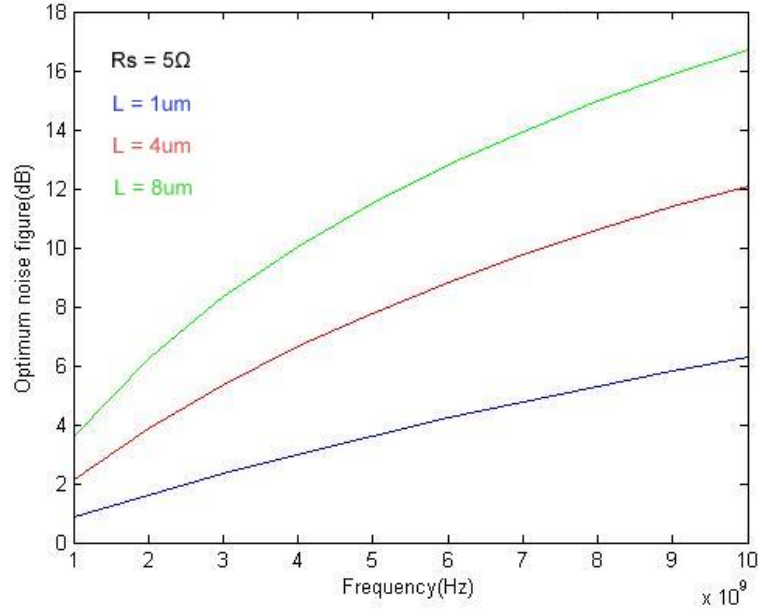


Figure 4.20: Variation of Optimum Noise Figure with Frequency for $R_s = 5\Omega$

The value of noise figure is supposed to decrease as R_s decreases from 15Ω to 5Ω . From Figure 4.20 we can see that noise figure has decreased from approximately 20 dB to 17 dB for $L = 8\mu\text{m}$.

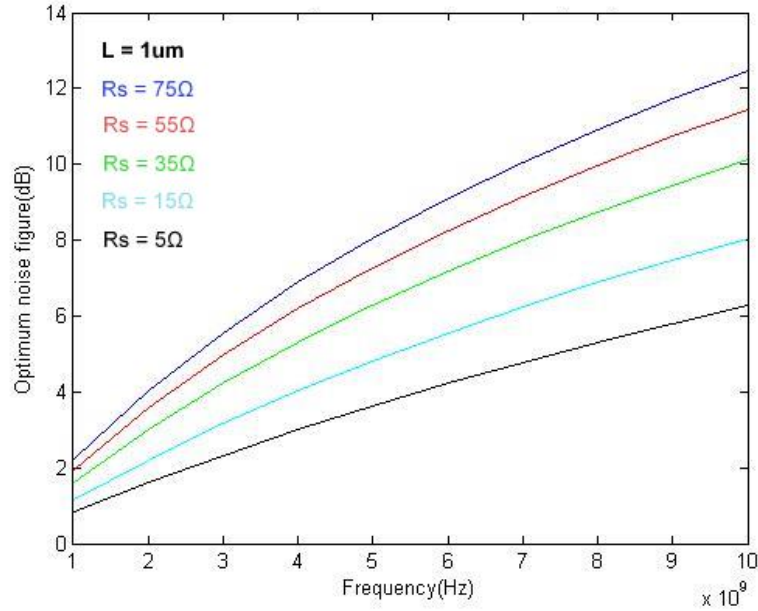


Figure 4.21: Variation of Optimum Noise Figure with Frequency for $L = 1\mu\text{m}$

The value of noise figure is supposed to decrease as R_s decreases from 75Ω to 5Ω . From Figure 4.21 we can see that noise figure has decreased from approximately 13 dB to 7 dB for $L = 1\mu\text{m}$.

4.6 Gate-drain capacitance

$$C_{gd} = \frac{ZL}{2\sqrt{2}} \left(\frac{q\epsilon_s N_d}{V_{bi} - (V_{gs} - V_{ds})} \right)^{1/2} + \frac{\pi}{2} \epsilon_s Z \quad (4.28)$$

It can be seen from equation (4.28) that gate-drain capacitance (C_{GD}) is directly proportional to the gate length (L). If we decrease L , C_{GD} will decrease. In the following figures the value of L has been decreased from $4\mu\text{m}$ to $0.25\mu\text{m}$. As a result we can see that the value of C_{GD} decreases. The aspect ratio is assumed to be 25. Hence as L decreases, gate width (Z) decreases as well.

Page A.28 includes the MATLAB code used for this simulation.

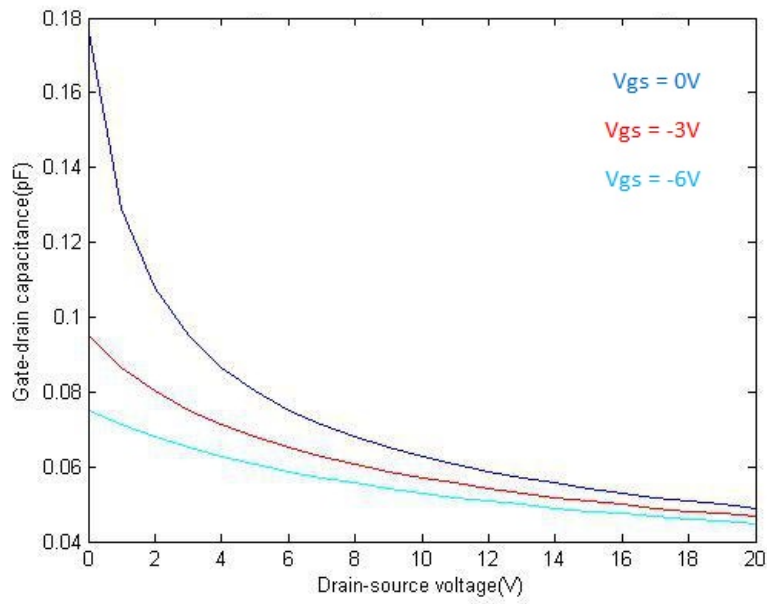


Figure 4.22: Variation of Gate-Drain Capacitance with Drain-Source Voltage for different Gate-Source Voltage

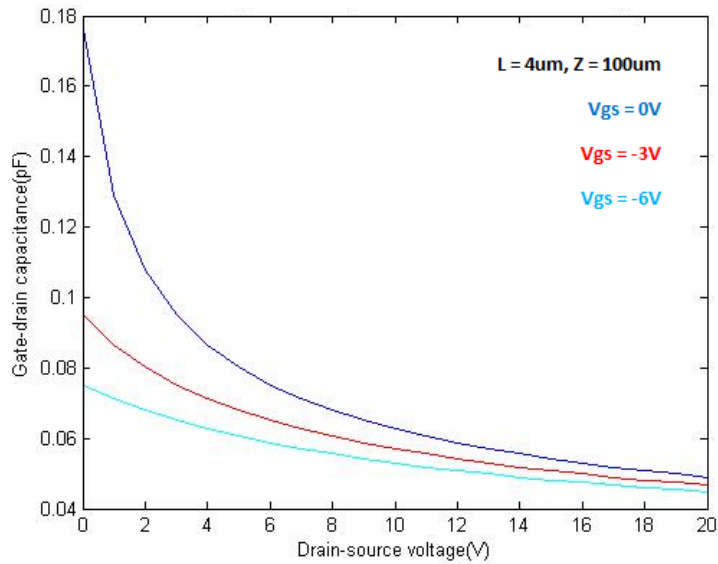


Figure 4.23: Variation of Gate-Drain Capacitance with Drain-Source Voltage for $L = 4\mu\text{m}$, $Z=100\mu\text{m}$

In Figure 4.23 we can see that for $L = 4\mu\text{m}$, the value of C_{GD} for $V_{gs} = 0\text{V}$ is approximately 0.18pF .

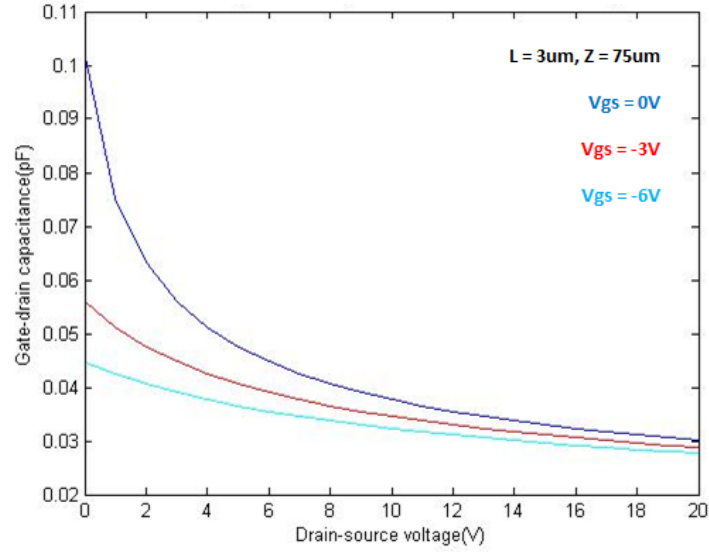


Figure 4.24: Variation of Gate-Drain Capacitance with Drain-Source Voltage for $L = 3\mu\text{m}$, $Z = 75\mu\text{m}$

The value of C_{GD} is supposed to decrease as L decreases from $4\mu\text{m}$ to $3\mu\text{m}$. From Figure 4.24 we can see that C_{GD} has decreased from approximately 0.18pF to 0.1pF for $V_{gs} = 0\text{V}$.

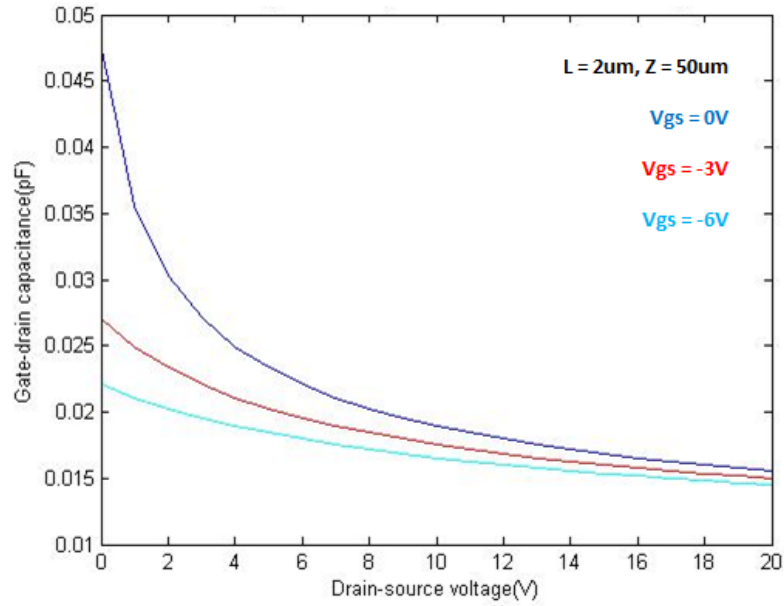


Figure 4.25: Variation of Gate-Drain Capacitance with Drain-Source Voltage for $L = 2\mu\text{m}$, $Z=50\mu\text{m}$

The value of C_{GD} is supposed to decrease as L decreases from $3\mu\text{m}$ to $2\mu\text{m}$. From Figure 4.25 we can see that C_{GD} has decreased from approximately 0.1pF to 0.046pF for $V_{gs} = 0V$.

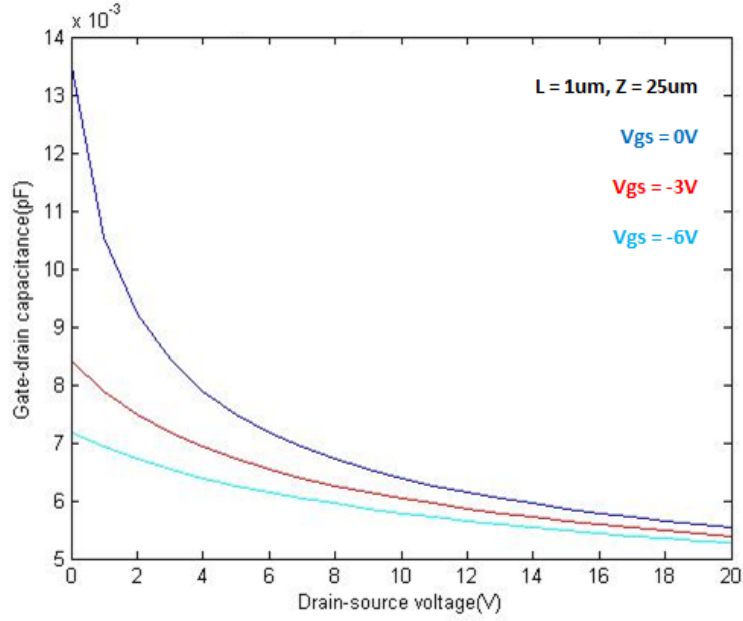


Figure 4.26: Variation of Gate-Drain Capacitance with Drain-Source Voltage for $L = 1\mu\text{m}$, $Z=25\mu\text{m}$

The value of C_{GD} is supposed to decrease as L decreases from $2\mu\text{m}$ to $1\mu\text{m}$. From Figure 4.26 we can see that C_{GD} has decreased from approximately 0.046pF to $13.5 \times 10^{-3}\text{pF}$ for $V_{gs} = 0V$.

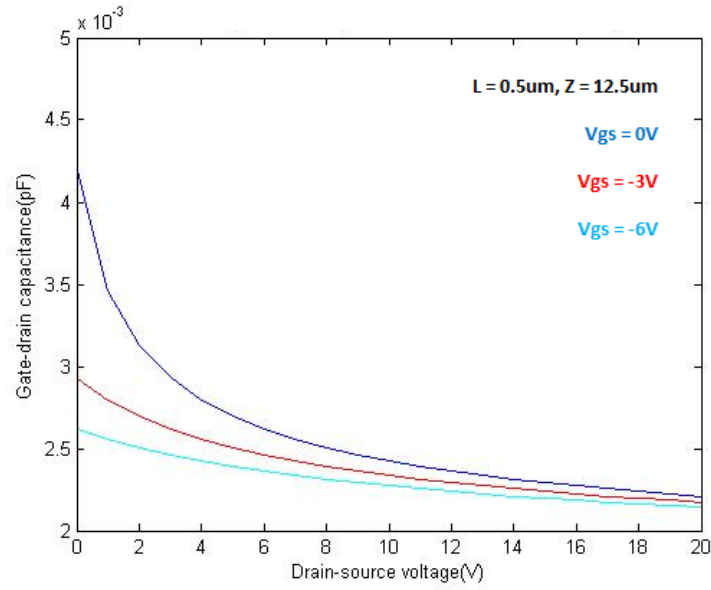


Figure 4.27: Variation of Gate-Drain Capacitance with Drain-Source Voltage for $L = 0.5\mu\text{m}$, $Z=12.5\mu\text{m}$

The value of C_{GD} is supposed to decrease as L decreases from $1\mu\text{m}$ to $0.5\mu\text{m}$. From Figure 4.27 we can see that C_{GD} has decreased from approximately $13.5 \times 10^{-3} \text{ pF}$ to $4.2 \times 10^{-3} \text{ pF}$ for $V_{GS} = 0\text{V}$.

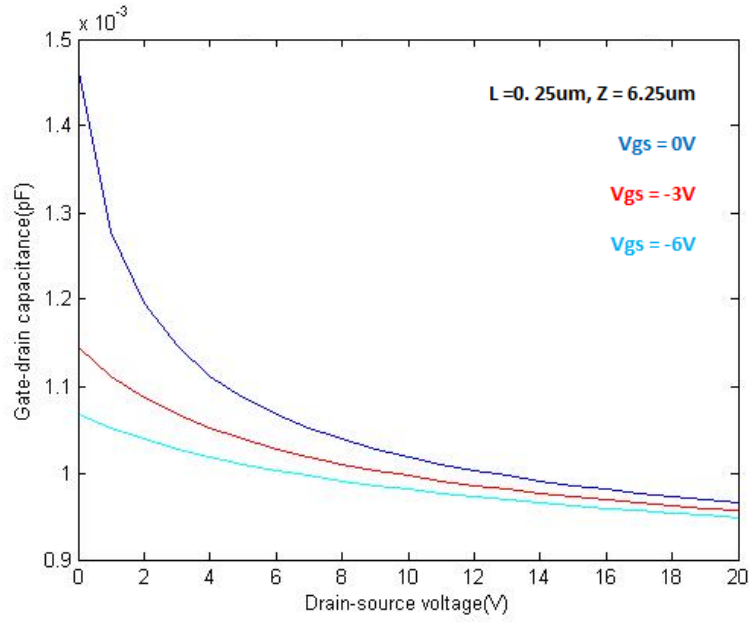


Figure 4.28: Variation of Gate-Drain Capacitance with Drain-Source Voltage for $L = 0.25\mu\text{m}$, $Z=6.25\mu\text{m}$

The value of C_{GD} is supposed to decrease as L decreases from $0.5\mu\text{m}$ to $0.25\mu\text{m}$. From Figure 4.28 we can see that C_{GD} has decreased from approximately $4.2 \times 10^{-3}\text{pF}$ to $1.5 \times 10^{-3}\text{pF}$ for $V_{gs} = 0\text{V}$.

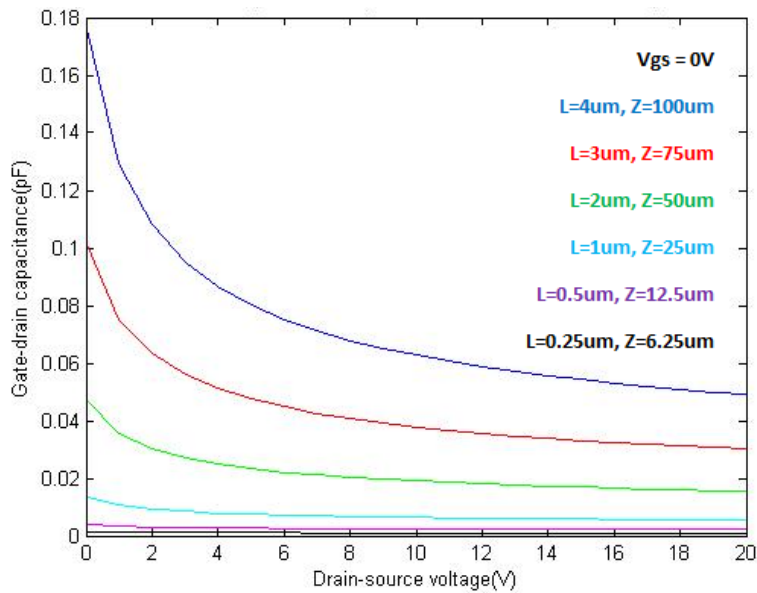


Figure 4.29: Variation of Gate-Drain Capacitance with Drain-Source Voltage for $V_{gs} = 0\text{V}$

The value of C_{GD} is supposed to decrease as L decreases from $4\mu\text{m}$ to $0.25\mu\text{m}$. From figure 4.29 we can see that C_{GD} has decreased from approximately 0.18pF to $1.5 \times 10^{-3}\text{pF}$ for $V_{GS} = 0\text{V}$.

4.7 Gate-source capacitance

$$C_{gs} = \frac{ZL}{2\sqrt{2}} \left(\frac{q\epsilon_s N_d}{V_{bi} - V_{gs}} \right)^{1/2} + \frac{\pi}{2} \epsilon_s Z \quad (4.29)$$

It can be seen from equation (4.29) that gate-source capacitance (C_{GS}) is directly proportional to the gate length (L). If we decrease L , C_{GS} will decrease. In the following figure the value of L has been decreased from $4\mu\text{m}$ to $0.25\mu\text{m}$. As a result we can see that the value of C_{GS} decreases. The aspect ratio is assumed to be 25. Hence as L decreases, gate width (Z) decreases as well.

The corresponding MATLAB code used to demonstrate this variation is on page A.29.

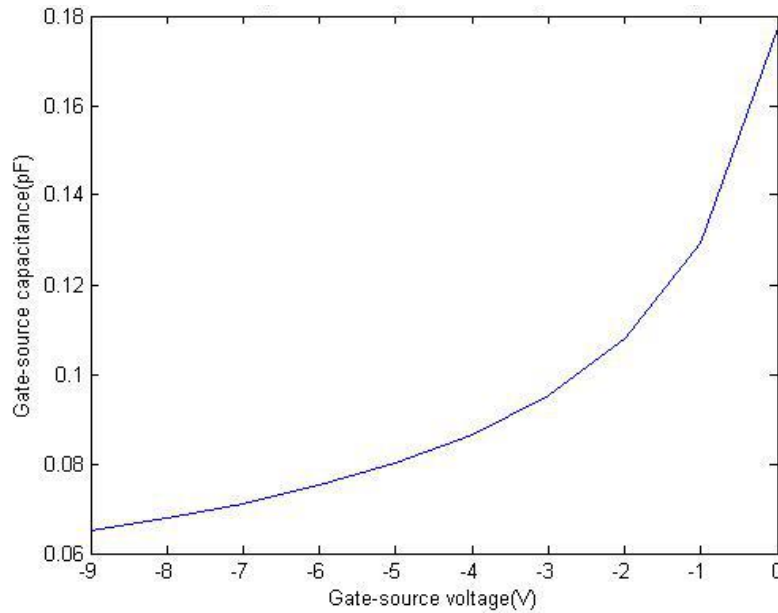


Figure 4.30: Variation of Gate-Source Capacitance with Gate-Source Voltage

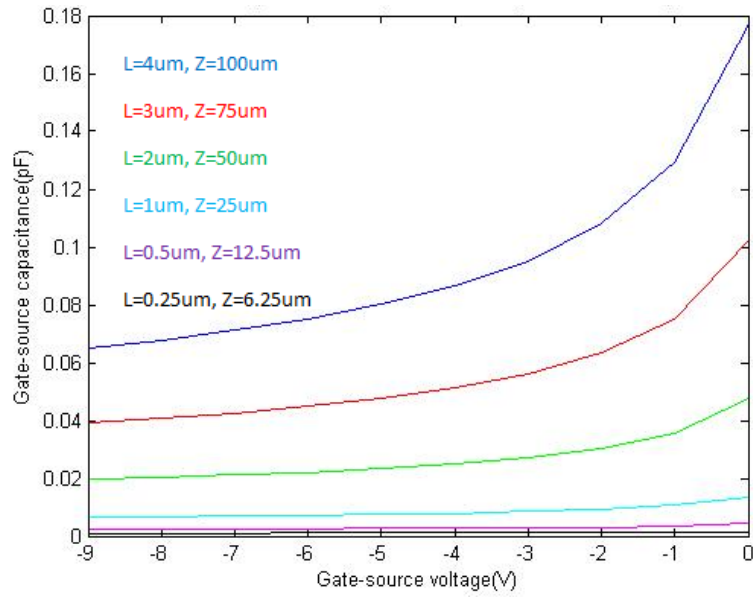


Figure 4.31: Variation of Gate-Source Capacitance with Gate-Source Voltage for different gate lengths

The value of C_{GS} is supposed to decrease as L decreases from $4\mu\text{m}$ to $0.25\mu\text{m}$. From Figure 4.31 we can see that C_{GS} has decreased from approximately 0.18pF to less than $1.5 \times 10^{-3}\text{pF}$.

4.8 Total internal device capacitance

$$C_t = C_{gd} + C_{gs} \quad (4.30)$$

Code added on page A.30 has been used to demonstrate the following variations.

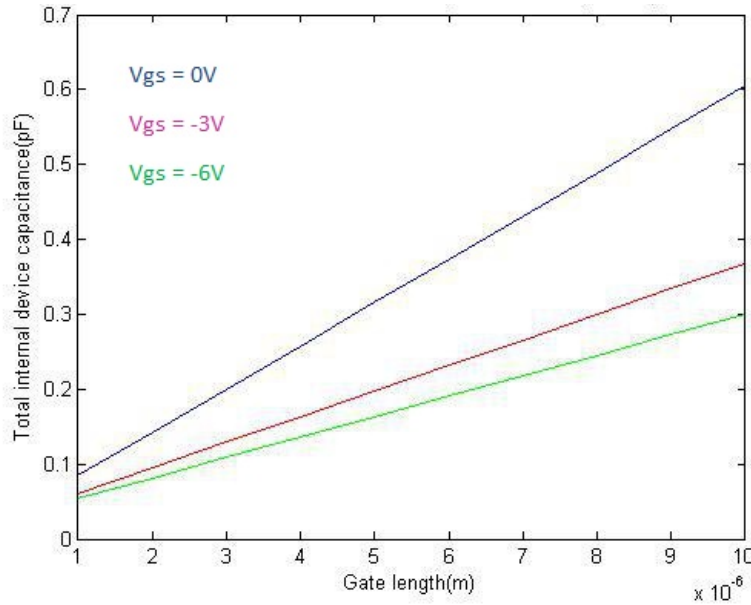


Figure 4.32: Variation of total internal device capacitance with gate length for different gate-source voltage

C_{GD} and C_{GS} are directly proportional to the gate length (L) as it can be seen from equations (4.28) and (4.29). We know from equation (4.30) that total internal device capacitance is the sum of C_{GD} and C_{GS} . Therefore, we can conclude that total internal device capacitance is directly proportional to the gate length (L). If we decrease L , C_t will decrease. In the following figure the value of L has been decreased from $6\mu\text{m}$ to $0.25\mu\text{m}$. As a result we can see that the value of C_t decreases as well.

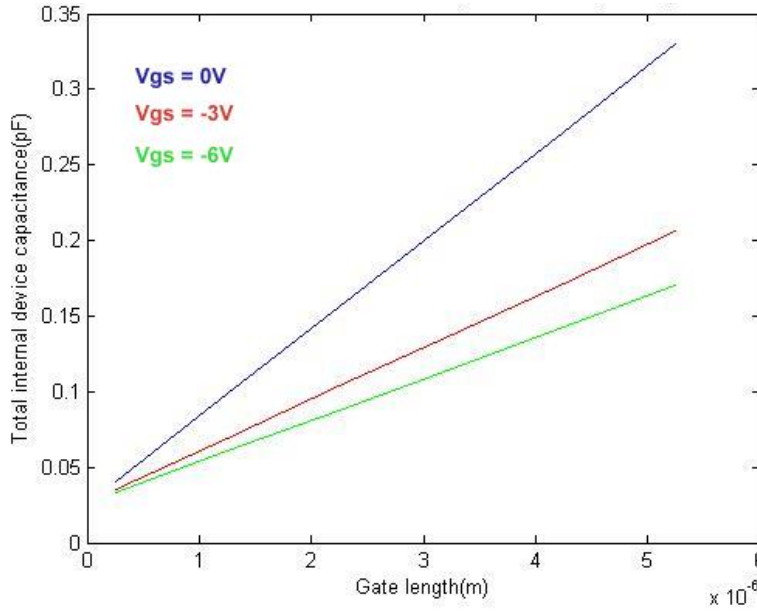


Figure 4.33: Variation of total internal device capacitance with gate length for different gate-source voltage

The value of C_t is supposed to decrease as L decreases from $6\mu\text{m}$ to $0.25\mu\text{m}$. From Figure 4.33 we can see that C_t has decreased as L is decreased beyond $1\mu\text{m}$. The value decreases to approximately $0.04\mu\text{m}$ for $V_{GS} = 0V$.

CHAPTER 5

CONCLUSIONS

In this thesis, we have attempted to demonstrate the effects of gate length modulation and parasitic resistance on GaN MESFET parameters such as the transconductance, total internal capacitance, and noise figure. Also the channel potential distribution has been investigated in both one dimensional and two dimensional plots. The one dimensional channel distribution carried out for various applied potential confirms that there lies a point in the middle where along the channel length the potential is maximum. The two dimensional investigation (taking into consideration the channel length and channel depth) shows that the potential decreases with increase in channel length. Also, the potential at the source side is less than the potential at the drain side as expected.

The variation of transconductance with gate-source voltage shows there is a linear increase in the transconductance with increase in gate-source voltage, and for a fixed drain-source voltage the MESFET with lowest parasitic resistance gives the highest transconductance.

The internal capacitance is seen to increase with increasing gate length and the highest value is obtained with the least negative gate-source voltage.

The optimum noise figure is also seen to increase with increase in frequency. Keeping the gate length constant, the lowest noise figure is obtained with the device with the lowest parasitic resistance.

The parameters have shown the desired trends with variation and can be said to have good agreement with the expected results.

CHAPTER 6

SUGGESTIONS FOR FURTHER RESEARCH

An analytical two-dimensional channel potential distribution model based on the Poisson's equation is presented in this thesis assuming long-channel GaN MESFET. This potential distribution model can be extended for short-channel MESFETs with some assumptions and modifications.

Other practical parameters can be taken into consideration and the effect of gate length modulation and parasitic resistance observed which might help to make a more accurate conclusion about the variation of these parameters and their respective effect on the power and frequency output of GaN MESFET. The possible parameters are discussed below.

Cut-off frequency

Cut-off frequency is a boundary in a system's frequency response at which energy flowing through the system begins to be reduced.

The expression of cut-off frequency is as follows:

$$f_t = \frac{g_m}{2\pi(C_{gs} + C_{gd})}$$

With the decrease in gate length, the cut-off frequency increases due to the decrease in internal device capacitance and increase in transconductance of the device [14].

Transit time and RC time constant

Transit time is the time for a charge carrier to cross the channel region from the source to the drain region.

The equation for transit time is as follows:

$$\tau_r = \frac{1}{2\pi f_t}$$

RC time constant is an important parameter when the MESFET is operated as a switch or a memory device.

The equation for RC time constant is as follows:

$$\tau_{RC} = R_{ds}(C_{gs} + C_{gd})$$

The time constant is more than transit time resulting from input capacitance and transconductance [14].

Maximum Power Density

The maximum power output is obtained from the expression:

$$P_{\max} = \frac{I_{\text{dsat}}(V_B - V_{\text{dsat}})}{8} \quad [14].$$

REFERENCES

- [1] Sheet1_MESFETBackground.pdf – provided by Supervisor
- [2] http://epcco.com/epc/documents/producttraining/Appnote_GaNfundamentals.pdf
- [3] Chapter-3, GaN material technology - http://itri2.org/ttec/hte_j/report/03.pdf
- [4] http://en.wikipedia.org/wiki/Band_gap
- [5] http://en.wikipedia.org/wiki/Electron_mobility
- [6] http://en.wikipedia.org/wiki/Saturation_velocity
- [7] http://en.wikipedia.org/wiki/Thermal_conductivity
- [8] GaN vs SiC - http://www.digikey.com/Web%20Export/Supplier%20Content/Microsemi_278/PDF/Microsemi_GalliumNitride_VS_SiliconCarbide.pdf?redirected=
- [9] Azam, Sher (Linköping University, Department of Physics, Chemistry and Biology, Materials Science) (Linköping University, The Institute of Technology), Linköping Studies in Science and Technology. Thesis, ISSN 0280-7971; 1374, “Wide Bandgap Semiconductor (SiC & GaN) Power Amplifiers in Different Classes”.
- [10] Potential Performance of SiC and GaN Based Metal Semiconductor Field Effect transistors H. Arabshahi Department of Physics, Ferdowsi University of Mashhad, P.O. Box 91775-1436, Mashhad, Iran (Received on 23 July, 2008).
- [11] Pulsed measurements of GaN MESFETs B. Boudart, S. Trassaert, C. Gaquiere, D. Theron and Y. Crosner Institut d’Electronique et de Microelectronique du Nord – DHS U.M.R. - C.N.R.S. 8520- USTL – Avenue Poincare- B.P. 69 59652 VILLENEUVE D’ASCQ CEDEX – France.
- [12] Investigation of cross sectional potential distribution M. Kaneko, A. Hinoki, A. Suzuki, T. Araki, Y. Nanishi
- [13] Double-ion-implanted GaN MESFETs with extremely low source/drain resistance

- [14] A complete analytical model of GaN MESFET for microwave frequency applications -
S.Bose, Adarsh, A.Kumar, Simrata, M.Gupta, R.S. Gupta, Received 11 April 2001;
revised 23 May 2001; accepted 4 June 2001.
- [15] Provided by Supervisor

APPENDIX A

MATLAB CODES FOR SIMULATION

One dimensional channel potential variations, for different values of applied voltage

```

clear all;
clc;
close all;
Phi_m = 5.15; % work function of the metal
kai = 4.1; % electron affinity of the semiconductor
Phi_bo = Phi_m - kai; % barrier height
Nc = 2.234*10^19; % effective density of state
Nd = 10^16; % doping concentration
T = 300; % temperature
q = 1.6*10^-19; % charge of electron
k = 1.38*10^-23; % Boltzman constant
Phi_n = (k*T/q)*log(Nc/Nd);
Vbi = Phi_bo - Phi_n; % built in potential
eps0 = 8.854*10^-12; % permittivity of vacuum
eps = 8.9*eps0;

Va = 0; % applied voltage
w=sqrt((2*eps*(Vbi-Va))/(q*Nd));
A=(q*Nd)/(2*eps);
x=0:10^-6:1000*10^-6;
y=-A*x.^2+A*2*w*x-(Vbi-Va);
plot(x,y);
hold on;

Va=-0.5; % applied voltage
w=sqrt((2*eps*(Vbi-Va))/(q*Nd));
A=(q*Nd)/(2*eps);
x=0:10^-6:1000*10^-6;
y=-A*x.^2+A*2*w*x-(Vbi-Va);
plot(x,y,'r');

Va=-1; % applied voltage
w=sqrt((2*eps*(Vbi-Va))/(q*Nd));
A=(q*Nd)/(2*eps);
x=0:10^-6:1000*10^-6;
y=-A*x.^2+A*2*w*x-(Vbi-Va);
plot(x,y,'g');

Va=-1.5; % applied voltage

```

```

w=sqrt((2*eps*(Vbi-Va))/(q*Nd));
A=(q*Nd)/(2*eps);
x=0:10^-6:1000*10^-6;
y=-A*x.^2+A*2*w*x-(Vbi-Va);
plot(x,y,'c');

```

```

Va=-2;                                     % applied voltage
w=sqrt((2*eps*(Vbi-Va))/(q*Nd));
A=(q*Nd)/(2*eps);
x=0:10^-6:1000*10^-6;
y=-A*x.^2+A*2*w*x-(Vbi-Va);
plot(x,y,'k');

```

Two Dimensional Channel Potential

Channel Potential:

```
clear all;

clc;

close all;

x=0e-6:0.01e-6:1e-6;

y=0:0.005e-6:0.2e-6;

p=0.1e-6;

q=0.2e-6;

for i=1:length(x)

for j=1:length(y)

z(j,i)=real(mesfet(x(i),y(j)));

if (j>1)

if(z(j,i)<z(j-1,i))

z(j,i)=z(j-1,i);

end

end

end

end

[X,Y] = meshgrid(x,y);

surf(X,Y,z);
```

Mesfet Function:

```
function Z=mesfet(x,y)
```



```

%% Constant Parameters

me = 9.1094e-31; %Mass of Electron

k=1.3807e-23; %Boltzman Constant

h=6.6261e-34; %Planc's Constant

h_bar=1.0546e-34; %Reduced Planc's Constant

e=1.6022e-19; %Charge of Electron

eps0=8.8542e-12; %Permittivity of Vacuum

%% Material Related Parameters

eff_me=0.22*me; %Electron Effective mass (GaN)

ki=4.1; %Electron Effinity (GaN)

Fm=4.55; %Metal(Tungsten) Work Function

eps=9.5*eps0; %Permittivity of GaN

%% Applied Parameters

T=300; %Temperature

Nd=10^23; %Channel Doping Concentration(/m^3)

Vg=-1.5; %Gate Voltage

Vd=1.5; %Drain Voltage

Vs=0; %Source Voltage

Vb=0; %Body Bias

Vgs=Vg-Vs; %Gate to Source Voltage

Vds=Vd-Vs; %Drain to Source Voltage

Vbs=Vb-Vs; %Body to Source Voltage

aa=0.2e-6; %Channel Thickness

L=1e-6; %Gate Length

%% Effective Density of State in Conduction Band, Nc

```

```

Nc=2*((2*pi*eff_me*k*T)/h^2)^(3/2); %per meter cube

%% Calculation of Thermal Voltage Vt

Vt=(k*T)/e;

%% Potential Difference Between Conduction Band and Fermi Level, Fn

Fn=Vt*log(Nc/Nd);

%% Schottky Barrier Height, Fbo

Fbo=Fm-ki;

%% Built in Potential, Vbi

Vbi=Fbo-Fn;

%% Space Charge Width

W=sqrt((2*eps*(Vbi-Vgs+Vds))/(e*Nd)); %meter

%% 2D Potential

V1=Vgs-Vbi; %Upper Boundary Potential

V2=Vs; %Source Terminal Potential

V3=Vds; %Drain Terminal Potential

h2= sqrt((2*eps*(Vbi-Vgs+Vds))/(e*Nd));

h1= sqrt((2*eps*(Vbi-Vgs))/(e*Nd));

dh=h2-h1;

h=h2-(dh/L)*x;

a=((2*y*dh)/L)/(y^2-2*h2*y);

b=((4*y*dh)/L)/(y^2-2*y*h2);

c=-(e*Nd/eps)/(y^2-2*h2*y);

p1=(sqrt(-((x+1/a)*b)/a)*besseli(1,2*sqrt(-((x+1/a)*b)/a)))/(a*x+1);

p2=(sqrt(-((x+1/a)*b)/a)*besselk(1,2*sqrt(-((x+1/a)*b)/a)))/(a*x+1);

p3=c/b;

```

$$M=y^2-2*y*h;$$

$$M_0=y^2-2*y*h2;$$

$$M_L=y^2-2*y*h1;$$

$$p1_0=(\sqrt{-((1/a)*b)/a}*\text{besseli}(1,2*\sqrt{-((1/a)*b)/a}));$$

$$p1_L=(\sqrt{-((L+1/a)*b)/a}*\text{besseli}(1,2*\sqrt{-((L+1/a)*b)/a}))/(\text{a}*L+1);$$

$$p2_0=(\sqrt{-((1/a)*b)/a}*\text{besselk}(1,2*\sqrt{-((1/a)*b)/a}));$$

$$p2_L=(\sqrt{-((L+1/a)*b)/a}*\text{besselk}(1,2*\sqrt{-((L+1/a)*b)/a}))/(\text{a}*L+1);$$

$$Q1=M_0*p1_0;$$

$$Q2=M_0*p2_0;$$

$$Q3=V3-V1-M_0*p3;$$

$$Q4=M_L*p1_L;$$

$$Q5=M_L*p2_L;$$

$$Q6=V2-V1-M_L*p3;$$

$$Q=Q2*Q4-Q1*Q5;$$

$$R=Q2*Q6-Q3*Q5;$$

$$S=Q1*Q6-Q3*Q4;$$

$$d1=R/Q;$$

$$d2=S/Q;$$

$$A=d1*p1-d2*p2+p3;$$

$$Fi=A*y^2-2*A*h*y+V1;$$

$$Z=Fi;$$

Variation of Drain-Source Current with Drain-Source Voltage

```
clc;

clear all;

close all;

% variable

u = 0.15;

eps = 9.5*8.8542e-12;

max_iter= 100;

tol =.000000001;

a = 7.5*(10^-8);

d = 0.15e-6;

Vp = 16;

% fixed

q = 1.6*(10^-19);

Z = 100*(10^-6);

Nd = 1*(10^23);

L = 4*(10^-6);

Rs = 75;

Rd = 75;

Vbi = 1;

Vgs = 0;

% Vds = 5;

Vds = [0:1:10];

Ids(1) = 0;

for i=1:length(Vds)
```

```

for k = 1:max_iter

    Ids(k+1) = ((q*Z*u*Nd*a)/L)*(Vds(i)-Ids(k)*(Rs+Rd)-(2/(3*sqrt(Vp)))*((Vbi-Vgs+Vds(i)-Ids(k)*Rd)^(3/2) - (Vbi-Vgs+Ids(k)*Rs)^(3/2)));

    err = abs((Ids(k+1)-Ids(k))/Ids(k+1));

    if(err<tol)

        sol(i) = Ids(k+1);

        break;

    end

end

sol(i) = (Ids(k+1))*1000;

end

plot(Vds, sol),ylabel('Drain-source current (mA)'), xlabel('Drain-source voltage(V)'), title('Ids-Vds characteristics for GaN MESFET')

hold on;

Vgs = -3;

Vds = [0:1:10];

Ids(1) = 0;

for i=1:length(Vds)

    for k = 1:max_iter

        Ids(k+1) = ((q*Z*u*Nd*a)/L)*(Vds(i)-Ids(k)*(Rs+Rd)-(2/(3*(sqrt(Vp)))*((Vbi-Vgs+Vds(i)-(Ids(k)*Rd))^(3/2)-(Vbi-Vgs+(Ids(k)*Rs))^(3/2))));

        err = abs((Ids(k+1)-Ids(k))/Ids(k+1));

        if(err<tol)

            sol(i) = Ids(k+1);

            break;

        end

    end

end

```

```

        sol(i) = (Ids(k+1))*1000;

    end

    plot (Vds, sol, 'r')

    hold on;

    Vgs = -6;

    % Vds = 5;

    Vds = [0:1:10];

    Ids(1) = 0;

    for i=1:length(Vds)

        for k = 1:max_iter

            Ids(k+1) = ((q*Z*u*Nd*a)/L)*(Vds(i)-Ids(k)*(Rs+Rd)-(2/(3*(sqrt(Vp))))*((Vbi-Vgs+Vds(i)-(Ids(k)*Rd))^(3/2)-
            (Vbi-Vgs+( Ids(k)*Rs))^(3/2)));

            err = abs((Ids(k+1)-Ids(k))/Ids(k+1));

            if(err<tol)

                sol(i) = Ids(k+1);

                break;

            end

        end

    end

    sol(i) = (Ids(k+1))*1000;

    end

    plot (Vds, sol, 'g')

    hold on;

    Vgs = -9;

    % Vds = 5;

    Vds = [0:1:10];

```

```

Ids(1) = 0;

for i=1:length(Vds)

for k = 1:max_iter

    Ids(k+1) = ((q*Z*u*Nd*a)/L)*(Vds(i)-Ids(k)*(Rs+Rd)-(2/(3*(sqrt(Vp))))*(Vbi-Vgs+Vds(i)-(Ids(k)*Rd))^(3/2)-
(Vbi-Vgs+( Ids(k)*Rs))^(3/2)));

    err = abs((Ids(k+1)-Ids(k))/Ids(k+1));

    if(err<tol)

        sol(i) = Ids(k+1);

        break;

    end

end

sol(i) = (Ids(k+1))*1000;

end

plot (Vds, sol, 'c')

hold on;

Kd = 1;

Vsat = 0.26*10^4;

Es = Vsat/u;

Vgs = 0;

Vt = Vbi-Vp;

V1s = (Es*L*(Vgs-Vt))/(Es*L+(Vgs-Vt));

eps = 9.5*8.8542*10^-12;

Vds = [10:1:20];

for i = 1:length(Vds)

    Ls(i)=L-((2*a)/pi)*asinh((pi*Kd*(Vds(i)-V1s))/(2*a*Es));

```

```

V2s(i) = Vds(i)-V1s;

Lsb(i) = ((1-Kd)*V2s(i))/(Es*cosh((pi*Ls(i))/(2*a)));

B(i)=(2*eps*Vsat*Z)/(a*(Vp+3*Es*Ls(i))) ;

Idsat(i)= (1+2*B(i)*Rs*(Vgs-Vt)-sqrt(1+4*B(i)*Rs*(Vgs-Vt)))/(2*B(i)*Rs^2);

Idsatb(i)=(Idsat(i)*(1+(Ls(i)+Lsb(i))/L))*1000;

end

plot(Vds,Idsatb)

hold on;

Vgs = -3;

Vsat = 0.28*10^4;

Vds = [10:1:20];

for i = 1:length(Vds)

    Ls(i)=L-((2*a)/pi)*asinh((pi*Kd*(Vds(i)-V1s))/(2*a*Es));

    V2s(i) = Vds(i)-V1s;

    Lsb(i) = ((1-Kd)*V2s(i))/(Es*cosh((pi*Ls(i))/(2*a)));

    B(i)=(2*eps*Vsat*Z)/(a*(Vp+3*Es*Ls(i))) ;

    Idsat(i)= (1+2*B(i)*Rs*(Vgs-Vt)-sqrt(1+4*B(i)*Rs*(Vgs-Vt)))/(2*B(i)*Rs^2);

    Idsatb(i)=(Idsat(i)*(1+(Ls(i)+Lsb(i))/L))*1000;

end

plot(Vds,Idsatb,'r')

hold on;

Vgs = -6;

Vsat = 0.29*10^4;

Vds = [10:1:20];

for i = 1:length(Vds)

```



```

Ls(i)=L-((2*a)/pi)*asinh((pi*Kd*(Vds(i)-V1s))/(2*a*Es));

V2s(i) = Vds(i)-V1s;

Lsb(i) = ((1-Kd)*V2s(i))/(Es*cosh((pi*Ls(i))/(2*a)));

B(i)=(2*eps*Vsat*Z)/(a*(Vp+3*Es*Ls(i))) ;

Idsat(i)= (1+2*B(i)*Rs*(Vgs-Vt)-sqrt(1+4*B(i)*Rs*(Vgs-Vt)))/(2*B(i)*Rs^2);

Idsatb(i)=(Idsat(i)*(1+(Ls(i)+Lsb(i))/L))*1000;

end

plot(Vds,Idsatb,'g')

hold on;

Vgs = -9;

Vsat = 0.19*10^4;

Vds = [10:1:20];

for i = 1:length(Vds)

    Ls(i)=L-((2*a)/pi)*asinh((pi*Kd*(Vds(i)-V1s))/(2*a*Es));

    V2s(i) = Vds(i)-V1s;

    Lsb(i) = ((1-Kd)*V2s(i))/(Es*cosh((pi*Ls(i))/(2*a)));

    B(i)=(2*eps*Vsat*Z)/(a*(Vp+3*Es*Ls(i))) ;

    Idsat(i)= (1+2*B(i)*Rs*(Vgs-Vt)-sqrt(1+4*B(i)*Rs*(Vgs-Vt)))/(2*B(i)*Rs^2);

    Idsatb(i)=(Idsat(i)*(1+(Ls(i)+Lsb(i))/L))*1000;

end

plot(Vds,Idsatb,'c')

```

Variation of Transconductance with Gate-Source Voltage

```

clc;

close all;

clear all;

a = 7.5*(10^-8);

Kd = 0.6;

Vsat = 0.27*10^4;

u = 0.15;

Es = Vsat/u;

L = 4*(10^-6);

Vbi = 1;

Vp = 16;

Vt = Vbi-Vp;

eps = 9.5*8.8542*10^-12;

Rs = 75;

Z = 100*(10^-6);

Vds = 10;

gm = zeros(1,10);

syms Vgs

gyb=diff((((1+2*((2*eps*Vsat*Z)/(a*(Vp+3*Es*(L-((2*a)/pi)*asinh((pi*Kd*(Vds-((Es*L*(Vgs-Vt))/(Es*L+(Vgs-Vt)))))/(2*a*Es)))))))*Rs*(Vgs-Vt)-sqrt(1+4*((2*eps*Vsat*Z)/(a*(Vp+3*Es*(L-((2*a)/pi)*asinh((pi*Kd*(Vds-((Es*L*(Vgs-Vt))/(Es*L+(Vgs-Vt)))))/(2*a*Es)))))))*Rs*(Vgs-Vt))/((2*((2*eps*Vsat*Z)/(a*(Vp+3*Es*(L-((2*a)/pi)*asinh((pi*Kd*(Vds-((Es*L*(Vgs-Vt))/(Es*L+(Vgs-Vt)))))/(2*a*Es))))))*Rs^2))*(1+((L-((2*a)/pi)*asinh((pi*Kd*(Vds-((Es*L*(Vgs-Vt))/(Es*L+(Vgs-Vt)))))/(2*a*Es))))+(((1-Kd)*(Vds-((Es*L*(Vgs-Vt))/(Es*L+(Vgs-Vt)))))/(Es*cosh((pi*(L-((2*a)/pi)*asinh((pi*Kd*(Vds-((Es*L*(Vgs-Vt))/(Es*L+(Vgs-Vt)))))/(2*a*Es))))/(2*a))))/L)))));

gy = gyb/(1+gyb*Rs)

gm(1)=(subs(gy,Vgs,-9))*1000/(Z*10^3);

```

```

gm(2)=(subs(gy,Vgs,-8))*1000/(Z*10^3);

gm(3)=(subs(gy,Vgs,-7))*1000/(Z*10^3);

gm(4)=(subs(gy,Vgs,-6))*1000/(Z*10^3);

gm(5)=(subs(gy,Vgs,-5))*1000/(Z*10^3);

gm(6)=(subs(gy,Vgs,-4))*1000/(Z*10^3);

gm(7)=(subs(gy,Vgs,-3))*1000/(Z*10^3);

gm(8)=(subs(gy,Vgs,-2))*1000/(Z*10^3);

gm(9)=(subs(gy,Vgs,-1))*1000/(Z*10^3);

gm(10)=(subs(gy,Vgs,0))*1000/(Z*10^3);

Vgs = [-9:1:0];

plot(Vgs,gm),xlabel('Gate-source voltage(V)'),ylabel('Transconductance(ms/mm)'),title('Variation of
transconductance with gate-source voltage')

hold on;

Vsat = 0.28*10^4;

Vds = 12;

gm = zeros(1,10);

syms Vgs

gyb=diff((((1+2*((2*eps*Vsat*Z)/(a*(Vp+3*Es*(L-((2*a)/pi)*asinh((pi*Kd*(Vds-((Es*L*(Vgs-
Vt))/(Es*L+(Vgs-Vt)))))/(2*a*Es)))))))*Rs*(Vgs-Vt)-sqrt(1+4*((2*eps*Vsat*Z)/(a*(Vp+3*Es*(L-
((2*a)/pi)*asinh((pi*Kd*(Vds-((Es*L*(Vgs-Vt))/(Es*L+(Vgs-Vt)))))/(2*a*Es)))))))*Rs*(Vgs-
Vt)))/(2*((2*eps*Vsat*Z)/(a*(Vp+3*Es*(L-((2*a)/pi)*asinh((pi*Kd*(Vds-((Es*L*(Vgs-Vt))/(Es*L+(Vgs-
Vt)))))/(2*a*Es)))))))*Rs^2)*(1+((L-((2*a)/pi)*asinh((pi*Kd*(Vds-((Es*L*(Vgs-Vt))/(Es*L+(Vgs-
Vt)))))/(2*a*Es)))+((1-Kd)*(Vds-((Es*L*(Vgs-Vt))/(Es*L+(Vgs-Vt)))))/(Es*cosh((pi*(L-
((2*a)/pi)*asinh((pi*Kd*(Vds-((Es*L*(Vgs-Vt))/(Es*L+(Vgs-Vt)))))/(2*a*Es)))/(2*a)))))/L)))));

gy = gyb/(1+gyb*Rs);

gm(1)=(subs(gy,Vgs,-9))*1000/(Z*10^3);

gm(2)=(subs(gy,Vgs,-8))*1000/(Z*10^3);

gm(3)=(subs(gy,Vgs,-7))*1000/(Z*10^3);

gm(4)=(subs(gy,Vgs,-6))*1000/(Z*10^3);

```

```

gm(5)=(subs(gy,Vgs,-5))*1000/(Z*10^3);

gm(6)=(subs(gy,Vgs,-4))*1000/(Z*10^3);

gm(7)=(subs(gy,Vgs,-3))*1000/(Z*10^3);

gm(8)=(subs(gy,Vgs,-2))*1000/(Z*10^3);

gm(9)=(subs(gy,Vgs,-1))*1000/(Z*10^3);

gm(10)=(subs(gy,Vgs,0))*1000/(Z*10^3);

Vgs = [-9:1:0];

plot(Vgs,gm,'r')

hold on;

Vsat = 0.29*10^4;

Vds = 15;

gm = zeros(1,10);

syms Vgs

gyb=diff((((1+2*((2*eps*Vsat*Z)/(a*(Vp+3*Es*(L-((2*a)/pi)*asinh((pi*Kd*(Vds-((Es*L*(Vgs-Vt))/(Es*L+(Vgs-Vt)))))/(2*a*Es)))))))*Rs*(Vgs-Vt)-sqrt(1+4*((2*eps*Vsat*Z)/(a*(Vp+3*Es*(L-((2*a)/pi)*asinh((pi*Kd*(Vds-((Es*L*(Vgs-Vt))/(Es*L+(Vgs-Vt)))))/(2*a*Es)))))))*Rs*(Vgs-Vt)))/(2*((2*eps*Vsat*Z)/(a*(Vp+3*Es*(L-((2*a)/pi)*asinh((pi*Kd*(Vds-((Es*L*(Vgs-Vt))/(Es*L+(Vgs-Vt)))))/(2*a*Es)))))))*Rs^2))*(1+((L-((2*a)/pi)*asinh((pi*Kd*(Vds-((Es*L*(Vgs-Vt))/(Es*L+(Vgs-Vt)))))/(2*a*Es))))+(((1-Kd)*(Vds-((Es*L*(Vgs-Vt))/(Es*L+(Vgs-Vt)))))/(Es*cosh((pi*(L-((2*a)/pi)*asinh((pi*Kd*(Vds-((Es*L*(Vgs-Vt))/(Es*L+(Vgs-Vt)))))/(2*a*Es))))/(2*a)))))/L));

gy = gyb/(1+gyb*Rs);

gm(1)=(subs(gy,Vgs,-9))*1000/(Z*10^3);

gm(2)=(subs(gy,Vgs,-8))*1000/(Z*10^3);

gm(3)=(subs(gy,Vgs,-7))*1000/(Z*10^3);

gm(4)=(subs(gy,Vgs,-6))*1000/(Z*10^3);

gm(5)=(subs(gy,Vgs,-5))*1000/(Z*10^3);

gm(6)=(subs(gy,Vgs,-4))*1000/(Z*10^3);

gm(7)=(subs(gy,Vgs,-3))*1000/(Z*10^3);

```

```
gm(8)=(subs(gy,Vgs,-2))*1000/(Z*10^3);  
gm(9)=(subs(gy,Vgs,-1))*1000/(Z*10^3);  
gm(10)=(subs(gy,Vgs,0))*1000/(Z*10^3);  
Vgs = [-9:1:0];  
plot(Vgs,gm,'g')
```

Variation of Optimum Noise Figure with Frequency

```
clc;

clear all;

close all;

q = 1.6*10^-19;

Z=100*10^-6;

Vbi=1;

Vds=5;

Rs=75;

Rg=5;

Nd=1*10^23;

eps=9.5*8.854*10^-12;

%for L = 1um

L=1*10^-6;

Vgs = -3;

gm
=(38685626227668133590597632/19768278308084420625*(11366411333352724322542099427302824
77371327921662890625/4313591466744102367146722413923140907781943107606491596976577639
87456/(22743861454796784249/18889465931478580854784000-
34498941656555872338340866277728375/178405961588244985132285746181186892047843328*asin
h(2000/9*pi*(5-(9/500*Vgs+27/100)/(7509/500+Vgs))))^2*(Vgs+15)*pi*(-
9/500/(7509/500+Vgs)+(9/500*Vgs+27/100)/(7509/500+Vgs)^2)/(81+4000000*pi^2*(5-
(9/500*Vgs+27/100)/(7509/500+Vgs))^2)^(1/2)+263577044107792275/38685626227668133590597632/
(22743861454796784249/18889465931478580854784000-
34498941656555872338340866277728375/178405961588244985132285746181186892047843328*asin
h(2000/9*pi*(5-(9/500*Vgs+27/100)/(7509/500+Vgs))))-
1/8796093022208/(19342813113834066795298816+263577044107792275/(22743861454796784249/18
889465931478580854784000-
34498941656555872338340866277728375/178405961588244985132285746181186892047843328*asin
h(2000/9*pi*(5-
(9/500*Vgs+27/100)/(7509/500+Vgs))))*(Vgs+15))^(1/2)*(113664113333527243225420994273028247
7371327921662890625/11150372599265311570767859136324180752990208/(22743861454796784249
/18889465931478580854784000-
```

$$34498941656555872338340866277728375/178405961588244985132285746181186892047843328*\sinh(2000/9*\pi*(5-(9/500*V_{gs}+27/100)/(7509/500+V_{gs})))^2*(V_{gs}+15)*\pi*(-9/500/(7509/500+V_{gs})+(9/500*V_{gs}+27/100)/(7509/500+V_{gs})^2)/(81+4000000*\pi^2*(5-(9/500*V_{gs}+27/100)/(7509/500+V_{gs}))^2)^{(1/2)}+263577044107792275/(22743861454796784249/18889465931478580854784000-$$

$$34498941656555872338340866277728375/178405961588244985132285746181186892047843328*\sinh(2000/9*\pi*(5-(9/500*V_{gs}+27/100)/(7509/500+V_{gs}))))*(22743861454796784249/18889465931478580854784000-$$

$$34498941656555872338340866277728375/178405961588244985132285746181186892047843328*\sinh(2000/9*\pi*(5-(9/500*V_{gs}+27/100)/(7509/500+V_{gs}))))*(2-56369097663014421875/1180591620717411303424*\sinh(2000/9*\pi*(5-(9/500*V_{gs}+27/100)/(7509/500+V_{gs}))+500/9*(2-2/5*(9/500*V_{gs}+27/100)/(7509/500+V_{gs}))/\cosh(18889465931478580854784/2833419889721787*\pi*(1/1000000-3607622250432923/75557863725914323419136*\sinh(2000/9*\pi*(5-(9/500*V_{gs}+27/100)/(7509/500+V_{gs})))))-766643147923463829740908139505075/1012945474241937133241379867066368*(1+263577044107792275/38685626227668133590597632/(22743861454796784249/18889465931478580854784000-$$

$$34498941656555872338340866277728375/178405961588244985132285746181186892047843328*\sinh(2000/9*\pi*(5-(9/500*V_{gs}+27/100)/(7509/500+V_{gs}))))*(V_{gs}+15)-1/4398046511104*(19342813113834066795298816+263577044107792275/(22743861454796784249/18889465931478580854784000-$$

$$34498941656555872338340866277728375/178405961588244985132285746181186892047843328*\sinh(2000/9*\pi*(5-(9/500*V_{gs}+27/100)/(7509/500+V_{gs}))))*(V_{gs}+15))^{(1/2)}*\pi*(-9/500/(7509/500+V_{gs})+(9/500*V_{gs}+27/100)/(7509/500+V_{gs})^2)/(81+4000000*\pi^2*(5-(9/500*V_{gs}+27/100)/(7509/500+V_{gs}))^2)^{(1/2)}*(2-56369097663014421875/1180591620717411303424*\sinh(2000/9*\pi*(5-(9/500*V_{gs}+27/100)/(7509/500+V_{gs}))+500/9*(2-2/5*(9/500*V_{gs}+27/100)/(7509/500+V_{gs}))/\cosh(18889465931478580854784/2833419889721787*\pi*(1/1000000-3607622250432923/75557863725914323419136*\sinh(2000/9*\pi*(5-(9/500*V_{gs}+27/100)/(7509/500+V_{gs})))))+38685626227668133590597632/19768278308084420625*(1+263577044107792275/38685626227668133590597632/(22743861454796784249/18889465931478580854784000-$$

$$34498941656555872338340866277728375/178405961588244985132285746181186892047843328*\sinh(2000/9*\pi*(5-(9/500*V_{gs}+27/100)/(7509/500+V_{gs}))))*(V_{gs}+15)-1/4398046511104*(19342813113834066795298816+263577044107792275/(22743861454796784249/18889465931478580854784000-$$

$$34498941656555872338340866277728375/178405961588244985132285746181186892047843328*\sinh(2000/9*\pi*(5-(9/500*V_{gs}+27/100)/(7509/500+V_{gs}))))*(V_{gs}+15))^{(1/2)}*(22743861454796784249/18889465931478580854784000-$$

$$34498941656555872338340866277728375/178405961588244985132285746181186892047843328*\sinh(2000/9*\pi*(5-(9/500*V_{gs}+27/100)/(7509/500+V_{gs}))))*(-7046137207876802734375/73786976294838206464*\pi*(-9/500/(7509/500+V_{gs})+(9/500*V_{gs}+27/100)/(7509/500+V_{gs})^2)/(81+4000000*\pi^2*(5-(9/500*V_{gs}+27/100)/(7509/500+V_{gs}))^2)^{(1/2)}+500/9*(-9/1250/(7509/500+V_{gs})+2/5*(9/500*V_{gs}+27/100)/(7509/500+V_{gs})^2)/\cosh(18889465931478580854784/2833419889721787*\pi*(1/1000000-3607622250432923/75557863725914323419136*\sinh(2000/9*\pi*(5-(9/500*V_{gs}+27/100)/(7509/500+V_{gs})))))+901905562608230750000/25500779007496083*(2-2/5*(9/500*V_{gs}+27/100)/(7509/500+V_{gs}))/\cosh(18889465931478580854784/2833419889721787*\pi*(1/$$

$$\begin{aligned}
&1000000-3607622250432923/75557863725914323419136*\sinh(2000/9*\pi*(5- \\
&(9/500*V_{gs}+27/100)/(7509/500+V_{gs}))))^2*\sinh(18889465931478580854784/2833419889721787*\pi*(1 \\
&/1000000-3607622250432923/75557863725914323419136*\sinh(2000/9*\pi*(5- \\
&(9/500*V_{gs}+27/100)/(7509/500+V_{gs}))))*\pi^2*(- \\
&9/500/(7509/500+V_{gs})+(9/500*V_{gs}+27/100)/(7509/500+V_{gs})^2)/(81+4000000*\pi^2*(5- \\
&(9/500*V_{gs}+27/100)/(7509/500+V_{gs})^2)^{(1/2)))/(1+38685626227668133590597632/263577044107792 \\
&275*(1136641133335272432254209942730282477371327921662890625/431359146674410236714672 \\
&241392314090778194310760649159697657763987456/(22743861454796784249/188894659314785808 \\
&54784000- \\
&34498941656555872338340866277728375/178405961588244985132285746181186892047843328*\sin \\
&h(2000/9*\pi*(5-(9/500*V_{gs}+27/100)/(7509/500+V_{gs}))))^2*(V_{gs}+15)*\pi*(- \\
&9/500/(7509/500+V_{gs})+(9/500*V_{gs}+27/100)/(7509/500+V_{gs})^2)/(81+4000000*\pi^2*(5- \\
&(9/500*V_{gs}+27/100)/(7509/500+V_{gs})^2)^{(1/2)}+263577044107792275/38685626227668133590597632/ \\
&(22743861454796784249/18889465931478580854784000- \\
&34498941656555872338340866277728375/178405961588244985132285746181186892047843328*\sin \\
&h(2000/9*\pi*(5-(9/500*V_{gs}+27/100)/(7509/500+V_{gs}))))- \\
&1/8796093022208/(19342813113834066795298816+263577044107792275/(22743861454796784249/18 \\
&889465931478580854784000- \\
&34498941656555872338340866277728375/178405961588244985132285746181186892047843328*\sin \\
&h(2000/9*\pi*(5- \\
&(9/500*V_{gs}+27/100)/(7509/500+V_{gs}))))*(V_{gs}+15))^{(1/2)}*(113664113333527243225420994273028247 \\
&7371327921662890625/11150372599265311570767859136324180752990208/(22743861454796784249 \\
&/18889465931478580854784000- \\
&34498941656555872338340866277728375/178405961588244985132285746181186892047843328*\sin \\
&h(2000/9*\pi*(5-(9/500*V_{gs}+27/100)/(7509/500+V_{gs}))))^2*(V_{gs}+15)*\pi*(- \\
&9/500/(7509/500+V_{gs})+(9/500*V_{gs}+27/100)/(7509/500+V_{gs})^2)/(81+4000000*\pi^2*(5- \\
&(9/500*V_{gs}+27/100)/(7509/500+V_{gs})^2)^{(1/2)}+263577044107792275/(22743861454796784249/18889 \\
&465931478580854784000- \\
&34498941656555872338340866277728375/178405961588244985132285746181186892047843328*\sin \\
&h(2000/9*\pi*(5- \\
&(9/500*V_{gs}+27/100)/(7509/500+V_{gs}))))*(22743861454796784249/18889465931478580854784000- \\
&34498941656555872338340866277728375/178405961588244985132285746181186892047843328*\sin \\
&h(2000/9*\pi*(5-(9/500*V_{gs}+27/100)/(7509/500+V_{gs}))))*(2- \\
&56369097663014421875/1180591620717411303424*\sinh(2000/9*\pi*(5- \\
&(9/500*V_{gs}+27/100)/(7509/500+V_{gs}))))+500/9*(2- \\
&2/5*(9/500*V_{gs}+27/100)/(7509/500+V_{gs}))/\cosh(18889465931478580854784/2833419889721787*\pi*(1/ \\
&1000000-3607622250432923/75557863725914323419136*\sinh(2000/9*\pi*(5- \\
&(9/500*V_{gs}+27/100)/(7509/500+V_{gs})))))- \\
&57498236094259787230568110462880625/1012945474241937133241379867066368*(1+26357704410 \\
&7792275/38685626227668133590597632/(22743861454796784249/18889465931478580854784000- \\
&34498941656555872338340866277728375/178405961588244985132285746181186892047843328*\sin \\
&h(2000/9*\pi*(5-(9/500*V_{gs}+27/100)/(7509/500+V_{gs}))))*(V_{gs}+15)- \\
&1/4398046511104*(19342813113834066795298816+263577044107792275/(22743861454796784249/1 \\
&8889465931478580854784000- \\
&34498941656555872338340866277728375/178405961588244985132285746181186892047843328*\sin \\
&h(2000/9*\pi*(5-(9/500*V_{gs}+27/100)/(7509/500+V_{gs}))))*(V_{gs}+15))^{(1/2)}*\pi*(- \\
&9/500/(7509/500+V_{gs})+(9/500*V_{gs}+27/100)/(7509/500+V_{gs})^2)/(81+4000000*\pi^2*(5- \\
&(9/500*V_{gs}+27/100)/(7509/500+V_{gs})^2)^{(1/2)}*(2- \\
&56369097663014421875/1180591620717411303424*\sinh(2000/9*\pi*(5- \\
&(9/500*V_{gs}+27/100)/(7509/500+V_{gs}))))+500/9*(2-
\end{aligned}$$


```

2/5*(9/500*Vgs+27/100)/(7509/500+Vgs))/cosh(18889465931478580854784/2833419889721787*pi*(1/
1000000-3607622250432923/75557863725914323419136*asinh(2000/9*pi*(5-
(9/500*Vgs+27/100)/(7509/500+Vgs)))))+38685626227668133590597632/263577044107792275*(1+2
63577044107792275/38685626227668133590597632/(22743861454796784249/1888946593147858085
4784000-
34498941656555872338340866277728375/178405961588244985132285746181186892047843328*asin
h(2000/9*pi*(5-(9/500*Vgs+27/100)/(7509/500+Vgs))))*(Vgs+15)-
1/4398046511104*(19342813113834066795298816+263577044107792275/(22743861454796784249/1
8889465931478580854784000-
34498941656555872338340866277728375/178405961588244985132285746181186892047843328*asin
h(2000/9*pi*(5-
(9/500*Vgs+27/100)/(7509/500+Vgs))))*(Vgs+15))^(1/2))*(22743861454796784249/188894659314785
80854784000-
34498941656555872338340866277728375/178405961588244985132285746181186892047843328*asin
h(2000/9*pi*(5-(9/500*Vgs+27/100)/(7509/500+Vgs))))*(-
7046137207876802734375/73786976294838206464*pi*(-
9/500/(7509/500+Vgs)+(9/500*Vgs+27/100)/(7509/500+Vgs)^2)/(81+4000000*pi^2*(5-
(9/500*Vgs+27/100)/(7509/500+Vgs))^2)^(1/2)+500/9*(-
9/1250/(7509/500+Vgs)+2/5*(9/500*Vgs+27/100)/(7509/500+Vgs)^2)/cosh(1888946593147858085478
4/2833419889721787*pi*(1/1000000-
3607622250432923/75557863725914323419136*asinh(2000/9*pi*(5-
(9/500*Vgs+27/100)/(7509/500+Vgs)))))+901905562608230750000/25500779007496083*(2-
2/5*(9/500*Vgs+27/100)/(7509/500+Vgs))/cosh(18889465931478580854784/2833419889721787*pi*(1/
1000000-3607622250432923/75557863725914323419136*asinh(2000/9*pi*(5-
(9/500*Vgs+27/100)/(7509/500+Vgs))))^2*sinh(18889465931478580854784/2833419889721787*pi*(1
/1000000-3607622250432923/75557863725914323419136*asinh(2000/9*pi*(5-
(9/500*Vgs+27/100)/(7509/500+Vgs)))))*pi^2*(-
9/500/(7509/500+Vgs)+(9/500*Vgs+27/100)/(7509/500+Vgs)^2)/(81+4000000*pi^2*(5-
(9/500*Vgs+27/100)/(7509/500+Vgs))^2)^(1/2)));

```

```

Cgs = (((Z*L)/(2*2^0.5))*sqrt((q*eps*Nd)/(Vbi-Vgs)) + (pi/2)*eps*Z);

```

```

Cgd = (((Z*L)/(2*2^0.5))*sqrt((q*eps*Nd)/(Vbi-(Vgs-Vds))) + (pi/2)*eps*Z);

```

```

ft = gm/(2*pi*(Cgs+Cgd));

```

```

f = [1*10^9:1*10^9:10*10^9];

```

```

for i = 1:length(f)

```

```

    fo(i)=10*log(1+2.5*(f(i)/ft)*sqrt(gm*(Rs+Rg)));

```

```

end

```

```

plot(f,fo,xlabel('Frequency(Hz)'),ylabel('Optimum noise figure(dB)'),title('Variation of optimum noise
figure with frequency'))

```

```

hold on;

```

%for L = 4um

$L=4*10^{-6}$;

$V_{gs} = -3$;

gm

$$\begin{aligned} &= (38685626227668133590597632/19768278308084420625 * (11366411333352724322542099427302824 \\ &77371327921662890625/4313591466744102367146722413923140907781943107606491596976577639 \\ &87456/(22743861454796784249/18889465931478580854784000- \\ &34498941656555872338340866277728375/178405961588244985132285746181186892047843328 * \operatorname{asin} \\ &h(2000/9 * \pi * (5 - (9/500 * V_{gs} + 27/100)/(7509/500 + V_{gs}))))^2 * (V_{gs} + 15) * \pi * (- \\ &9/500/(7509/500 + V_{gs}) + (9/500 * V_{gs} + 27/100)/(7509/500 + V_{gs})^2)/(81 + 4000000 * \pi^2 * (5 - \\ &(9/500 * V_{gs} + 27/100)/(7509/500 + V_{gs}))^2)^{1/2} + 263577044107792275/38685626227668133590597632/ \\ &(22743861454796784249/18889465931478580854784000- \\ &34498941656555872338340866277728375/178405961588244985132285746181186892047843328 * \operatorname{asin} \\ &h(2000/9 * \pi * (5 - (9/500 * V_{gs} + 27/100)/(7509/500 + V_{gs})))) - \\ &1/8796093022208/(19342813113834066795298816 + 263577044107792275/(22743861454796784249/18 \\ &889465931478580854784000- \\ &34498941656555872338340866277728375/178405961588244985132285746181186892047843328 * \operatorname{asin} \\ &h(2000/9 * \pi * (5 - \\ &(9/500 * V_{gs} + 27/100)/(7509/500 + V_{gs})))) * (V_{gs} + 15)^{1/2} * (113664113333527243225420994273028247 \\ &7371327921662890625/11150372599265311570767859136324180752990208/(22743861454796784249 \\ &/18889465931478580854784000- \\ &34498941656555872338340866277728375/178405961588244985132285746181186892047843328 * \operatorname{asin} \\ &h(2000/9 * \pi * (5 - (9/500 * V_{gs} + 27/100)/(7509/500 + V_{gs}))))^2 * (V_{gs} + 15) * \pi * (- \\ &9/500/(7509/500 + V_{gs}) + (9/500 * V_{gs} + 27/100)/(7509/500 + V_{gs})^2)/(81 + 4000000 * \pi^2 * (5 - \\ &(9/500 * V_{gs} + 27/100)/(7509/500 + V_{gs}))^2)^{1/2} + 263577044107792275/(22743861454796784249/18889 \\ &465931478580854784000- \\ &34498941656555872338340866277728375/178405961588244985132285746181186892047843328 * \operatorname{asin} \\ &h(2000/9 * \pi * (5 - \\ &(9/500 * V_{gs} + 27/100)/(7509/500 + V_{gs})))) * (22743861454796784249/18889465931478580854784000- \\ &34498941656555872338340866277728375/178405961588244985132285746181186892047843328 * \operatorname{asin} \\ &h(2000/9 * \pi * (5 - (9/500 * V_{gs} + 27/100)/(7509/500 + V_{gs})))) * (2 - \\ &56369097663014421875/1180591620717411303424 * \operatorname{asinh}(2000/9 * \pi * (5 - \\ &(9/500 * V_{gs} + 27/100)/(7509/500 + V_{gs}))) + 500/9 * (2 - \\ &2/5 * (9/500 * V_{gs} + 27/100)/(7509/500 + V_{gs}))/\cosh(18889465931478580854784/2833419889721787 * \pi * (1/ \\ &1000000 - 3607622250432923/75557863725914323419136 * \operatorname{asinh}(2000/9 * \pi * (5 - \\ &(9/500 * V_{gs} + 27/100)/(7509/500 + V_{gs})))))) - \\ &766643147923463829740908139505075/1012945474241937133241379867066368 * (1 + 2635770441077 \\ &92275/38685626227668133590597632/(22743861454796784249/18889465931478580854784000- \\ &34498941656555872338340866277728375/178405961588244985132285746181186892047843328 * \operatorname{asin} \\ &h(2000/9 * \pi * (5 - (9/500 * V_{gs} + 27/100)/(7509/500 + V_{gs})))) * (V_{gs} + 15) - \\ &1/4398046511104 * (19342813113834066795298816 + 263577044107792275/(22743861454796784249/1 \\ &8889465931478580854784000- \\ &34498941656555872338340866277728375/178405961588244985132285746181186892047843328 * \operatorname{asin} \\ &h(2000/9 * \pi * (5 - (9/500 * V_{gs} + 27/100)/(7509/500 + V_{gs})))) * (V_{gs} + 15)^{1/2}) * \pi * (- \\ &9/500/(7509/500 + V_{gs}) + (9/500 * V_{gs} + 27/100)/(7509/500 + V_{gs})^2)/(81 + 4000000 * \pi^2 * (5 - \\ &(9/500 * V_{gs} + 27/100)/(7509/500 + V_{gs}))^2)^{1/2} * (2 - \end{aligned}$$

$$\begin{aligned}
&56369097663014421875/1180591620717411303424*\sinh(2000/9*\pi*(5- \\
&(9/500*V_{gs}+27/100)/(7509/500+V_{gs}))) + 500/9*(2- \\
&2/5*(9/500*V_{gs}+27/100)/(7509/500+V_{gs}))/\cosh(18889465931478580854784/2833419889721787*\pi*(1/ \\
&1000000-3607622250432923/75557863725914323419136*\sinh(2000/9*\pi*(5- \\
&(9/500*V_{gs}+27/100)/(7509/500+V_{gs})))) + 38685626227668133590597632/19768278308084420625*(1 \\
&+263577044107792275/38685626227668133590597632/(22743861454796784249/18889465931478580 \\
&854784000- \\
&34498941656555872338340866277728375/178405961588244985132285746181186892047843328*\sin \\
&h(2000/9*\pi*(5-(9/500*V_{gs}+27/100)/(7509/500+V_{gs}))))*(V_{gs}+15)- \\
&1/4398046511104*(19342813113834066795298816+263577044107792275/(22743861454796784249/1 \\
&8889465931478580854784000- \\
&34498941656555872338340866277728375/178405961588244985132285746181186892047843328*\sin \\
&h(2000/9*\pi*(5- \\
&(9/500*V_{gs}+27/100)/(7509/500+V_{gs}))))*(V_{gs}+15))^{(1/2)}*(22743861454796784249/188894659314785 \\
&80854784000- \\
&34498941656555872338340866277728375/178405961588244985132285746181186892047843328*\sin \\
&h(2000/9*\pi*(5-(9/500*V_{gs}+27/100)/(7509/500+V_{gs}))))*(- \\
&7046137207876802734375/73786976294838206464*\pi*(- \\
&9/500/(7509/500+V_{gs})+(9/500*V_{gs}+27/100)/(7509/500+V_{gs})^2)/(81+4000000*\pi^2*(5- \\
&(9/500*V_{gs}+27/100)/(7509/500+V_{gs}))^2)^{(1/2)}+500/9*(- \\
&9/1250/(7509/500+V_{gs})+2/5*(9/500*V_{gs}+27/100)/(7509/500+V_{gs})^2)/\cosh(1888946593147858085478 \\
&4/2833419889721787*\pi*(1/1000000- \\
&3607622250432923/75557863725914323419136*\sinh(2000/9*\pi*(5- \\
&(9/500*V_{gs}+27/100)/(7509/500+V_{gs})))) + 901905562608230750000/25500779007496083*(2- \\
&2/5*(9/500*V_{gs}+27/100)/(7509/500+V_{gs}))/\cosh(18889465931478580854784/2833419889721787*\pi*(1/ \\
&1000000-3607622250432923/75557863725914323419136*\sinh(2000/9*\pi*(5- \\
&(9/500*V_{gs}+27/100)/(7509/500+V_{gs}))))^2*\sinh(18889465931478580854784/2833419889721787*\pi*(1 \\
&/1000000-3607622250432923/75557863725914323419136*\sinh(2000/9*\pi*(5- \\
&(9/500*V_{gs}+27/100)/(7509/500+V_{gs}))))*\pi^2*(- \\
&9/500/(7509/500+V_{gs})+(9/500*V_{gs}+27/100)/(7509/500+V_{gs})^2)/(81+4000000*\pi^2*(5- \\
&(9/500*V_{gs}+27/100)/(7509/500+V_{gs}))^2)^{(1/2)))/(1+38685626227668133590597632/263577044107792 \\
&275*(1136641133335272432254209942730282477371327921662890625/431359146674410236714672 \\
&241392314090778194310760649159697657763987456/(22743861454796784249/188894659314785808 \\
&54784000- \\
&34498941656555872338340866277728375/178405961588244985132285746181186892047843328*\sin \\
&h(2000/9*\pi*(5-(9/500*V_{gs}+27/100)/(7509/500+V_{gs}))))^2*(V_{gs}+15)*\pi*(- \\
&9/500/(7509/500+V_{gs})+(9/500*V_{gs}+27/100)/(7509/500+V_{gs})^2)/(81+4000000*\pi^2*(5- \\
&(9/500*V_{gs}+27/100)/(7509/500+V_{gs}))^2)^{(1/2)}+263577044107792275/38685626227668133590597632/ \\
&(22743861454796784249/18889465931478580854784000- \\
&34498941656555872338340866277728375/178405961588244985132285746181186892047843328*\sin \\
&h(2000/9*\pi*(5-(9/500*V_{gs}+27/100)/(7509/500+V_{gs}))))- \\
&1/8796093022208/(19342813113834066795298816+263577044107792275/(22743861454796784249/18 \\
&889465931478580854784000- \\
&34498941656555872338340866277728375/178405961588244985132285746181186892047843328*\sin \\
&h(2000/9*\pi*(5- \\
&(9/500*V_{gs}+27/100)/(7509/500+V_{gs}))))*(V_{gs}+15))^{(1/2)}*(113664113333527243225420994273028247 \\
&7371327921662890625/11150372599265311570767859136324180752990208/(22743861454796784249 \\
&/18889465931478580854784000- \\
&34498941656555872338340866277728375/178405961588244985132285746181186892047843328*\sin \\
&h(2000/9*\pi*(5-(9/500*V_{gs}+27/100)/(7509/500+V_{gs}))))^2*(V_{gs}+15)*\pi*(-
\end{aligned}$$

$$\begin{aligned}
& 9/500/(7509/500+V_{gs})+(9/500*V_{gs}+27/100)/(7509/500+V_{gs})^2/(81+4000000*\pi^2*(5- \\
& (9/500*V_{gs}+27/100)/(7509/500+V_{gs}))^2)^{(1/2)}+263577044107792275/(22743861454796784249/18889 \\
& 465931478580854784000- \\
& 34498941656555872338340866277728375/178405961588244985132285746181186892047843328*\operatorname{asin} \\
& h(2000/9*\pi*(5- \\
& (9/500*V_{gs}+27/100)/(7509/500+V_{gs}))))*(22743861454796784249/18889465931478580854784000- \\
& 34498941656555872338340866277728375/178405961588244985132285746181186892047843328*\operatorname{asin} \\
& h(2000/9*\pi*(5-(9/500*V_{gs}+27/100)/(7509/500+V_{gs}))))*(2- \\
& 56369097663014421875/1180591620717411303424*\operatorname{asinh}(2000/9*\pi*(5- \\
& (9/500*V_{gs}+27/100)/(7509/500+V_{gs}))+500/9*(2- \\
& 2/5*(9/500*V_{gs}+27/100)/(7509/500+V_{gs}))/\cosh(18889465931478580854784/2833419889721787*\pi*(1/ \\
& 1000000-3607622250432923/75557863725914323419136*\operatorname{asinh}(2000/9*\pi*(5- \\
& (9/500*V_{gs}+27/100)/(7509/500+V_{gs})))))- \\
& 57498236094259787230568110462880625/1012945474241937133241379867066368*(1+26357704410 \\
& 7792275/38685626227668133590597632/(22743861454796784249/18889465931478580854784000- \\
& 34498941656555872338340866277728375/178405961588244985132285746181186892047843328*\operatorname{asin} \\
& h(2000/9*\pi*(5-(9/500*V_{gs}+27/100)/(7509/500+V_{gs}))))*(V_{gs}+15)- \\
& 1/4398046511104*(19342813113834066795298816+263577044107792275/(22743861454796784249/1 \\
& 8889465931478580854784000- \\
& 34498941656555872338340866277728375/178405961588244985132285746181186892047843328*\operatorname{asin} \\
& h(2000/9*\pi*(5-(9/500*V_{gs}+27/100)/(7509/500+V_{gs}))))*(V_{gs}+15))^{(1/2)}*\pi*(- \\
& 9/500/(7509/500+V_{gs})+(9/500*V_{gs}+27/100)/(7509/500+V_{gs})^2/(81+4000000*\pi^2*(5- \\
& (9/500*V_{gs}+27/100)/(7509/500+V_{gs}))^2)^{(1/2)}*(2- \\
& 56369097663014421875/1180591620717411303424*\operatorname{asinh}(2000/9*\pi*(5- \\
& (9/500*V_{gs}+27/100)/(7509/500+V_{gs}))+500/9*(2- \\
& 2/5*(9/500*V_{gs}+27/100)/(7509/500+V_{gs}))/\cosh(18889465931478580854784/2833419889721787*\pi*(1/ \\
& 1000000-3607622250432923/75557863725914323419136*\operatorname{asinh}(2000/9*\pi*(5- \\
& (9/500*V_{gs}+27/100)/(7509/500+V_{gs}))))))+38685626227668133590597632/263577044107792275*(1+2 \\
& 63577044107792275/38685626227668133590597632/(22743861454796784249/1888946593147858085 \\
& 4784000- \\
& 34498941656555872338340866277728375/178405961588244985132285746181186892047843328*\operatorname{asin} \\
& h(2000/9*\pi*(5-(9/500*V_{gs}+27/100)/(7509/500+V_{gs}))))*(V_{gs}+15)- \\
& 1/4398046511104*(19342813113834066795298816+263577044107792275/(22743861454796784249/1 \\
& 8889465931478580854784000- \\
& 34498941656555872338340866277728375/178405961588244985132285746181186892047843328*\operatorname{asin} \\
& h(2000/9*\pi*(5- \\
& (9/500*V_{gs}+27/100)/(7509/500+V_{gs}))))*(V_{gs}+15))^{(1/2)}*(22743861454796784249/188894659314785 \\
& 80854784000- \\
& 34498941656555872338340866277728375/178405961588244985132285746181186892047843328*\operatorname{asin} \\
& h(2000/9*\pi*(5-(9/500*V_{gs}+27/100)/(7509/500+V_{gs}))))*(- \\
& 7046137207876802734375/73786976294838206464*\pi*(- \\
& 9/500/(7509/500+V_{gs})+(9/500*V_{gs}+27/100)/(7509/500+V_{gs})^2/(81+4000000*\pi^2*(5- \\
& (9/500*V_{gs}+27/100)/(7509/500+V_{gs}))^2)^{(1/2)}+500/9*(- \\
& 9/1250/(7509/500+V_{gs})+2/5*(9/500*V_{gs}+27/100)/(7509/500+V_{gs})^2)/\cosh(1888946593147858085478 \\
& 4/2833419889721787*\pi*(1/1000000- \\
& 3607622250432923/75557863725914323419136*\operatorname{asinh}(2000/9*\pi*(5- \\
& (9/500*V_{gs}+27/100)/(7509/500+V_{gs}))))+901905562608230750000/25500779007496083*(2- \\
& 2/5*(9/500*V_{gs}+27/100)/(7509/500+V_{gs}))/\cosh(18889465931478580854784/2833419889721787*\pi*(1/ \\
& 1000000-3607622250432923/75557863725914323419136*\operatorname{asinh}(2000/9*\pi*(5- \\
& (9/500*V_{gs}+27/100)/(7509/500+V_{gs}))))))^2*\sinh(18889465931478580854784/2833419889721787*\pi*(1
\end{aligned}$$

```

/1000000-3607622250432923/75557863725914323419136*asinh(2000/9*pi*(5-
(9/500*Vgs+27/100)/(7509/500+Vgs))))*pi^2*(-
9/500/(7509/500+Vgs)+(9/500*Vgs+27/100)/(7509/500+Vgs)^2)/(81+4000000*pi^2*(5-
(9/500*Vgs+27/100)/(7509/500+Vgs))^2)^(1/2)));

Cgs = (((Z*L)/(2*2^0.5))*sqrt((q*eps*Nd)/(Vbi-Vgs)) + (pi/2)*eps*Z);

Cgd = (((Z*L)/(2*2^0.5))*sqrt((q*eps*Nd)/(Vbi-(Vgs-Vds))) + (pi/2)*eps*Z);

ft = gm/(2*pi*(Cgs+Cgd));

f = [1*10^9:1*10^9:10*10^9];

for i = 1:length(f)

    fo(i)=10*log(1+2.5*(f(i)/ft)*sqrt(gm*(Rs+Rg)));

end

plot(f,fo,'r')

hold on;

%for L = 8um

L=8*10^-6;

Vgs = -3;

gm
=(38685626227668133590597632/19768278308084420625*(11366411333352724322542099427302824
77371327921662890625/4313591466744102367146722413923140907781943107606491596976577639
87456/(22743861454796784249/18889465931478580854784000-
34498941656555872338340866277728375/178405961588244985132285746181186892047843328*asin
h(2000/9*pi*(5-(9/500*Vgs+27/100)/(7509/500+Vgs))))^2*(Vgs+15)*pi*(-
9/500/(7509/500+Vgs)+(9/500*Vgs+27/100)/(7509/500+Vgs)^2)/(81+4000000*pi^2*(5-
(9/500*Vgs+27/100)/(7509/500+Vgs))^2)^(1/2)+263577044107792275/38685626227668133590597632/
(22743861454796784249/18889465931478580854784000-
34498941656555872338340866277728375/178405961588244985132285746181186892047843328*asin
h(2000/9*pi*(5-(9/500*Vgs+27/100)/(7509/500+Vgs))))-
1/8796093022208/(19342813113834066795298816+263577044107792275/(22743861454796784249/18
889465931478580854784000-
34498941656555872338340866277728375/178405961588244985132285746181186892047843328*asin
h(2000/9*pi*(5-
(9/500*Vgs+27/100)/(7509/500+Vgs))))*(Vgs+15))^1/2*(113664113333527243225420994273028247
7371327921662890625/11150372599265311570767859136324180752990208/(22743861454796784249
/18889465931478580854784000-
34498941656555872338340866277728375/178405961588244985132285746181186892047843328*asin

```

$$\begin{aligned} & h(2000/9*\pi*(5-(9/500*V_{gs}+27/100)/(7509/500+V_{gs})))^2*(V_{gs}+15)*\pi*(- \\ & 9/500/(7509/500+V_{gs})+(9/500*V_{gs}+27/100)/(7509/500+V_{gs})^2)/(81+4000000*\pi^2*(5- \\ & (9/500*V_{gs}+27/100)/(7509/500+V_{gs}))^2)^{(1/2)}+263577044107792275/(22743861454796784249/18889 \\ & 465931478580854784000- \\ & 34498941656555872338340866277728375/178405961588244985132285746181186892047843328*\operatorname{asin} \\ & h(2000/9*\pi*(5- \\ & (9/500*V_{gs}+27/100)/(7509/500+V_{gs}))))*(22743861454796784249/18889465931478580854784000- \\ & 34498941656555872338340866277728375/178405961588244985132285746181186892047843328*\operatorname{asin} \\ & h(2000/9*\pi*(5-(9/500*V_{gs}+27/100)/(7509/500+V_{gs}))))*(2- \\ & 56369097663014421875/1180591620717411303424*\operatorname{asinh}(2000/9*\pi*(5- \\ & (9/500*V_{gs}+27/100)/(7509/500+V_{gs}))+500/9*(2- \\ & 2/5*(9/500*V_{gs}+27/100)/(7509/500+V_{gs}))/\cosh(18889465931478580854784/2833419889721787*\pi*(1/ \\ & 1000000-3607622250432923/75557863725914323419136*\operatorname{asinh}(2000/9*\pi*(5- \\ & (9/500*V_{gs}+27/100)/(7509/500+V_{gs})))))- \\ & 766643147923463829740908139505075/1012945474241937133241379867066368*(1+2635770441077 \\ & 92275/38685626227668133590597632/(22743861454796784249/18889465931478580854784000- \\ & 34498941656555872338340866277728375/178405961588244985132285746181186892047843328*\operatorname{asin} \\ & h(2000/9*\pi*(5-(9/500*V_{gs}+27/100)/(7509/500+V_{gs}))))*(V_{gs}+15)- \\ & 1/4398046511104*(19342813113834066795298816+263577044107792275/(22743861454796784249/1 \\ & 8889465931478580854784000- \\ & 34498941656555872338340866277728375/178405961588244985132285746181186892047843328*\operatorname{asin} \\ & h(2000/9*\pi*(5-(9/500*V_{gs}+27/100)/(7509/500+V_{gs}))))*(V_{gs}+15))^{(1/2)}*\pi*(- \\ & 9/500/(7509/500+V_{gs})+(9/500*V_{gs}+27/100)/(7509/500+V_{gs})^2)/(81+4000000*\pi^2*(5- \\ & (9/500*V_{gs}+27/100)/(7509/500+V_{gs}))^2)^{(1/2)}*(2- \\ & 56369097663014421875/1180591620717411303424*\operatorname{asinh}(2000/9*\pi*(5- \\ & (9/500*V_{gs}+27/100)/(7509/500+V_{gs}))+500/9*(2- \\ & 2/5*(9/500*V_{gs}+27/100)/(7509/500+V_{gs}))/\cosh(18889465931478580854784/2833419889721787*\pi*(1/ \\ & 1000000-3607622250432923/75557863725914323419136*\operatorname{asinh}(2000/9*\pi*(5- \\ & (9/500*V_{gs}+27/100)/(7509/500+V_{gs})))))+38685626227668133590597632/19768278308084420625*(1 \\ & +263577044107792275/38685626227668133590597632/(22743861454796784249/18889465931478580 \\ & 854784000- \\ & 34498941656555872338340866277728375/178405961588244985132285746181186892047843328*\operatorname{asin} \\ & h(2000/9*\pi*(5-(9/500*V_{gs}+27/100)/(7509/500+V_{gs}))))*(V_{gs}+15)- \\ & 1/4398046511104*(19342813113834066795298816+263577044107792275/(22743861454796784249/1 \\ & 8889465931478580854784000- \\ & 34498941656555872338340866277728375/178405961588244985132285746181186892047843328*\operatorname{asin} \\ & h(2000/9*\pi*(5- \\ & (9/500*V_{gs}+27/100)/(7509/500+V_{gs}))))*(V_{gs}+15))^{(1/2)}*(22743861454796784249/188894659314785 \\ & 80854784000- \\ & 34498941656555872338340866277728375/178405961588244985132285746181186892047843328*\operatorname{asin} \\ & h(2000/9*\pi*(5-(9/500*V_{gs}+27/100)/(7509/500+V_{gs}))))*(- \\ & 7046137207876802734375/73786976294838206464*\pi*(- \\ & 9/500/(7509/500+V_{gs})+(9/500*V_{gs}+27/100)/(7509/500+V_{gs})^2)/(81+4000000*\pi^2*(5- \\ & (9/500*V_{gs}+27/100)/(7509/500+V_{gs}))^2)^{(1/2)}+500/9*(- \\ & 9/1250/(7509/500+V_{gs})+2/5*(9/500*V_{gs}+27/100)/(7509/500+V_{gs})^2)/\cosh(1888946593147858085478 \\ & 4/2833419889721787*\pi*(1/1000000- \\ & 3607622250432923/75557863725914323419136*\operatorname{asinh}(2000/9*\pi*(5- \\ & (9/500*V_{gs}+27/100)/(7509/500+V_{gs}))))+901905562608230750000/25500779007496083*(2- \\ & 2/5*(9/500*V_{gs}+27/100)/(7509/500+V_{gs}))/\cosh(18889465931478580854784/2833419889721787*\pi*(1/ \\ & 1000000-3607622250432923/75557863725914323419136*\operatorname{asinh}(2000/9*\pi*(5-
\end{aligned}$$


```

1000000-3607622250432923/75557863725914323419136*asinh(2000/9*pi*(5-
(9/500*Vgs+27/100)/(7509/500+Vgs)))))+38685626227668133590597632/263577044107792275*(1+2
63577044107792275/38685626227668133590597632/(22743861454796784249/1888946593147858085
4784000-
34498941656555872338340866277728375/178405961588244985132285746181186892047843328*asin
h(2000/9*pi*(5-(9/500*Vgs+27/100)/(7509/500+Vgs))))*(Vgs+15)-
1/4398046511104*(19342813113834066795298816+263577044107792275/(22743861454796784249/1
8889465931478580854784000-
34498941656555872338340866277728375/178405961588244985132285746181186892047843328*asin
h(2000/9*pi*(5-
(9/500*Vgs+27/100)/(7509/500+Vgs))))*(Vgs+15))^(1/2))*(22743861454796784249/188894659314785
80854784000-
34498941656555872338340866277728375/178405961588244985132285746181186892047843328*asin
h(2000/9*pi*(5-(9/500*Vgs+27/100)/(7509/500+Vgs))))*(-
7046137207876802734375/73786976294838206464*pi*(-
9/500/(7509/500+Vgs)+(9/500*Vgs+27/100)/(7509/500+Vgs)^2)/(81+4000000*pi^2*(5-
(9/500*Vgs+27/100)/(7509/500+Vgs))^2)^(1/2)+500/9*(-
9/1250/(7509/500+Vgs)+2/5*(9/500*Vgs+27/100)/(7509/500+Vgs)^2)/cosh(1888946593147858085478
4/2833419889721787*pi*(1/1000000-
3607622250432923/75557863725914323419136*asinh(2000/9*pi*(5-
(9/500*Vgs+27/100)/(7509/500+Vgs)))))+901905562608230750000/25500779007496083*(2-
2/5*(9/500*Vgs+27/100)/(7509/500+Vgs))/cosh(18889465931478580854784/2833419889721787*pi*(1/
1000000-3607622250432923/75557863725914323419136*asinh(2000/9*pi*(5-
(9/500*Vgs+27/100)/(7509/500+Vgs))))^2*sinh(18889465931478580854784/2833419889721787*pi*(1
/1000000-3607622250432923/75557863725914323419136*asinh(2000/9*pi*(5-
(9/500*Vgs+27/100)/(7509/500+Vgs)))))*pi^2*(-
9/500/(7509/500+Vgs)+(9/500*Vgs+27/100)/(7509/500+Vgs)^2)/(81+4000000*pi^2*(5-
(9/500*Vgs+27/100)/(7509/500+Vgs))^2)^(1/2)))));

```

```

Cgs = (((Z*L)/(2*2^0.5))*sqrt((q*eps*Nd)/(Vbi-Vgs)) + (pi/2)*eps*Z);

```

```

Cgd = (((Z*L)/(2*2^0.5))*sqrt((q*eps*Nd)/(Vbi-(Vgs-Vds))) + (pi/2)*eps*Z);

```

```

ft = gm/(2*pi*(Cgs+Cgd));

```

```

f = [1*10^9:1*10^9:10*10^9];

```

```

for i = 1:length(f)

```

```

    fo(i)=10*log(1+2.5*(f(i)/ft)*sqrt(gm*(Rs+Rg)));

```

```

end

```

```

plot(f,fo,'g')

```


Variation of Gate-Drain Capacitance with Drain-Source Voltage

```
clear all;

clc;

close all;

Z = 100*10^-6;

L = 4*10^-6;

q = 1.6*10^-19;

Eo = 8.85*10^-12;

E = 9.5*Eo;

Nd = 10^23;

Vbi = 1;

Vds = [0:1:20];

Vgs = 0;

Cgd = (((Z*L)/(2*2^0.5)).*sqrt((q*E*Nd)/(Vbi-(Vgs-Vds)))) + (pi./2)*E*Z)*10^12;

plot(Vds,Cgd, xlabel('Drain-source voltage(V)'),ylabel('Gate-drain capacitance(pF)'),title('Variation of gate-drain
capacitance with drain-source voltages'))

hold on;

Vgs = -3;

Cgd = (((Z*L)/(2*2^0.5)).*sqrt((q*E*Nd)/(Vbi-(Vgs-Vds)))) + (pi./2)*E*Z)*10^12;

plot(Vds,Cgd,'r')

hold on;

Vgs = -6;

Cgd = (((Z*L)/(2*2^0.5)).*sqrt((q*E*Nd)/(Vbi-(Vgs-Vds)))) + (pi./2)*E*Z)*10^12;

plot(Vds,Cgd,'c')
```

Variation of Gate-Source Capacitance with respect to Gate-Source Voltage

```
clear all;

clc;

close all;

Z = 100*10^-6;

L = 4*10^-6;

q = 1.6*10^-19;

Eo = 8.85*10^-12;

E = 9.5*Eo;

Nd = 10^23;

Vbi = 1;

Vgs = [-9:1:0];

Cgs = (((Z*L)/(2*2^0.5)).*sqrt((q*E*Nd)/(Vbi-Vgs)) + (pi./2)*E*Z)*10^12;

plot(Vgs,Cgs), xlabel('Gate-source voltage(V)'),ylabel('Gate-source capacitance(pF)'),title('Variation of gate-source capacitance with gate-source voltage')
```

Variation of Total Internal Device Capacitance with Gate Length

```

clc;

close all;

clear all;

Z=100*10^-6;

q=1.6022*10^-19;

eps=9.5*8.854*10^-12;

Nd=1*10^23;

Vbi=1;

Vds=5;

Vgs=0;

L = [1*(10^-6):1*(10^-6):10*(10^-6)];

for i = 1:length(L)

    Cgs = ((Z*L/(2*sqrt(2))))*(sqrt(q*eps*Nd/(Vbi-Vgs)))+(pi*eps*Z)/2)*10^12

    Cgd = ((Z*L/(2*sqrt(2))))*(sqrt(q*eps*Nd/(Vbi-(Vgs-Vds))))+(pi*eps*Z)/2)*10^12

end

Ct = Cgs+Cgd;

plot(L,Ct),xlabel('Gate length(m)'),ylabel('Total internal device capacitance(pF)'), title('Variation of total internal device capacitance with gate length')

hold on;

Vgs=-3;

L = [1*(10^-6):1*(10^-6):10*(10^-6)];

for i = 1:length(L)

    Cgs = ((Z*L/(2*sqrt(2))))*(sqrt(q*eps*Nd/(Vbi-Vgs)))+(pi*eps*Z)/2)*10^12

    Cgd = ((Z*L/(2*sqrt(2))))*(sqrt(q*eps*Nd/(Vbi-(Vgs-Vds))))+(pi*eps*Z)/2)*10^12

```

```

end

Ct = Cgs+Cgd;

plot(L,Ct,'r')

hold on;

Vgs=-6;

L = [1*(10^-6):1*(10^-6):10*(10^-6)];

for i = 1:length(L)

    Cgs = ((Z*L/(2*sqrt(2))))*(sqrt(q*eps*Nd/(Vbi-Vgs)))+(pi*eps*Z)/2)*10^12

    Cgd = ((Z*L/(2*sqrt(2))))*(sqrt(q*eps*Nd/(Vbi-(Vgs-Vds)))+(pi*eps*Z)/2)*10^12

end

Ct = Cgs+Cgd;

plot(L,Ct,'g')

```